

THE ROLE OF PHOTORESPIRATION IN PLANT RESPONSE TO HIGH LIGHT AND
PATHOGEN INFECTION

By

Xiaotong Jiang

A DISSERTATION

Submitted to
Michigan State University
in partial fulfillment of the requirements
for the degree of

Plant Biology – Doctor of Philosophy
Molecular Plant Sciences – Dual Major

2024

ABSTRACT

Plants interact with the dynamic environment constantly. Photorespiration is a physiological process that occurs simultaneously with photosynthesis and is often considered wasteful. However, photorespiration involves the coordination of multiple organelles and connects with various primary metabolic pathways, thus its response to the environment greatly influences the fate of plants. The roles of photorespiration in plant interaction with the dynamic environment are still not very clear. To investigate the underlying mechanisms, I applied various strategies to dissect the roles of photorespiration in plant response to both abiotic and biotic environmental factors.

Previous studies from my lab found that some Arabidopsis photorespiratory mutants only exhibit obvious photosynthetic phenotypes under high and dynamic light conditions, suggesting that photorespiration is regulated by high light. To identify potential modulators of photorespiration under such conditions, I performed a genetic screen for suppressors of the Arabidopsis photorespiratory mutant, *hpr1*, which is defective in the peroxisomal hydroxypyruvate reductase 1. A suppressor that partially rescued the small rosette of the *hpr1* mutant was mapped to *GLYR1*, which encodes the cytosolic glyoxylate reductase 1 that converts glyoxylate to glycolate. Independent loss-of-function alleles of *GLYR1* also recapitulated the partial rescue of *hpr1* in plant appearance and photosynthetic and photorespiratory activities. Interestingly, *glyr1* also suppressed the phenotypes of the photorespiratory mutant *catalase 2*, but not a null allele of the *PLGG1* (*Plastidic Glycolate Glycerate Transporter 1*) gene. Further investigations using metabolic and genetic tools provided evidence of a possible cytosolic glyoxylate shunt, which is triggered under high light conditions and in the absence of a properly functional main photorespiratory pathway. This shunt reduces the accumulated cytosolic glyoxylate to hydroxypyruvate, thus helping with carbon recycling through the cytosolic HPR2 enzyme. These findings support the metabolic flexibility of the photorespiration network under stress conditions.

My transcriptomic analysis of *hpr1* and its suppressor *glyr1 hpr1* also supports the existence of this non-canonical cytosolic pathway. Drastic transcriptional reprogramming that involves broad cellular functions was found in the *hpr1* mutant, which can be largely reverted by defective GLYR1. The rescuing effect of *glyr1* is only prominent when HPR1 is absent, supporting the view that the accumulation of photorespiratory intermediates in *hpr1* causes a

stressful cellular environment that disrupts biological processes globally, and that *glyr1* partially prevents this metabolic accumulation.

To investigate the role of photorespiration in plant response to biotic stress, I analyzed the performance of photorespiratory mutants in plant immune response. My data showed that deficiencies of the peroxisomal photorespiratory enzyme HPR1 and the chloroplastic transporter PLGG1 compromised response in both layers of immunity, pattern-triggered immunity and effector-triggered immunity, and these defects can be rescued when the plants were grown under high CO₂ conditions. These findings suggest that HPR1 and PLGG1 contribute to plant immune response via the photorespiratory pathway.

My research broadens our understanding of the role of photorespiration in plants under stress conditions, which may help with agricultural efforts to improve crop performance in response to the changing environment.

ACKNOWLEDGEMENTS

First, I really appreciate my mentor, Dr. Jianping Hu, for her generous guidance and support throughout my whole Ph.D. She is always patient, thoughtful, and professional. She gives me a lot of freedom to explore my own interests in research, treats my thoughts and questions seriously, and is always around when I need help. I learned numerous research skills including experiments, writing and presentations from her, which are valuable for me. I always feel lucky to have her as my mentor.

Next, I thank my committee members, Drs. Berkley Walker, Sheng Yang He and Gregg Howe, for their technical support, helpful instructions and insightful feedback. Dr. Walker's expertise in photorespiration is essential for my research, which I heavily rely on in the last 6 years. I've learned a lot from Dr. He, who is very experienced in plant immunity and continues supporting me after he left MSU. Dr. Howe also generously shares his thoughts and lab resources all the time.

I also thank previous and current members in the Hu Lab. I am happy to have overlaps and communications with many postdocs in the lab, including Drs. Stefanie Tietz, Ronghui Pan, Anne Rea, Linqi Han, Amanda Koenig, and Hiruni Weerasooriya. They all kindly share their knowledge and experiences of research and life, and provide me with vital help in designing experiments and troubleshooting. I have been obtaining a lot of assistance from undergraduate students and rotating students, including Linnea Hartz, Joy Li, Michael Nikolovski, Krishen Patel, Lillian Bieszke, Asia Hawkins, Carter Pasternak and Emily Schley. I also had many nice interactions with visiting student Katarzyna Krawczyk. Special thanks to lab members who directly contributed to my work: Drs. Stefanie Tietz and Jiying Li for performing EMS mutagenesis and the initial screening; Dr. Amanda Koenig and Joy Li for performing the GLYR1 localization experiment.

People from other labs and research facilities also help me a lot. I thank David Hall for performing DEPI experiments; Cassandra Johnny (MSU Mass Spectrometry and Metabolomics Core) and Drs. Xinyu Fu and Kelem Alamrie for technical support in metabolic measurements; Drs. John Froehlich and Sarah Stainbrook for technical support in immunoblot; Nicholas Panchy (MSU Bioinformatics Core) for analyzing the RNA-seq data; Drs. Ludmila Roze and Luke Gregory for technical support in experiments related to enzyme activity; Drs. Li Zhang and Pai Li for technical support in experiments related to immunity; Melinda Frame (MSU Center for

Advanced Microscopy) for technical support in confocal microscope; Dr. Alex Costa (Università degli Studi Milano) for sharing seeds and constructs of HyPer-sensor; Dr. Brad Day for sharing *rps2-101c* seeds and *Pst* DC3000 (*avrRpt2*) stain; and Jim Klug, Cody Keilen and Nick Deason for growth chamber support. Drs. Qiang Guo, Deserah Strand, Kaila Smith, Hussien Alameldin, Andre Velasquez and many other people in the MSU community all contributed to my research at a certain point, which I am grateful for.

I also appreciate the support from my family and friends over the last 6 years. No matter where they are and if they understand what I am doing, they have been using their own ways to constantly back me up. I always feel power, warmth and love from them, which I am deeply appreciated. I thank my cat Bellatrix for her intimate company during most of my Ph.D., making me feel that I have a home here.

Finally, I want to thank myself for persistently overcoming all the difficulties and eventually reaching the destination of the Ph.D. journey.

TABLE OF CONTENTS

LIST OF ABBREVIATIONS	vii
CHAPTER 1. Background.....	1
1.1 Photorespiration	1
1.2 The role of photorespiration under high light stress	2
1.3 The role of photorespiration in plant immunity	8
1.4 Summary	16
Figures	17
Tables	18
CHAPTER 2. A photorespiratory glyoxylate shunt in the cytosol supports photosynthesis and plant growth under high light conditions in Arabidopsis.....	19
2.1 Introduction.....	19
2.2 Results.....	22
2.3 Discussions	29
2.4 Methods	32
Figures	38
CHAPTER 3. Defective GLYR1 largely reverts the broad transcriptional reprogramming of the <i>hpr1</i> mutant under high light conditions.....	45
3.1 Introduction.....	45
3.2 Results.....	45
3.3 Discussions	49
3.4 Methods	50
Figures	52
Tables	62
CHAPTER 4. The role of photorespiration in plant immunity.....	66
4.1 Introduction.....	66
4.2 Results.....	67
4.3 Discussion and future directions.....	71
4.4 Methods	72
Figures	76
CHAPTER 5. Summary and future perspectives.....	86
REFERENCES	88
APPENDIX.....	103

LIST OF ABBREVIATIONS

2-OG	2-Oxoglutarate
2-PG	2-Phosphoglycolate
3-PGA	3-Phosphoglycerate
AAN	Aminoacetonitrile
BASS6	Bile acid sodium symporter 6
CAT	Catalase
CEF	Cyclic electron flow
CFU	Colony-forming units
DAMP	Damage-associated molecular pattern
DEG	Differentially expressed gene
dpi/hpi	Day(s)/hour(s) post infiltration
ETI	Effector-triggered immunity
FOC	<i>Fusarium oxysporum</i> f. sp. <i>cucumerinum</i>
G6P	Glucose-6-phosphate
GABA	γ -Aminobutyric acid
GDC	Glycine decarboxylase complex
GGAT	Glutamate:glyoxylate aminotransferase
GLYK	Glycerate kinase
GLYR1	Glyoxylate reductase 1
GOX	Glycolate oxidase
HPR	Hydroxypyruvate reductase
HR	Hypersensitive response
INH	Isonicotinic acid hydrazide
JA	Jasmonate
MAMP	Microbe-associated molecular pattern
NLR	Nucleotide-binding/leucine-rich-repeat receptor
NPQ	Non-photochemical quenching
PGLP	2-PG phosphatase
PLGG1	Plastidial glycolate/glycerate transporter 1
PMDH	Peroxisomal malate dehydrogenase

PR1	Pathogenesis-related 1
PRR	Pattern recognition receptor
PS	Photosystem
<i>Pst</i>	<i>Pseudomonas syringae</i> pv. <i>tomato</i>
PTI	Pattern-triggered immunity
PTM	Post-translational modification
qE	Energy-dependent quenching
ROS	Reactive oxygen species
Rubisco	RuBP carboxylase/oxygenase
RuBP	Ribulose-1,5-bisphosphate
SA	Salicylic acid
SCN	Soybean cyst nematode
SGAT	Serine:glyoxylate aminotransferase
SHMT	Serine hydroxymethyltransferase
THF	Tetrahydrofolate

CHAPTER 1*. Background

1.1 Photorespiration

Photorespiration, a biological pathway that is closely linked to photosynthesis, is initiated by the oxygenation of ribulose 1,5-bisphosphate (RuBP) catalyzed by ribulose 1,5-bisphosphate carboxylase-oxygenase (rubisco), producing 2-phosphoglycolate (2-PG) which can inhibit cellular functions when accumulated. In this pathway, 2-PG is first dephosphorylated by 2-PG phosphatase (PGLP) to produce glycolate, which is then transported out of the chloroplast by plastidial glycolate/glycerate transporter 1 (PLGG1) and bile acid sodium symporter 6 (BASS6). Upon entering the peroxisome, glycolate is converted to glyoxylate by glycolate oxidase (GOX), producing H₂O₂ that is then scavenged by catalases (CATs). Both glutamate:glyoxylate aminotransferase (GGAT) and serine:glyoxylate aminotransferase (SGAT) catalyze the conversion of glyoxylate to glycine. After transporting to the mitochondrion, glycine is converted to serine by the glycine decarboxylase complex (GDC) and serine hydroxymethyltransferase (SHMT), accompanying the tetrahydrofolate (THF) cycle and releasing CO₂ and NH₃. Serine is then transported back to the peroxisome, converted to hydroxypyruvate by SGAT, and subsequently reduced to glycerate by hydroxypyruvate reductase 1 (HPR1). HPR2 is an HPR isoform that reduces hydroxypyruvate to glycerate in the cytosol. Finally, glycerate is imported into the chloroplast through PLGG1 and phosphorylated to 3-phosphoglycerate (3-PGA) by glycerate kinase (GLYK) to recycle back to the Calvin-Benson cycle. Photorespiration consumes ATP in the chloroplast and NAD(P)H in the peroxisome and the cytosol, and releases NADH in the mitochondrion (Eisenhut *et al.*, 2019) (**Fig. 1.1**).

Because photorespiration itself, the regeneration of RuBP from 3-PGA, and the re-fixation of released CO₂ and NH₃ consume massive energy, this pathway significantly reduces photosynthetic efficiency (Walker *et al.*, 2016b). Therefore, the photorespiratory pathway has become a major target for genetic engineering with the goal to increase crop yield (Betti *et al.*, 2016; South *et al.*, 2018). However, photorespiration is essential to C₃ plants and even vital for C₄ plants such as maize (Zelitch *et al.*, 2009) and *Flaveria bidentis* (Levey *et al.*, 2019), highlighting its importance to plant survival. Photorespiration has tight connections with nitrogen, sulfate and one-carbon (C₁) metabolisms (Shi & Bloom, 2021), and has also been

* This chapter is partially adapted from Jiang, X., Walker, B. J., He, S. Y., & Hu, J. (2023). The role of photorespiration in plant immunity. *Frontiers in Plant Science*, 14(February), 1–8.

shown to play roles in plant response to both abiotic (Voss *et al.*, 2013) and biotic stresses (Sørhagen *et al.*, 2013).

1.2 The role of photorespiration under high light stress

1.2.1 Plant response to high light conditions

Light is an essential energy source and a critical environmental cue for plants, but its intensity often fluctuates beyond the ranges optimal for plant growth. For example, plants frequently experience high light conditions that exceed $2000 \mu\text{mol m}^{-2} \text{s}^{-1}$ on sunny days, posing significant stress to plants in the field (Ort, 2001; Mishra *et al.*, 2012). To cope with this stress, plants have developed responses at various levels, from molecular, cellular, to organismal (Szymańska *et al.*, 2017; Shi *et al.*, 2022a).

When light intensities exceed photosynthetic capacity, the generation of reactive oxygen species (ROS) from the photosynthetic apparatus is enhanced (Shi *et al.*, 2022a). In chloroplasts, superoxide ($\text{O}_2^{\cdot-}$) and single oxygen ($^1\text{O}_2$) produced by Photosystems (PSs) I and II can cause photodamage to protein complexes and subsequently inactivate the electron transport chain (Roach & Krieger-Liszkay, 2014; Krieger-Liszkay & Shimakawa, 2022; Sharma *et al.*, 2023). To mitigate photodamage, the antioxidant system in chloroplasts is activated to scavenge ROS. This system includes nonenzymatic components such as carotenoids, ascorbate, and glutathione, as well as enzymes like catalase and superoxide dismutase (Szymańska *et al.*, 2017; Foyer, 2018; Bassi & Dall'osto, 2021). Plants also regulate photosynthetic electron transport to suppress ROS generation. Energy-dependent quenching (qE), the main and rapidly reversing component of non-photochemical quenching (NPQ), can safely dissipate the excessive energy absorbed by light-harvesting complexes as heat (Ruban, 2016; Bassi & Dall'osto, 2021). Additionally, cyclic electron flow (CEF) around PSI is activated under high light as a photoprotective strategy, increasing proton release into the thylakoid lumen and subsequently prompting ATP synthesis and energy dissipation as qE (Shikanai, 2007; Chaux *et al.*, 2015).

Despite their damaging nature, chloroplastic ROS also function as retrograde signaling molecules, transmitting environmental cues to the nucleus to coordinate whole-cell response (Li & Kim, 2022; Foyer & Hanke, 2022). Gene expression analyses have shown dynamic and temporal transcriptional reprogramming under high light and indicated the involvement of hormones, light signaling, metabolites, and developmental processes, in addition to ROS and photosynthesis (Rossel *et al.*, 2002; Kleine *et al.*, 2007; Suzuki *et al.*, 2015; Zhao *et al.*, 2016;

Crisp *et al.*, 2017; Huang *et al.*, 2019b). Another protective mechanism employed by the plant at cellular and organismal levels is the reduction of light absorption through processes such as chloroplast and leaf movement (Takahashi & Badger, 2011; Wada, 2013), and anthocyanin accumulation (Zheng *et al.*, 2021; Ma *et al.*, 2021).

Overall, plants employ various strategies at different levels to survive high light conditions through complicated responses. A deeper understanding of the underlying mechanisms of these responses will ultimately enable us to develop crops that are more resilient to high light.

1.2.2 The role of photorespiration under high light conditions

As a metabolic process closely related to photosynthesis, photorespiration has been shown to support the performance of photosynthesis, especially under stress conditions.

Under regular growth conditions, many photorespiratory mutants exhibit compromised photosynthesis and growth in ambient air (Timm & Bauwe, 2013; Timm *et al.*, 2016). Under high CO₂ environments where rubisco oxygenation is inhibited, these photorespiratory mutants are largely recovered (Timm & Bauwe, 2013; Timm *et al.*, 2016). Although the exact reasons for these air-grown phenotypes are not clear, the accumulated photorespiratory intermediates in these mutants, such as 2-PG, glyoxylate, and glycerate, can inhibit the activities of photosynthesis-related enzymes (Timm *et al.*, 2016). Additionally, several *Arabidopsis* photorespiratory mutants, including *hpr1*, *plgg1*, *cat2* and *gox1*, display much more pronounced photosynthetic phenotypes under high and dynamic light conditions than low and constant light conditions, highlighting the increased importance of photorespiration under high light (Li *et al.*, 2019a).

During high light and other abiotic stresses, increased photorespiratory flux rates and enzyme activities, and accumulations of photorespiratory metabolites are often observed, suggesting that photorespiration plays an important role in maintaining photosynthetic performance and helping with plant survival under these conditions (Muraoka *et al.*, 2000; Voss *et al.*, 2013; Ma *et al.*, 2014; Huang *et al.*, 2014, 2015; Sunil *et al.*, 2019; Osei-Bonsu *et al.*, 2021; Shi *et al.*, 2022b). Under stresses, photorespiration is believed to function as an alternative electron sink that consumes excessive energy produced by the photosynthetic light reactions, preventing over-reduction of the electron transport chain and ROS-induced photodamage (Wingler *et al.*, 2000; Ort & Baker, 2002; Voss *et al.*, 2013; Huang *et al.*, 2019a). However, an

alternative perspective suggests that photorespiration facilitates the synthesis of new PSII proteins during the repair of photodamage rather than preventing photodamage itself (Takahashi *et al.*, 2007; Wang *et al.*, 2022), a function not necessarily due to energy consumption in photorespiration. A recent work also challenged the idea of photorespiration as an alternative sink, as it observed decreased PSII efficiency (Φ_{II}) and increased photoinhibition under high O₂ conditions that cause increased energy demand of photorespiration, contradicting the protective role of photorespiration (Smith *et al.*, 2023). Further investigations indicated a new role of photorespiration in avoiding substrate limitation in ATP synthesis (Smith *et al.*, 2023). In addition, photorespiration can upregulate CEF and the alternative oxidase pathway in mitochondria to protect photosynthesis indirectly (Sunil *et al.*, 2019). Finally, since photorespiration generates hydrogen peroxide (H₂O₂), an important signaling molecule, this pathway may directly contribute to signal transduction in high light response (Voss *et al.*, 2013).

In summary, photorespiration has a notable role in supporting photosynthesis under high light and other abiotic stresses, but the underlying mechanisms require further investigation.

1.2.3 The role of the hydroxypyruvate reductase (HPR) family in photorespiration and other processes

As a major enzyme in photorespiration, HPR catalyzes the reduction of hydroxypyruvate to glycerate (**Fig. 1.1**). In Arabidopsis, three members of the HPR family have been shown to function in photorespiration (Timm *et al.*, 2008, 2011). The peroxisomal HPR1 plays a major role in reducing hydroxypyruvate with NADH as the co-factor, whereas HPR2 and HPR3 in the cytosol have low activities and prefer NADPH as the co-factor (Timm *et al.*, 2008, 2011; Xu *et al.*, 2018a; Wang *et al.*, 2022). All three enzymes can also reduce glyoxylate using NADH and NADPH, and HPR2 and HPR3 are additionally involved in the tyrosine conversion pathway, catalyzing the reduction of 4-hydroxyphenylpyruvic acid to 4-hydroxyphenyllactic acid (Timm *et al.*, 2008, 2011; Xu *et al.*, 2018a). Based on phylogenetic analysis, HPR1 is present across green plants, HPR2 is conserved in land plants, and HPR3 is angiosperm-specific (Xu *et al.*, 2018a).

HPR enzymes play an important role in photosynthesis. The knockout mutant of *HPR1* shows compromised photosynthetic performance and growth phenotypes in the air, with additive effects observed in the *hpr1 hpr2* double mutant and *hpr1 hpr2 hpr3* triple mutant (Timm *et al.*, 2008, 2011). Under high light conditions, *hpr1* exhibits stronger phenotypes, including a

decrease in PSII efficiency, an increase in NPQ, CEF activation, H₂O₂ accumulation, and diminished levels of chlorophyll and anthocyanin (Li *et al.*, 2019a; Wang *et al.*, 2022). Further investigation of *hpr1* in high light found that 2-PG accumulation inhibited the activity of triose phosphate isomerase, an enzyme of the Calvin-Benson cycle that converts glyceraldehyde 3-phosphate to dihydroxyacetone phosphate, resulting in a cytosolic bypass and glucose-6-phosphate (G6P) shunt in the Calvin-Benson cycle (Li *et al.*, 2019b). The G6P shunt consumes ATP, which triggers high rates of CEF to balance energy demand (Li *et al.*, 2019b). Consistent with the activation of the G6P shunt, increased CO₂ release was also observed in *hpr1* (Cousins *et al.*, 2011; Timm *et al.*, 2021). However, there are other possible explanations for this extra CO₂ release, as the non-enzymatic decarboxylation of hydroxypyruvate and serine consumption through serine decarboxylase also seem to occur in *hpr1* (Cousins *et al.*, 2011; Timm *et al.*, 2021). Additionally, HPR1 was found to play a role in maintaining the repair of PSII under HL (Wang *et al.*, 2022).

HPR enzymes have a broad influence on the level of metabolites in the plant. Deficiencies in one or more HPRs increase the levels of most photorespiratory intermediates, including glycolate, glycine, serine, hydroxypyruvate and glycerate, and these metabolic phenotypes are affected by photoperiods (Timm *et al.*, 2008, 2011, 2021). Consistent with the impaired photosynthesis, carbohydrate levels are largely decreased in the *hpr1* mutant (Timm *et al.*, 2021). Levels for other metabolites related to photorespiration, such as intermediates in the tricarboxylic acid cycle and many amino acids, are elevated or reduced in *hpr1* (Timm *et al.*, 2008, 2011, 2021). Interestingly, different from its daytime-dependent accumulation pattern in the wild-type plants, serine was found to be constitutively elevated in the *hpr1* mutant, inhibiting the expression of photorespiratory genes and reducing the level of the corresponding enzymes (Timm *et al.*, 2013). Additionally, the accumulated glycolate can replace the bicarbonate ligand in PSII in *hpr1*, shifting the midpoint potential of the quinone acceptor and reducing ¹O₂ generation (Messant *et al.*, 2018).

HPR1 is closely connected in function with peroxisomal malate dehydrogenase (PMDH). PMDH is a component of the malate valve, a powerful system that transfers reducing equivalents (Selinski & Scheibe, 2019). In photosynthetic tissue, PMDH was believed to provide the NADH required by HPR1 to reduce hydroxypyruvate in the peroxisome (Reumann & Weber, 2006). However, an Arabidopsis mutant lacking both *PMDH* genes showed only a weak decrease in

photosynthesis despite more CO₂ release from photorespiration, indicating that hydroxypyruvate reduction is not totally dependent on PMDH (Cousins *et al.*, 2008). Additionally, it was suggested that in germinating seeds, PMDH oxidizes the NADH produced by β -oxidation, which is opposite to its function in photosynthetic tissue, and HPR1 can partially compensate for this role when PMDH is absent (Pracharoenwattana *et al.*, 2010).

Other than high light, HPR1 also seems to play a positive role in other abiotic stresses. The level of NADH-dependent HPR is elevated in barley during drought stress (Wingler *et al.*, 1999), and the Arabidopsis *hpr1* mutant is more susceptible to drought compared to the wild-type (Li & Hu, 2015). Additionally, defective HPR1 in Arabidopsis leads to decreases in ozone tolerance (Saji *et al.*, 2017).

Taken together, HPRs not only are important enzymes in photorespiration, but also show functions in processes related to photosynthesis, primary metabolism, energetics, and stress response. Mutants of the HPRs are valuable tools to examine the role of photorespiration in various pathways.

1.2.4 Regulation of photorespiration

As photorespiration is tightly linked to primary metabolic pathways and crucial to plant survival under certain environmental conditions, this pathway is expected to be regulated. Although research in this area is still scarce, some regulatory mechanisms of photorespiration are emerging (Timm & Hagemann, 2020; Timm, 2020; Aroca *et al.*, 2023).

Photorespiratory flux is determined by the ratio of CO₂ to O₂. A low CO₂/O₂ ratio around Rubisco favors photorespiration, while high CO₂ or low O₂ concentrations inhibit it (Timm & Bauwe, 2013; Fu *et al.*, 2023). A shift from high to low CO₂ levels alters the level of photorespiratory metabolites, mostly inducing their accumulation (Timm *et al.*, 2012; Eisenhut *et al.*, 2017). Surprisingly, this reduction in CO₂ does not cause obvious changes in the expression of photorespiratory genes (Pérez-Delgado *et al.*, 2013; Eisenhut *et al.*, 2017), suggesting that photorespiratory enzymes may have high capacities to handle variable fluxes (Timm, 2020).

Light seems to regulate photorespiration. Most of the photorespiratory genes are up-regulated by light and during photomorphogenesis, and show diurnal changes in transcript and protein levels (Lutziger & Oliver, 2001; Foyer *et al.*, 2009; Kaur *et al.*, 2013; Timm *et al.*, 2013; Wang *et al.*, 2022). Light-responsive elements were also found in the upstream regions of photorespiratory genes (Aroca *et al.*, 2023). Additionally, light triggers the alternative splicing of

HPR in pumpkin, preferentially producing the cytosolic over the peroxisomal localized isoform (Mano *et al.*, 1999), possibly to reduce the level of the hydroxypyruvate that escapes from peroxisomes.

Photorespiration can also regulate itself. As mentioned above, high levels of serine disrupt the diel fluctuation of photorespiratory gene expression and their protein levels in *Arabidopsis* (Timm *et al.*, 2013). In addition, applying glycine to *Arabidopsis* enhances the accumulation of *GDC* and *SHMT1* transcripts during the day (Timm *et al.*, 2013). Moreover, GDC was suggested to be a key enzyme that controls photorespiratory flux, as overexpressing the H- or L-subunit of GDC decreased the level of photorespiratory intermediates (Timm & Hagemann, 2020).

Besides the above-mentioned light-responsive elements in the promoters and the alternative splicing of *HPR*, more evidence shows that photorespiration genes are regulated by upstream regions and introns. Multiple regulatory elements were found in a nucleosome-depleted region within the *Arabidopsis CAT2* promoter, regulating its transcript abundance (Laxa, 2017). The intron within the 5'UTR of *Arabidopsis GGAT1* was shown to boost gene expression by recruiting RNA polymerase II (Laxa *et al.*, 2016). Interestingly, the expression of the P-protein of GDC in the C4 species *Flaveria trinervia* is tissue-specific and regulated by both the two tandem sub-promoters and alternative splicing (Wiludda *et al.*, 2012). Additionally, bioinformatic analysis predicted that upstream regulatory elements and 5'UTR introns are prevalent in *Arabidopsis* photorespiratory genes (Laxa & Fromm, 2018), suggesting that photorespiration is under active transcriptional and post-transcriptional regulation.

Post-translational modifications (PTMs) also occur in photorespiratory proteins. Phosphorylation plays an important role in maintaining enzyme activity or cofactor binding in GOXs (Jossier *et al.*, 2020), SHMT1 (Liu *et al.*, 2019) and HPR1 (Liu *et al.*, 2020). Thioredoxins in mitochondria can modify the redox status of the GDC L-protein, thereby regulating glycine decarboxylation (Reinholdt *et al.*, 2019; da Fonseca-Pereira *et al.*, 2020). Furthermore, many potential sites for phosphorylation, ubiquitination, acetylation, and redox modifications have been identified in photorespiratory enzymes (Hodges, 2022; Aroca *et al.*, 2023), suggesting the possible involvement of additional PTMs in regulating photorespiration.

In conclusion, photorespiration is clearly regulated through various mechanisms. Current evidence indicates that photorespiration responds to environmental factors such as CO₂, O₂ and

light, receives feedback from its own metabolites and enzymes, and is regulated at transcriptional, post-transcriptional and post-translational levels. These findings highlight the flexibility and importance of photorespiration, underscoring the need for further research in this important area.

1.3 The role of photorespiration in plant immunity*

1.3.1 Plant immune system

In nature, plants are constantly exposed to a dynamic external biotic environment, which drives the development of the plant immune system. As the first layer of immunity, elicitors from pathogenic and nonpathogenic microbes, known as microbe-associated molecular patterns (MAMPs), are recognized by plasma membrane-localized receptors known as pattern recognition receptors (PRRs) to activate pattern-triggered immunity (PTI) (Yu *et al.*, 2017). Flg22, a peptide from the conserved domain of the bacterial flagellin, is one of the MAMPs. PTI also comprises plant responses to plant-derived endogenous elicitors generated in response to wounding or infection, such as small peptides and nucleotides, which are called damage-associated molecular patterns (DAMPs) (Yu *et al.*, 2017). During PTI, intracellular signaling, transcriptional reprogramming, and other physiological responses culminate to limit pathogen growth. These events include increases in cytosolic Ca²⁺ concentration, reactive oxygen species (ROS) burst, and biosynthesis of phytohormones such as salicylic acid (SA) and jasmonate (JA) (Yu *et al.*, 2017). To infect successfully, most pathogens can secrete virulent effectors into plant cells to suppress plant defense (Deslandes & Rivas, 2012). As the second layer of immunity, plants use intracellular nucleotide-binding/leucine-rich-repeat (NLR) receptors to recognize effectors, either directly or indirectly, leading to the activation of effector-triggered immunity (ETI) (Cui *et al.*, 2015). ETI responses are similar to, but stronger than, those of the PTI, and often cause local programmed cell death called the hypersensitive response (HR) (Cui *et al.*, 2015) (**Fig. 1.1**). Recent studies reveal that PTI and ETI are not simply two independent and distinct pathways but work together to regulate immune responses (Ngou *et al.*, 2021; Pruitt *et al.*, 2021; Yuan *et al.*, 2021).

* The majority of this section was published: Jiang, X., Walker, B. J., He, S. Y., & Hu, J. (2023). The role of photorespiration in plant immunity. *Frontiers in Plant Science*, 14(February), 1–8. Only minor modifications were made from the original publication.

The plant immune system appears to take advantage of photorespiration. For example, tightly connected with plant primary metabolism (Shi & Bloom, 2021), photorespiration can provide signals, substrates, or energy for immunity in face of pathogen invasion. In addition, the coupled response of photorespiration to environmental signals like dynamic light intensities (Fu & Walker, 2022) may represent a way for immunity to integrate environmental cues for optimal response.

There have been no unequivocal conclusions so far on how the level of photorespiratory enzymes is regulated in response to pathogen infections. Some studies show that photorespiratory genes are generally suppressed by pathogen infection (Zabala *et al.*, 2015; Giraldo – González *et al.*, 2021; Kalapos *et al.*, 2021; Yue *et al.*, 2021), whereas in other studies certain photorespiratory genes show increased expression (Mitsuya *et al.*, 2009; Ahammed *et al.*, 2018; Silva *et al.*, 2023). At the protein level, both up- and down-regulation of the photorespiratory enzymes in presence of pathogens have been observed (Segarra *et al.*, 2007; Zhao *et al.*, 2013; Ma *et al.*, 2020; He *et al.*, 2021). These discrepancies are likely due to the different plant-pathogen systems used and may indicate the complex nature of the response of various photorespiratory genes to stress at the gene expression and protein levels.

1.3.2 Photorespiratory ROS: important players in immune response

ROS such as H₂O₂ are crucial signaling molecules during plant-pathogen interactions (Camejo *et al.*, 2016). Photorespiration is a major source of H₂O₂ in photosynthetic cells (Foyer *et al.*, 2009), and photorespiratory organelles such as peroxisomes also contain H₂O₂-scavenging systems such as catalases (see below). Not surprisingly, studies of the roles of photorespiration in plant immunity have been mainly focused on H₂O₂ (**Table 1.1**).

GOX (**Fig. 1.1**) contributes to disease resistance through its H₂O₂-producing capability. GOX-silenced tobacco plants show compromised non-host resistance to bacterial pathogens *Pseudomonas syringae* pv. *tomato* (*Pst*) strain T1, *P. syringae* pv. *glycinea* and *Xanthomonas campestris* pv. *vesicatoria*, as well as reduced ETI responses to the effector AvrPto (Rojas *et al.*, 2012). Consistently, *GOX*-deficient *Arabidopsis* mutants show compromised non-host resistance to *P. syringae* pv. *syringae* strain B728A and *P. syringae* pv. *tabaci*, and reduced ETI responses to the effectors AvrB and AvrRps4 (Rojas *et al.*, 2012). Null mutants of HAOX (hydroxy-acid oxidase), the enzyme that belongs to the same L-2-HAOX family as GOX (Esser *et al.*, 2014), exhibit *gox*-like phenotypes in response to pathogens (Rojas *et al.*, 2012). The *Arabidopsis gox*

and *hoax* mutants also have decreased H₂O₂ levels after *P. syringae* pv. *tabaci* infection, which is independent of the H₂O₂-producing enzyme, NADPH oxidase (Rojas & Mysore, 2012; Rojas *et al.*, 2012). In addition, reducing *GOX2* expression in tomato lowers H₂O₂ levels in the leaf and increases plant susceptibility to the compatible pathogen *Pst* DC3000, a phenotype that can be rescued by H₂O₂ pre-treatment (Ahammed *et al.*, 2018). Similarly, decreases in the level of H₂O₂ and increases in *Pst* DC3000 susceptibility were seen after application of isonicotinic acid hydrazide (INH), an inhibitor that blocks the conversion of glycine to serine in photorespiration and suppresses GOX activity (Ahammed *et al.*, 2018). These results suggest that the H₂O₂ produced by GOX family members is important to immunity. However, silencing *GOX1* in rice results in enhanced resistance to the compatible pathogen *X. oryzae* pv. *oryzae* (Chern *et al.*, 2013). Additionally, three members from the tobacco GOX family contribute differently to H₂O₂ levels and defense (Xu *et al.*, 2018b), yet all five members of the Arabidopsis GOX family work additively to increase resistance (Rojas *et al.*, 2012). These inconsistent results regarding the function of different GOX members may be due to distinct plant-pathogen systems utilized and the functional divergence of family members in different plant lineages.

The function of the H₂O₂-scavenging enzyme CAT (**Fig. 1.1**) in immune response has been investigated extensively. Without pathogen infection, CAT-deficient mutants show SA accumulation, induced expression of the SA-pathway marker gene *PR1* (pathogenesis-related 1), cell death, along with H₂O₂ accumulation in tobacco (Takahashi *et al.*, 1997; Chamnongpol *et al.*, 1998; Mittler *et al.*, 1999) and Arabidopsis (Chaouch *et al.*, 2010; Chaouch & Noctor, 2010). In addition, SA was found to bind to CAT and inhibit CAT activity to increase the level of H₂O₂ in a variety of plant species (Chen *et al.*, 1993; Sánchez-Casas & Klessig, 1994). The inhibition of CAT activity by SA analogs correlates with the induction of the *PR1* gene and plant resistance to tobacco mosaic virus (Conrath *et al.*, 1995). Suppression of CAT2 by SA in Arabidopsis also leads to decreases in auxin and JA biosynthesis (Yuan *et al.*, 2017). This is consistent with the increased biotroph resistance that is dependent on SA and repressed by auxin, and decreased JA-dependent necrotroph resistance in the *cat2* mutant (Yuan *et al.*, 2017). This data supports the role of CAT2 as a mediator between SA and auxin/JA signaling pathways in response to different pathogens. CAT2 also seems to connect Ca²⁺ signaling to the JA pathway, as the calmodulin-binding protein IQM1 (IQ-Motif Containing Protein 1) positively regulates JA biosynthesis by enhancing CAT2 function at both the transcription and enzymatic activity levels (Lv *et al.*,

2019). The transcription factor GBF1 (G-box binding factor 1) downregulates *CAT2* expression during pathogen response, leading to high H₂O₂ levels (Giri *et al.*, 2017), reinforcing the view that photorespiratory H₂O₂, whose level is modulated by CATs, may act as a hub in coordinating defense responses.

Moreover, pathogens often target CAT to help with infection, which also suggests the importance of photorespiratory H₂O₂ in immunity. Effectors from the bacterial pathogen *Ralstonia solanacearum* (Sun *et al.*, 2017) and the root-knot nematode *Meloidogyne incognita* (Zhao *et al.*, 2021) inhibit CAT activity via physical interaction with the enzyme, and the 2b protein from the *Cucumber mosaic virus* induces CAT3 degradation in *Arabidopsis* (Murota *et al.*, 2017). However, some pathogens seem to regulate the level of CAT positively. For example, the *Pepino mosaic virus* utilizes Triple Gene Block Protein 1 (TGBp1) to promote the activity of CAT1 and reduce H₂O₂ levels in tomato (Mathioudakis *et al.*, 2013). Interestingly, the oomycete pathogen *Phytophthora sojae* has two effectors that interact with CATs and regulate H₂O₂ homeostasis in opposite directions (Zhang *et al.*, 2015).

Evidence suggesting that CAT and GOX act together to regulate H₂O₂ homeostasis in defense has been reported. Under sub-ambient CO₂ conditions, enhanced resistance to the biotrophic oomycete *Hyaloperonospora arabidopsidis* and high intracellular ROS content were observed in *Arabidopsis* (Williams *et al.*, 2018). This resistant phenotype is abolished in the *gox1* or *haox1* mutants under the same low CO₂ conditions after pathogen inoculation, and the *CAT2* gene is down-regulated by infection (Williams *et al.*, 2018), suggesting that both boosted GOX and suppressed CAT contribute to ROS accumulation. More direct evidence comes from rice, where SA treatment disrupts the physical interaction between GOX and CAT and induces H₂O₂ accumulation (Zhang *et al.*, 2016). These results suggest that H₂O₂ homeostasis during plant-pathogen interaction is possibly regulated by the association and disassociation of GOX and CAT.

Besides peroxisomal H₂O₂, mitochondrial ROS can be influenced by photorespiration and are involved in defense as well. The P-protein and H-protein of GDC, the mitochondrial multienzyme complex that catalyzes glycine decarboxylation (**Fig. 1.1**), are repressed in activity by the victorin toxin produced by the fungus *Cochliobolus victoriae* (Navarre and Wolpert, 1995). Victorin treatment triggers mitochondrial ROS burst and subsequent apoptotic response in oat, a similar result to that caused by the GDC inhibitor aminoacetonitrile (AAN) (Yao *et al.*,

2002). In addition, silencing *GDC-T* or *GDC-P* in tobacco suppresses victorin-triggered cell death and ETI response to the effector AvrPto (Gilbert & Wolpert, 2013). Furthermore, the bacterial elicitor harpin also inhibits GDC activity in Arabidopsis, resembling the inhibition by AAN treatment (Cristina Palmieri *et al.*, 2010). Therefore, it is likely that GDC plays a role in reducing the level of ROS during plant-pathogen interaction to avoid damages caused by excess ROS. Moreover, the degradation of SHMT1, the enzyme that synthesizes serine in mitochondrion (**Fig. 1.1**), can induce mitochondrial ROS accumulation and other defense responses in tobacco and rice plants, conferring broad-spectrum resistance to the rice stripe virus, the rice blast fungus *Magnaporthe oryzae*, and the bacterial leaf blight pathogen *X. oryzae* pv. *oryzae* (Fu *et al.*, 2022).

The peroxisomal aminotransferase GGAT, which converts glyoxylate to glycine (**Fig. 1.1**), is also connected with H₂O₂. Compared to wild-type plants, the Arabidopsis *ggat1* mutant is more resistant to the necrotrophic fungal pathogen *Botrytis cinerea* and contains lower H₂O₂ concentrations upon infection, whereas a higher H₂O₂ level is observed when the plants are uninfected (González-lópez *et al.*, 2021). How GGAT regulates H₂O₂ and whether this change in H₂O₂ levels imposes significant impacts on immune responses remains unknown.

The impact of photorespiration on ROS levels may differ among the three photorespiratory organelles during plant-pathogen interactions. In the chloroplast, photorespiration may actually prevent ROS production during plant immune response. As the major source of chloroplastic ROS, the photosynthetic electron transport chain produces excessive reducing equivalents and ATP under stress conditions (Voss *et al.*, 2013). Therefore, photorespiration may function as an alternative sink for these reducing equivalents and ATP to decrease ROS accumulation in the chloroplast and protect photosystems from photodamage (Voss *et al.*, 2013). Meanwhile, it is likely that the high photorespiratory rate under stress conditions enhances H₂O₂ production in the peroxisome, and increases NADH production by GDC in mitochondria to increase the level of mitochondrial ROS. Nonetheless, these hypotheses remain to be tested under pathogen defense conditions.

In conclusion, extensive evidence has demonstrated the key roles of ROS in plant immune response. The level of H₂O₂ is impacted by photorespiratory enzymes such as GOXs and CATs in peroxisomes and GDC in mitochondria, and potentially other photorespiratory proteins as well.

1.3.3 Involvement of photorespiratory metabolites in immunity

Photorespiration involves a variety of metabolites connected to several primary metabolic pathways, including photosynthesis, C1 metabolism, amino acid metabolism, and nitrogen and sulfate assimilation (Shi & Bloom, 2021). Metabolite analysis of Arabidopsis suspension cultured cells in which immunity was activated by *Pst* DC3000, mutant *Pst* DC3000 (D28E), or *flg22*, revealed large-scale metabolic changes, including the glyoxylate and dicarboxylate metabolism and the amino acid metabolism that partially overlap with the photorespiratory pathway (Misra *et al.*, 2016). In cucumber, nitrate-induced resistance to the fungus *Fusarium oxysporum* f. sp. *cucumerinum* (FOC), along with the accumulation of most of the photorespiratory intermediates except serine, was observed (Sun *et al.*, 2021). As discussed below, specific photorespiratory metabolites have also been shown to be involved in plant-pathogen interactions (**Table 1.1**).

Catalyzing the bidirectional conversion of serine and THF to glycine and 5,10-methylene-THF, the photorespiratory enzyme SHMT (**Fig. 1.1**) is also a crucial enzyme in C1 metabolism (Hanson & Roje, 2001). GmSHMT08c, which encodes a cytosolic SHMT in soybean, was identified to be a resistant gene to the soybean cyst nematode (*Heterodera glycines*, SCN) (Liu *et al.*, 2012; Kandoth *et al.*, 2017). The resistance is resulted from two amino acid substitutions in the GmSHMT08c protein that impede THF binding and reduce catalytic activity of the enzyme (Liu *et al.*, 2012; Korasick *et al.*, 2020). GmSHMT08c confers SCN-resistance in soybean roots (Liu *et al.*, 2012), so it is less likely that photorespiration is involved in this resistance. Other members of the GmSHMT family do not seem to function in SCN resistance individually (Lakhssassi *et al.*, 2019). However, considering the probable functional redundancy of the five mitochondrial GmSHMT members, folate metabolism is a possible point at which photorespiration affects plant immunity. Moreover, the Arabidopsis *shmt1* mutant exhibits compromised defense responses to both biotrophic and necrotrophic pathogens (Moreno *et al.*, 2005). Silencing tomato *SHMT1* dampens resistance to *P. syringae* independent of H₂O₂, whereas overexpressing the gene enhances the resistance (Ahammed *et al.*, 2018). Further, Arabidopsis SHMT4 binds to SA (Manohar *et al.*, 2015), and rice SHMT1 interacts with the disease-resistance protein RPM1 (Wang *et al.*, 2021), although their roles in immunity in these contexts have not been shown. Taken together, SHMT plays a role in defense response in several plant species. Except for the potential connection to folate metabolism in

soybean, and the mitochondrial ROS triggered by SHMT1 degradation in tobacco and rice, the underlying mechanisms of the SHMTs in immunity are still unknown in most species.

The peroxisomal HPR enzyme that converts hydroxypyruvate to glycerate (**Fig. 1.1**) engages in immunity through photorespiratory metabolites. A soybean HPR interacts with P34, the receptor of the *P. syringae* elicitor syringolide, and applying glycerate and 3-PGA, products of the HPR-catalyzed reaction and the downstream step, respectively, restrains syringolide-triggered HR (Okinaka *et al.*, 2002). Additionally, the cytosolic Arabidopsis HPR2 protein binds to SA, but evidence for its role in immunity is lacking (Manohar *et al.*, 2015).

The role of photorespiration-associated amino acids in plant immunity has been illustrated in several studies. In rice, 18 different amino acids, among which glutamate, glycine and serine are photorespiratory intermediates (**Fig. 1.1**), can induce systemic resistance against rice blast when individually applied to roots (Kadotani *et al.*, 2016). Soaking tomato fruits in glutamate solution reduces colonization of the fungal pathogen *Alternaria alternata* and activates several primary metabolic pathways such as nitrogen metabolism, the γ -aminobutyric acid (GABA) shunt, and SA signaling (Yang *et al.*, 2017). Consistently, glutamate can serve as a DAMP to induce Ca^{2+} signaling and thereafter defense responses in plants (Toyota *et al.*, 2018).

Taken together, current data provide evidence for the influence of photorespiratory metabolites on plant defense response. Further and in-depth studies are needed to elucidate the underlying mechanisms.

1.3.4 Influence of photorespiration on the biosynthesis of defense hormones

SA and JA are the two major phytohormones in plant defense (Pieterse *et al.*, 2012). SA is synthesized in plastids and in the cytosol (Lefevre *et al.*, 2020), and the biosynthesis and activation of JA involve plastids, peroxisomes and the cytosol (Wasternack & Song, 2017). Recently, CAT2-promoted JA biosynthesis in Arabidopsis was shown to be achieved by the direct interaction between the N-terminus of CAT2 and the JA biosynthetic enzymes acyl-CoA oxidase 2 (ACX2) and ACX3, without the requirement of H_2O_2 (Zhang *et al.*, 2021). Another study demonstrated that the JA-activated defense to the necrotrophic pathogen *Erwinia amylovora* is partially dependent on GOX2 and does not involve obvious changes in the level of H_2O_2 (Launay *et al.*, 2022), indicating that other mechanisms independent of H_2O_2 may exist in this immune response. Given the overlap of the locations for photorespiration and defense hormone biosynthesis in several subcellular compartments, it is possible that one or multiple

photorespiratory enzymes or metabolites serve as mediators or signals in the biosynthesis of SA and JA. Although evidence for the connection between photorespiration and defense hormone biosynthesis is still scarce, it is a promising research direction that merits further investigations.

1.3.5 Other photorespiratory components involved in defense

A few other photorespiratory enzymes are also involved in immunity, yet the mechanisms behind are inconclusive (**Table 1.1**).

In a *Pseudoperonospora cubensis*-resistant melon cultivar, genes encoding two aminotransferases - homologs of the Arabidopsis peroxisomal aminotransferase SGAT, which converts glyoxylate to glycine and serine to hydroxypyruvate (**Fig. 1.1**), were found among the resistance genes (Taler *et al.*, 2004). Overexpressing either gene confers resistance to the pathogen in the susceptible cultivar (Benjamin *et al.*, 2009). That the resistant melon cultivar also exhibits high GOX activities indicates that this SGAT-regulated resistance may be attributed to high H₂O₂ levels (Taler *et al.*, 2004). However, the positive role of SGAT in plant resistance to *P. syringae* in tomato was shown to be independent of H₂O₂ (Ahammed *et al.*, 2018). Additionally, Arabidopsis SGAT was identified as an SA-binding protein, with unknown consequences in defense (Manohar *et al.*, 2015). Further studies are needed to dissect the precise mechanism of the role of SGAT in immunity.

The chloroplast photorespiratory kinase GLYK, which phosphorylates glycerate to make 3-PGA (**Fig. 1.1**), appears to play a positive role in immunity at multiple levels. Full-length GLYK in potato is a target for the Irish potato famine pathogen *Phytophthora infestans* effector protein AVRvnt1 through protein binding, resulting in the impediment of GLYK trafficking into chloroplasts and enhancement of GLYK degradation, as well as the activation of the ETI response mediated by Rpi-vnt1.1, the NLR that recognizes AVRvnt1 (Gao *et al.*, 2020). *GLYK* silencing results in increased plant susceptibility to *P. infestans* lacking AVRvnt1 via an unknown mechanism (Gao *et al.*, 2020). Interestingly, the full-length GLYK protein is mainly produced under light (Gao *et al.*, 2020), when photorespiration operates, indicating that the function of GLYK in immunity likely depends on photorespiration.

1.3.6 Measurement of photorespiration rate in defense response

Measuring physiological parameters of photorespiration in plants after pathogen infection provides new perspectives in dissecting the relationship between photorespiration and defense. Photorespiration rate, which can be estimated by the difference of net CO₂ assimilation rate

between 2% and 21% O₂, is increased upon *Pst* DC3000 infection, whereas INH, the inhibitor that blocks the conversion of glycine to serine in photorespiration and suppresses GOX activity, suppresses this increase (Ahmed *et al.*, 2018). Other indicators of photorespiration rate used in the measurements include the photorespiratory CO₂ compensation point (Γ^*) and the ratio of glycine to serine (Gly/Ser). FOC-inoculated banana seedlings contain higher Γ^* than untreated plants (Dong *et al.*, 2016). In nitrate-induced FOC resistance cucumber plants, both Γ^* and Gly/Ser are increased (Sun *et al.*, 2021). Further studies are needed to determine whether the increased photorespiration rate reported in these studies contributes to defense responses. This quantitative approach may also be extended to additional studies aimed at dissecting the interplay between photorespiration and immunity.

1.4 Summary

Plants employ multiple layers of mechanisms, including photorespiration, to respond to high light conditions. Photorespiration has been shown to support photosynthetic performance, especially under stress conditions like high light. Research on the photorespiratory enzyme HPR further supports the impacts of photorespiration on photosynthesis, primary metabolism, energetics, and stress response. Emerging evidence for the regulation of photorespiration signifies the flexibility of this pathway and its role in plant response to the dynamic environment. Plants also use the immune system to protect themselves against pathogens. Studies demonstrate the key role of photorespiration in plant immunity through changes in ROS homeostasis, while other mechanisms such as the participation of photorespiratory metabolites, the direct impact of photorespiration on defense hormone biosynthesis, and so on, are also emerging. A more precise understanding of the contribution of photorespiration to plant physiology and plant interaction with the environment is vital for developing crops with both high yield and stress resilience.

Figures

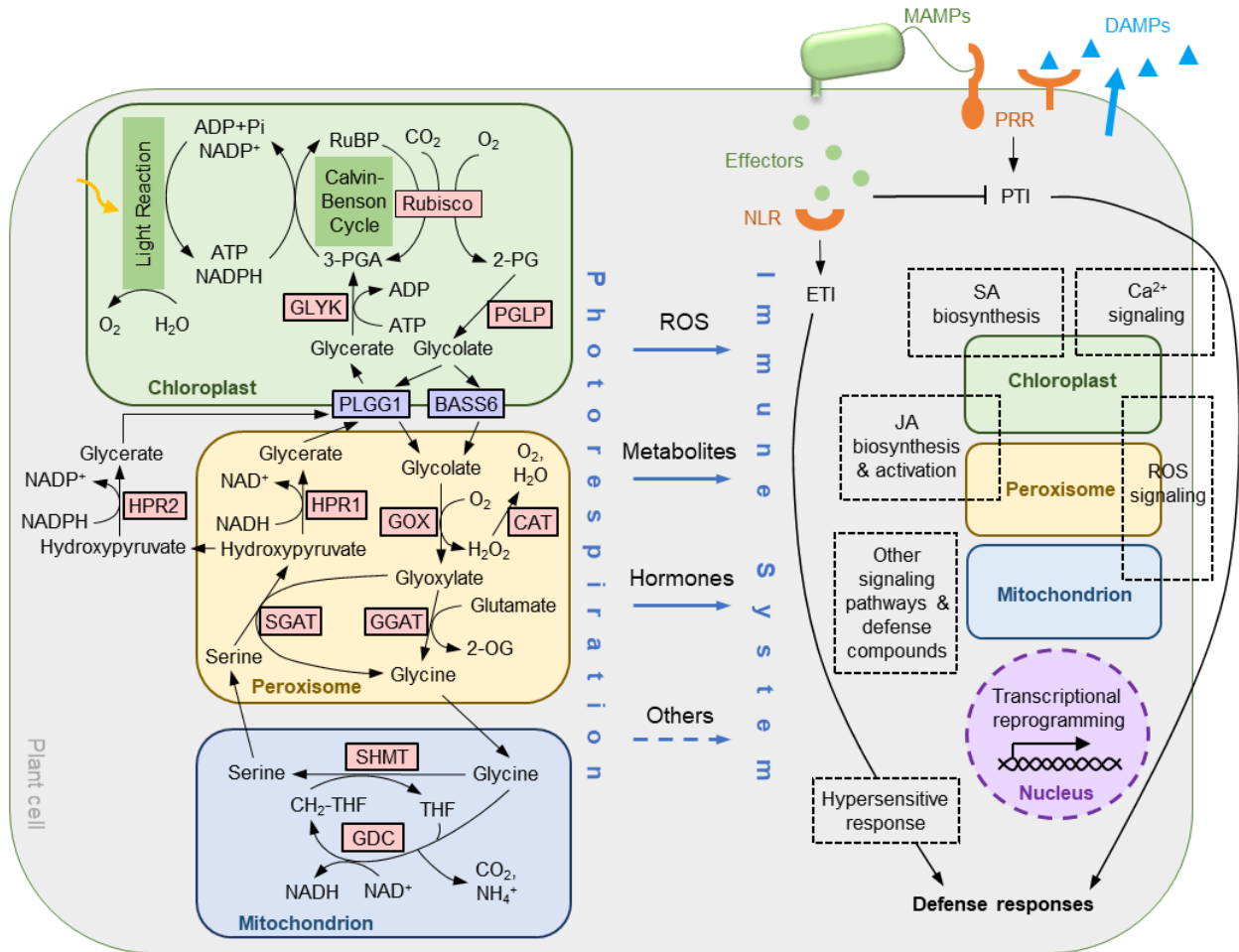


Figure 1.1. The known photorespiratory pathway and a working model for the connections between photorespiration and plant immunity. ROS, photorespiratory metabolites, defense hormones, and possibly other mechanisms connect the photorespiratory pathway to key components of the immune network. See main text for detailed information of the photorespiratory pathway and plant immune response pathways, as well as mechanisms/potential mechanisms for their connections. Overlaps between some subcomponents of the immune response network and the photorespiratory organelles indicate the involvement of the particular organelles. Abbreviations: 2-OG, 2-oxoglutarate; 2-PG, 2-phosphoglycolate; 3-PGA, 3-phosphoglycerate; BASS6, bile acid sodium symporter 6; CAT, catalase; GGAT, glutamate:glyoxylate aminotransferase; GDC, glycine decarboxylase complex; GLYK, glycerate kinase; GOX, glycolate oxidase; HPR, hydroxypyruvate reductase; PGLP, 2-PG phosphatase; PLGG1, plastidial glycolate/glycerate transporter 1; Rubisco, RuBP carboxylase/oxygenase; RuBP, ribulose-1,5-bisphosphate; SGAT, serine:glyoxylate aminotransferase; SHMT, serine hydroxymethyltransferase; THF, tetrahydrofolate; MAMP, microbe-associated molecular pattern; DAMP, damage-associated molecular pattern; PRR, pattern recognition receptor; NLR, nucleotide-binding/leucine-rich-repeat receptor; PTI, pattern-triggered immunity; ETI, effector-triggered immunity; ROS, reactive oxygen species; SA, salicylic acid; JA, jasmonate.

Tables

Table 1.1. Photorespiratory enzymes that participate in defense response.

Enzyme	Full name	Function in immunity	References
GOX	Glycolate oxidase	Impacts ROS homeostasis and JA biosynthesis	(Rojas & Mysore, 2012; Rojas <i>et al.</i> , 2012; Chern <i>et al.</i> , 2013; Zhang <i>et al.</i> , 2016; Ahammed <i>et al.</i> , 2018; Williams <i>et al.</i> , 2018; Xu <i>et al.</i> , 2018b; Launay <i>et al.</i> , 2022)
CAT	Catalase	Impacts ROS homeostasis; suppressed by SA; promotes JA biosynthesis and mediates crosstalk between SA and JA/auxin, and between Ca ²⁺ and JA (<i>AtCAT2</i>)	(Chen <i>et al.</i> , 1993; Sánchez-Casas & Klessig, 1994; Conrath <i>et al.</i> , 1995; Takahashi <i>et al.</i> , 1997; Chamnongpol <i>et al.</i> , 1998; Mittler <i>et al.</i> , 1999; Chaouch <i>et al.</i> , 2010; Chaouch & Noctor, 2010; Mathioudakis <i>et al.</i> , 2013; Zhang <i>et al.</i> , 2015, 2016, 2021; Giri <i>et al.</i> , 2017; Murota <i>et al.</i> , 2017; Sun <i>et al.</i> , 2017; Yuan <i>et al.</i> , 2017; Williams <i>et al.</i> , 2018; Lv <i>et al.</i> , 2019; Zhao <i>et al.</i> , 2021)
GGAT	Glutamate: glyoxylate aminotransferase	Connects with H ₂ O ₂	(González-lópez <i>et al.</i> , 2021)
SGAT	Serine:glyoxylate aminotransferase	Positive role in resistance in melon and tomato; bound by SA (<i>AtSGAT</i>)	(Taler <i>et al.</i> , 2004; Benjamin <i>et al.</i> , 2009; Manohar <i>et al.</i> , 2015; Ahammed <i>et al.</i> , 2018)
GDC	Glycine decarboxylase complex	Impacts ROS homeostasis	(Navarre & Wolpert, 1995; Yao <i>et al.</i> , 2002; Cristina Palmieri <i>et al.</i> , 2010; Gilbert & Wolpert, 2013)
SHMT	Serine hydroxymethyl-transferase	Impacts ROS homeostasis; contributes to resistance possibly through folate metabolism; bound by SA (<i>AtSHMT4</i>); interacts with the disease-resistance protein RPM1 (<i>OsSHMT1</i>)	(Moreno <i>et al.</i> , 2005; Liu <i>et al.</i> , 2012; Manohar <i>et al.</i> , 2015; Kandoth <i>et al.</i> , 2017; Ahammed <i>et al.</i> , 2018; Lakhssassi <i>et al.</i> , 2019; Korasick <i>et al.</i> , 2020; Wang <i>et al.</i> , 2021; Fu <i>et al.</i> , 2022)
HPR	Hydroxypyruvate reductase	Interacts with syringolide receptor (<i>GmHPR</i>); bound by SA (<i>AtHPR2</i>)	(Okinaka <i>et al.</i> , 2002; Manohar <i>et al.</i> , 2015)
GLYK	Glycerate kinase	Positive role in resistance in potato	(Gao <i>et al.</i> , 2020)

CHAPTER 2*. A photorespiratory glyoxylate shunt in the cytosol supports photosynthesis and plant growth under high light conditions in *Arabidopsis*

2.1 Introduction

Light is an essential energy source and a critical environmental cue for plants, but its intensity often fluctuates beyond the ranges optimal for plant growth. For example, plants frequently experience high light conditions that exceed $2000 \mu\text{mol m}^{-2} \text{s}^{-1}$ on sunny days, posing significant stress to plants in the field (Ort, 2001; Mishra *et al.*, 2012). When light intensities surpass the photosynthetic capacity, generation of reactive oxygen species (ROS) from the photosynthetic apparatus is enhanced, which can cause photodamage to protein complexes and subsequently inactivate the electron transport chain (Krieger-Liszkay & Shimakawa, 2022; Sharma *et al.*, 2023). To cope with this stress, plants have developed strategies to respond at various levels, such as the antioxidant system to scavenge ROS, dissipation of excessive energy as non-photochemical quenching (NPQ), cyclic electron flow (CEF) to balance ATP/NADPH production, transcriptional reprogramming, chloroplast and leaf movement, and anthocyanin accumulation (Szymańska *et al.*, 2017; Shi *et al.*, 2022a).

Photorespiration, a metabolic process closely related to photosynthesis, is initiated after the oxygenation of ribulose 1,5-bisphosphate (RuBP) by the photosynthetic enzyme ribulose 1,5-bisphosphate carboxylase-oxygenase (rubisco) (Eisenhut *et al.*, 2019). Through a series of reactions residing sequentially in the chloroplast, peroxisome, mitochondrion, and the cytosol, the oxygenation product 2-phosphoglycolate (2-PG), which inhibits cell functions, is eventually converted to 3-phosphoglycerate (3-PGA) to be recycled back to the Calvin-Benson cycle in the chloroplast (Eisenhut *et al.*, 2019) (**Fig. 2.1**).

Although photorespiration is often considered a sub-optimal process because it consumes energy and releases pre-fixed carbon as CO_2 , a properly functional photorespiratory pathway supports photosynthetic performance, especially under stress conditions. In ambient air and under regular growth conditions, many photorespiratory mutants exhibit compromised photosynthesis and growth, phenotypes that are largely recovered (Timm & Bauwe, 2013; Timm *et al.*, 2016) under high CO_2 environments where rubisco oxygenation is inhibited (Timm & Bauwe, 2013; Timm *et al.*, 2016). Although the exact reasons for these air-grown phenotypes are

* This chapter has been submitted for publication. All the experiments were conducted by myself, except for the *GLYR1* localization study, which was performed by Dr. Amanda Koenig and Joy Li.

unclear, the accumulated photorespiratory intermediates in these mutants, such as 2-PG, glyoxylate, and glycerate, can inhibit the activities of photosynthesis-related enzymes (Timm *et al.*, 2016). Additionally, several *Arabidopsis* photorespiratory mutants, including *hydroxypyruvate reductase 1 (hpr1)*, *plastidial glycolate/glycerate transporter 1 (plgg1)*, *catalase 2 (cat2)* and *glycolate oxidase 1 (gox1)*, have much more severe photosynthetic phenotypes under high and dynamic light compared with low and constant light conditions, supporting the increased importance of a properly functional photorespiratory pathway under high light (Li *et al.*, 2019a). Under stress, photorespiration is believed to function as an alternative electron sink that consumes excessive energy produced by the photosynthetic light reactions (Wingler *et al.*, 2000; Ort & Baker, 2002; Voss *et al.*, 2013; Huang *et al.*, 2019a), although a recent work challenged the idea that photorespiration's role as an alternative electron sink is photoprotective (Smith *et al.*, 2023).

As a core enzyme in photorespiration, HPR catalyzes the reduction of hydroxypyruvate to produce glycerate (**Fig. 2.1**). In *Arabidopsis*, three HPR family members have been shown to function in photorespiration (Timm *et al.*, 2008, 2011). Peroxisomal HPR1 plays a major role in reducing hydroxypyruvate with NADH as the co-factor, whereas HPR2 and HPR3 in the cytosol have low activities and higher affinities for NADPH (Timm *et al.*, 2008, 2011; Xu *et al.*, 2018a; Wang *et al.*, 2022). HPR enzymes play an important role in photosynthesis, because the knockout mutant of *HPR1* shows compromised photosynthetic performance and growth in the air, with additive effects observed in *hpr1 hpr2* double mutant and *hpr1 hpr2 hpr3* triple mutant (Timm *et al.*, 2008, 2011). Under high light, *hpr1* exhibits stronger phenotypes, including decreases in the efficiency of photosystem II (PSII), increases in NPQ, activation of CEF, accumulation of H₂O₂, and a marked reduction in chlorophyll and anthocyanin (Li *et al.*, 2019a; Wang *et al.*, 2022). Further investigation of *hpr1* under high light found that 2-PG accumulation inhibited the activity of triose phosphate isomerase, an enzyme of the Calvin-Benson cycle that converts glyceraldehyde 3-phosphate to dihydroxyacetone phosphate. This inhibition results in a cytosolic bypass and glucose-6-phosphate (G6P) shunt in the Calvin-Benson cycle where the G6P shunt consumes ATP, triggering high rates of CEF to balance energy demand (Li *et al.*, 2019b). Consistent with the activation of the G6P shunt, increased CO₂ release was also observed in *hpr1* (Cousins *et al.*, 2011; Timm *et al.*, 2021). However, there are other possible explanations for this extra CO₂ release, as the non-enzymatic decarboxylation of

hydroxypyruvate and serine consumption through serine decarboxylase also seem to occur in *hpr1* (Cousins *et al.*, 2011; Timm *et al.*, 2021). Finally, HPR1 was found to maintain the repair of PSII under high light (Wang *et al.*, 2022).

HPR enzymes have a broad influence on the level of metabolites in the plant. Deficiency in one or more HPRs increases the level of most photorespiratory intermediates, including glycolate, glycine, serine, hydroxypyruvate and glycerate, and these metabolic phenotypes are affected by photoperiods (Timm *et al.*, 2008, 2011, 2021). Consistent with the impaired photosynthesis, carbohydrate levels are largely decreased in the *hpr1* mutant (Timm *et al.*, 2021). Levels for other metabolites related to photorespiration, such as intermediates in the tricarboxylic acid cycle and many amino acids, are elevated or reduced in *hpr1* (Timm *et al.*, 2008, 2011, 2021). Interestingly, different from its daytime-dependent accumulation pattern in the wild-type plants, serine was found to be constitutively elevated in the *hpr1* mutant, inhibiting the expression of photorespiratory genes and reducing the level of the corresponding enzymes (Timm *et al.*, 2013). Additionally, the accumulated glycolate can replace the bicarbonate ligand in PSII in *hpr1*, shifting the midpoint potential of the quinone acceptor and reducing the generation of single oxygen (Messant *et al.*, 2018).

While the main flux of photorespiration is well known, there are examples of alternative fluxes, such as the aforementioned cytosolic HPR2 and HPR3 enzymes that are partially redundant in function with HPR1. Understanding other routes of carbon flux associated with photorespiration is important to fully deciphering this metabolic network. In addition, photorespiration is tightly linked to primary metabolic pathways and crucial to plant survival under certain environmental conditions, thus this pathway is expected to be regulated. Although research in this area is still scarce, current evidence indicates that photorespiration responds to environmental factors such as CO₂, O₂ and light, receives feedback from its own metabolites and enzymes, and is regulated at transcriptional, post-transcriptional and post-translational levels (Timm & Hagemann, 2020; Timm, 2020; Aroca *et al.*, 2023). Taken together, mechanistic research into the flexibility and regulation of photorespiration will be highly valuable to completely elucidating the role of this pathway in plant physiology and plant interaction with the environment.

In this work, we investigated the regulation and flexibility of photorespiration by characterizing a genetic suppressor of the Arabidopsis *hpr1* mutant under high light, mapping the

underlying gene, and conducting follow-up genetic and metabolic flux analyses. We found that defective glyoxylate reductase 1 (GLYR1), a cytosolic enzyme that catalyzes the conversion of glyoxylate to glycolate, can rescue the mutant phenotypes of *hpr1* in plant growth, photosynthesis and levels of photorespiratory metabolites under high light conditions. Further examination showed that loss of function of *GLYR1* can also partially suppress the phenotype of *cat2*, but not *plgg1*. Combining transitional metabolic profiling, glyoxylate feeding, and genetic analyses, we provided evidence for a cytosolic photorespiratory shunt that converts accumulated glyoxylate to hydroxypyruvate, which can act, at least partially, through the cytosolic HPR2 enzyme to enhance carbon recycling. This cytosolic shunt seems to be especially critical under high light intensities when a high rate of photorespiratory flux is required to deal with increased rates of total rubisco oxygenation reaction and in the absence of a functional major photorespiratory pathway. Our findings suggest that the metabolic flexibility of photorespiration can help plants adjust to stress conditions, thus may provide help with future efforts in improving plant performance under high light conditions.

2.2 Results

2.2.1 Loss of function of glyoxylate reductase 1 (GLYR1) partially rescues the growth and metabolic phenotypes of the *hpr1* mutant

To identify proteins with a regulatory or modulatory role in photorespiration, we performed EMS mutagenesis on *Arabidopsis hpr1-1* mutant seeds and screened for genetic suppressors based on their growth and photosynthetic phenotypes under high light conditions ($\sim 700 \mu\text{mol m}^{-2} \text{s}^{-1}$). One suppressor, *shpr7* (*hpr1* suppressor number 7), was found to partially suppress the small rosette size of *hpr1-1* under high light relative to normal light conditions ($100 \mu\text{mol m}^{-2} \text{s}^{-1}$) (**Fig. 2.2a and b**).

To characterize and map the causal mutation in *shpr7*, we backcrossed *shpr7* to *hpr1-1*. The segregation ratio of *hpr1*-like vs. suppressor-like plants in the BC₁F₂ generation was 3:1, suggesting that the suppression is caused by a recessive mutation. To map the gene responsible for the suppression, genomic DNA extracted from 80 suppressor-like individuals in the BC₃F₂ generation was pooled for whole genome sequencing. We identified a point mutation in the exon of the *Glyoxylate Reductase 1 (GLYR1)* gene, which encodes an NADPH-dependent glyoxylate/succinic semialdehyde reductase (Hoover *et al.*, 2007; Zarei *et al.*, 2017), causing a glutamate (E)-to-lysine (K) substitution at amino acid 117 (**Fig. 2.2c**). RT-PCR analysis detected

similar levels of the *GLYR1* transcripts in *shpr7* and the wild-type (**Fig. A1a**), suggesting that this mutation does not lead to obvious changes in gene expression. To determine the effect of the E117K mutation at the protein level, peptide antibodies against amino acid 229-243 were generated, which detected an apparently decreased level of the GLYR1 protein (30.7kDa) in high light-grown *shpr7* (**Fig. 2.2d**), indicating that this point mutation may cause the protein to be less stable. The antigen peptide is from a highly identical region between AtGLYR1 and its homolog, AtGLYR2, where the two proteins differ only by one amino acid (Simpson *et al.*, 2008). We therefore reasoned that the weak signal in *glyr1-1* in the immunoblot might be derived from the mature form of GLYR2, after its N-terminal transit peptide for chloroplast and mitochondrial dual targeting is removed upon import into the organelles (**Fig. 2.2d**).

To confirm that loss-of-function mutations in *GLYR1* can lead to the suppression of *hpr1-1* like that shown in *shpr7*, we obtained three independent T-DNA insertion mutant lines of *GLYR1* (**Fig. 2.2c**). All three lines lacked detectable full-length *GLYR1* transcript (**Fig. A1b**) and showed comparable growth and morphologies to the wild-type (Col-0) plants (**Fig. A1c**). Double mutants generated by crossing these lines individually with *hpr1-1* all exhibited very similar phenotypes as *shpr7* (**Fig. 2.2a and b, Fig. A1c**), confirming that loss of function of GLYR1 can partially rescue the *hpr1-1* mutant phenotypes. Overexpressing the *GLYR1* gene (*35S::GLYR1*) in *shpr7* reverted its rosette size back to *hpr1*-like under high light (**Fig. 2.2e, Fig. A1d**), further confirming *GLYR1* as the causal gene for the suppression of *hpr1*. Since the three T-DNA mutants were indistinguishable from each other in their capability to suppress *hpr1-1*, we selected the *glyr1-1* allele for follow-up experiments.

GLYR1 was shown to catalyze the conversion of glyoxylate to glycolate, and succinic semialdehyde to γ -hydroxybutyrate (Zarei *et al.*, 2017). Because glyoxylate and glycolate are photorespiratory intermediates, we tested if the deficiency in GLYR1 also causes metabolic changes in the photorespiratory pathway (**Fig. 2.3**). Mutant *hpr1-1* grown under high light conditions had elevated levels of all the 6 photorespiratory metabolites tested, consistent with previous reports that knockout mutant of *HPRI* accumulates photorespiratory intermediates under normal growth conditions (Timm *et al.*, 2008, 2021). The suppressor *shpr7* and the double mutant *glyr1-1 hpr1-1* showed partial rescue of the accumulation of at least 5 of these metabolites, including glycolate, glyoxylate, serine, hydroxypyruvate, and glycerate, and

consistent with its wild-type-like plant appearance, the *glyr1-1* single mutant contained similar levels of these metabolites as Col-0 (**Fig. 2.3**).

Taken together, our results proved that reduced or loss of function of the GLYR1 protein in Arabidopsis can partially suppress the mutant phenotypes of *hpr1* in both plant growth and the content of photorespiratory metabolites.

2.2.2 Defects in GLYR1 also partially rescue the phenotypes of the photorespiratory mutant *cat2*, but not those of *plgg1*

To investigate if the suppression of *hpr1* by *glyr1* is specifically linked to HPR1 or broadly connected to components of the photorespiratory pathway, we crossed *glyr1-1* into two other photorespiratory mutants, *cat2-1* and *plgg1-1* (**Fig. 2.1**). Similar to *hpr1-1*, *cat2-1* and *plgg1-1* are also compromised in growth and photosynthesis under high light (Li *et al.*, 2019a). Interestingly, under high light, the double mutant *glyr1-1 cat2-1* exhibited a bigger rosette size than *cat2-1*, whereas the lack of a functional GLYR1 was unable to improve the growth of *plgg1-1* (**Fig. 2.4a**).

To determine if *glyr1* can also rescue the reduced photosynthetic efficiency in *cat2-1* and *plgg1-1*, as well as *hpr1-1*, we measured quantum efficiency of photosystem II (Φ_{II}), a critical parameter of photosynthesis, in mutant and Col-0 seedlings. A 3-day light regime, with normal light on the first day and light gradients on days 2 and 3, was applied (**Fig. 2.4b**). Consistent with their growth phenotypes, *hpr1-1*, *cat2-1* and *plgg1-1* had lower Φ_{II} values, especially under higher light intensities, whereas *glyr1-1* resembled Col-0 (**Fig. 2.4b**). As expected, GLYR1 deficiency helped to improve the photosynthetic performance of *hpr1-1* and *cat2-1*, but not *plgg1-1* (**Fig. 2.4b**).

2.2.3 GLYR1 localizes to the cytosol

Since the subcellular location of GLYR1 underlies the potential mechanism by which defective GLYR1 suppresses *hpr1* and *cat2* phenotypes, we sought to definitively determine its subcellular localization. While several studies purport GLYR1 localization in the cytosol, these findings did not sufficiently account for the putative peroxisomal targeting signal type 1 (PTS1) tripeptide (SRE>) at GLYR1's extreme C-terminus, which implies its potential localization in peroxisome matrix. Apple (*Malus domestica*) GLYR1 localizes to the cytosol, but *MdGLYR1* lacks the C-terminal putative PTS1 and therefore cannot be used to precisely infer the localization of *AtGLYR1* (Brikis *et al.*, 2017). An *AtGLYR1*-GFP fusion protein transiently

expressed in tobacco localized to the cytosol (Simpson *et al.*, 2008), but again peroxisomal targeting cannot be discounted as the C-terminal PTS1 was blocked in this construct. Indirect evidence of cytosolic localization was shown in pea where the majority of glyoxylate-reducing activity was found in the cytosolic fraction, yet a small amount was detected in the chloroplast (Givan *et al.*, 1988). Moreover, a study using an N-terminal fluorescent tag showed the cytosolic localization of *AtGLYR1* in tobacco BY-2 and Arabidopsis cells (Ching *et al.*, 2012), dispelling its peroxisomal localization. However, the fluorescence signals also appeared in chloroplast-like structures in Arabidopsis mesophyll cells. Because these data did not include chlorophyll fluorescence as a marker, we cannot definitively rule out chloroplast localization of *GLYR1*. Therefore, it was important to obtain evidence in which *AtGLYR1*'s cytosolic localization is unequivocally shown.

To this end, we generated a *35S::eYFP-GLYR1* construct and co-expressed it with the peroxisome marker mScarlet-SRL (Koenig *et al.*, 2023) in tobacco leaves. *GLYR1* appeared diffused throughout the cytosol, and no *GLYR1* signal was observed overlapping peroxisomal or chloroplast (visualized by chlorophyll autofluorescence) signals (**Fig. 2.4c**), confirming that *GLYR1* is solely localized to the cytosol.

2.2.4 Transitional metabolic profiling uncovers a close link between hydroxypyruvate and *GLYR1*

Based on *GLYR1*'s mutant phenotypes, its protein localization, and the previously reported enzyme activity, we hypothesized a photorespiratory glyoxylate shunt in the cytosol. This shunt drives the conversion of glyoxylate to hydroxypyruvate and triggers carbon flux back to the Calvin-Benson cycle, when the primary photorespiratory pathway is deficient and when plants are exposed to high light conditions. Serine was found to accumulate in the *hpr1-1* and *cat2-1* mutants (Timm *et al.*, 2008; Bao *et al.*, 2021), likely increasing the level of free serine in the cytosol. Likewise, we posited that impaired photorespiration in *hpr1-1* and *cat2-1* also causes increased glyoxylate leakage to the cytosol. The lack of a functional *GLYR1* protein leads to an increase in the cytosolic level of glyoxylate, but in plants containing a functional primary photorespiratory pathway, this increase may not reach a level high enough to drive an aminotransferase activity with serine. Only in photorespiratory mutants such as *hpr1* and *cat2*, which already accumulate cytosolic glyoxylate, can *GLYR1* deficiency further increase the level of glyoxylate to a threshold to react with serine, producing hydroxypyruvate and glycine. The

hydroxypyruvate generated from this reaction can then be directly catalyzed by a cytosolic HPR (such as HPR2) to produce glycerate, which returns to the Calvin-Benson cycle in the chloroplast following phosphorylation by glycerate kinase (**Fig. 2.1**). Under this hypothesis, the lack of GLYR1 function can activate a cytosolic pathway in *hpr1-1* and *cat2-1* to recycle photorespiratory carbon more efficiently back to photosynthesis, decreasing the inhibitory effects of photorespiratory intermediates and subsequently improving the performance of these two mutants to compensate for the lack of HPR1 or CAT2. By contrast, loss of PLGG1 blocks the transport of glycerate into chloroplasts, preventing carbon recycling by HPR2 and therefore failing to rescue *plgg1-1*.

To test this hypothesis, we first determined how quickly photorespiratory metabolites respond to high light. The partial rescue of photorespiratory metabolites observed earlier in this study (**Fig. 2.3**) was shown in plants after two weeks of growth under high light. Here we instead employed short-term treatment of photorespiratory conditions to avoid secondary effects from early metabolic events. Plants were grown under high CO₂ (2,000 ppm) and normal light conditions for 3 weeks before transfer to ambient CO₂ and high light conditions. Plant tissue was sampled for metabolite measurements after ~10 h illumination, as photorespiratory intermediates were reported to accumulate to high levels at the end of the day (Pick *et al.*, 2013; Timm *et al.*, 2013).

When growing under high CO₂, *hpr1-1* only had increased serine and slightly decreased glycerate concentrations (**Fig. A2**), consistent with previously reported measurements of the photorespiratory intermediates under 1% (10,000 ppm) CO₂ (Timm *et al.*, 2008). The *cat2-1* mutant performed similarly to Col-0 and importantly, *glyr1-1* did not alter the levels of the photorespiratory metabolites in *hpr1-1* or *cat2-1* (**Fig. A2**), indicating that the influence of *glyr1-1* is well suppressed under high CO₂. After 10 h of ambient CO₂ and high light conditions, the levels of 5 out of the 6 photorespiratory intermediates, including glycolate, glyoxylate, serine, hydroxypyruvate and glycerate, were significantly higher in *hpr1-1* compared to Col-0 (**Fig. 2.5**). In *cat2-1*, glycolate, serine and glycerate were increased, and hydroxypyruvate also had a small but obvious accumulation (**Fig. 2.5, Fig. A3**). Intriguingly, the metabolites best rescued by *glyr1-1* in both *hpr1-1* and *cat2-1* were glycolate and hydroxypyruvate (**Fig. 2.5**). Considering the enzymatic activity of GLYR1 in converting glyoxylate to glycolate, it is expected that *glyr1-1 hpr1-1* and *glyr1-1 cat2-1* have lower levels of glycolate. However, the dramatic rescue of

hydroxypyruvate in *hpr1-1* and *cat2-1* by *glyr1-1* after only a 10-h treatment suggested that hydroxypyruvate is closely related to the function of GLYR1, which supports the cytosolic shunt we proposed. As the growth and photosynthetic phenotypes of *cat2-1* were weaker than *hpr1-1*, hydroxypyruvate accumulation in *cat2-1* was relatively lower and rescued better than *hpr1-1*, with *glyr1 cat2* hydroxypyruvate content returning to wildtype levels at 22% that observed in *cat2* (**Fig. 2.5, Fig. A3**). Glycerate abundance in the mutants showed a similar trend as that of hydroxypyruvate, although the difference between *glyr1-1 hpr1-1* and *hpr1-1* was smaller, which is probably because the response of glycerate requires hydroxypyruvate as the primary responder and is therefore indirect.

In summary, transitional metabolic profile suggests a close connection between hydroxypyruvate and GLYR1 under high light conditions. It supports the role of the proposed cytosolic photorespiratory pathway, in which the accumulated glyoxylate caused by defective GLYR1 in the *hpr1* and *cat2* background is converted to hydroxypyruvate.

2.2.5 Feeding glyoxylate to the plant strongly inhibits growth of wild-type but can benefit *hpr1*

Based on our hypothesis, the availability of glyoxylate in the cytosol plays an important role in activating the non-canonical pathway in *hpr1-1*. To obtain further support for this role, we increased the level of free glyoxylate in the cytosol by directly supplying glyoxylate to the growth medium for *hpr1-1*.

Although the mechanism is still unclear, glyoxylate was reported to inhibit RuBP regeneration and rubisco activation (Mulligan *et al.*, 1983; Cook *et al.*, 1985; Chastain & Ogren, 1989; Campbell & Ogren, 1990; Lu *et al.*, 2014) and therefore is toxic to plants. In agreement with this, Col-0 plants grown in 0.4 mM glyoxylate exhibited strong growth inhibition and decreased fresh weight under normal or high light conditions (**Fig. 2.6**). However, *hpr1-1* maintained similar fresh weight after glyoxylate feeding (**Fig. 2.6b**), despite some suppression in root elongation (**Fig. 2.6a**), indicating that glyoxylate can be metabolized more quickly in *hpr1-1*, possibly through the cytosolic pathway we proposed. The *glyr1-1 hpr1-1* double mutant showed a small growth inhibition upon glyoxylate treatment (**Fig. 2.6**), possibly because the total glyoxylate amount from both internal and external sources exceeds the capacity of this cytosolic pathway. By contrast, 0.1 mM serine had no influence on plant growth in all the lines under normal or high light conditions (**Fig. A4**), indicating that the cytosolic serine in *hpr1-1* is

adequate for the cytosolic shunt we proposed. In summary, results from the glyoxylate feeding experiment showed that increasing glyoxylate availability in the cytosol can benefit *hpr1-1*, thus supporting our hypothesis.

2.2.6 The rescuing effect of *glyr1* in *hpr1* largely depends on HPR2

Our proposed photorespiratory glyoxylate shunt requires the activity of cytosolic HPR, so we investigated the role of HPR2 because it has a stronger role in photorespiration than HPR3 (Timm *et al.*, 2011). Null mutant *hpr2-3* (**Fig. A5**) was used to generate a triple knockout line *glyr1-1 hpr1-1 hpr2-3*. Because mutants defective in both *HPR1* and *HPR2* genes are already stunted, grow poorly in ambient air, and are intolerant to high light treatment, we first grew all the lines under high CO₂ and normal light conditions, during which all mutants showed comparable morphologies as Col-0 (**Fig. 2.7a**, Day 0). After three weeks and at the end of the dark period, plants were moved to ambient CO₂ and high light conditions, where they were kept for 9 days. This treatment led to much smaller rosettes in *hpr1-1* compared to Col-0, which was partially rescued in *glyr1-1 hpr1-1* and the original suppressor *shpr7* (**Fig. 2.7a**). At Day 9, although *hpr1-1 hpr2-3* and *glyr1-1 hpr1-1 hpr2-3* performed poorly compared with other lines, they looked similar to each other, supporting our conclusion that, at least at this time point, *glyr1-1*'s role in helping carbon recycle back to the chloroplast largely depends on a functional HPR2. At Day 18, *glyr1-1 hpr1-1 hpr2-3* became slightly bigger than *hpr1-1 hpr2-3* (**Fig. 2.7a**), indicating that *glyr1-1* may also act through other proteins (such as HPR3) for its role under longer photorespiratory conditions.

Transitional metabolic profiling was also performed on mutants grown under high CO₂ and normal light for 3 weeks followed by 10-h treatment with ambient CO₂ and high light. Similar to the rescued glycolate level in *glyr1-1 hpr1-1*, *glyr1-1 hpr1-1 hpr2-3* also showed a lower glycolate level than *hpr1-1 hpr2-3* (**Fig. 2.7b**), confirming that the glycolate production via GLYR1 is greatly lost. By contrast, the level of hydroxypyruvate was only slightly rescued in *glyr1-1 hpr1-1 hpr2-3* (**Fig. 2.7b**), supporting the importance of HPR2 in this cytosolic shunt.

The cytosolic shunt we proposed indicates an increased flux through HPR2 in *glyr1-1 hpr1-1* and *shpr7* compared to *hpr1-1*, which may require a higher activity of the HPR2 enzyme. To test this possibility, the maximal enzymatic activities of HPR in plants were measured, which showed that *glyr1-1 hpr1-1* and *shpr7* had comparable enzymatic activities of HPR to *hpr1-1* in the transitional (**Fig. A6a**) or stable stage (**Fig. A6b**) of high light treatment, using NADH or

NADPH as the co-factor. However, this assay measures the total maximal enzymatic activities of HPR in protein extract from plants, which is more correlated to the level of the HPR enzymes. Since the enzymes in the plant cell usually do not operate at their maximal capacities, the possible regulation of enzymatic levels to increase fluxes cannot be captured by this assay.

2.3 Discussions

In this study, we provided evidence for a cytosolic glyoxylate shunt of photorespiration that can improve carbon recycling in the absence of enzymes in the major photorespiratory pathway under high light, supporting the metabolic flexibility of the photorespiration network. Under high light, deficiency in GLYR1, a cytosolic enzyme that converts glyoxylate to glycolate, can partially rescue the phenotypes of the photorespiration mutants *hpr1* and *cat2* but not those of the glycolate/glycerate transporter mutant *plgg1*. Further investigations showed that hydroxypyruvate is closely connected to GLYR1's function, and the availability of glyoxylate and HPR2 in the cytosol are important for the suppression of *hpr1*. These results led us to propose a novel cytosolic photorespiratory shunt, which seems to be critical when the major photorespiratory pathway is compromised and when plants are exposed to photorespiratory conditions such as high light. Specifically, a reaction between glyoxylate and serine is catalyzed by an aminotransferase to produce hydroxypyruvate and glycine (**Fig. 2.1**). Via HPR2, cytosolic hydroxypyruvate is subsequently converted to glycerate that eventually returns to the Calvin-Benson cycle, thus reducing the accumulation of the toxic photorespiratory intermediates and enhancing carbon recycling (**Fig. 2.1**). We predict that, in wild-type plants, this shunt may only be activated under extremely high photorespiratory fluxes.

Plants contain two GLYR proteins, the cytosolic GLYR1 and the plastid/mitochondrion-dual localized GLYR2, both of which are believed to be involved in aldehyde detoxification during abiotic stress (Allan *et al.*, 2008; Mekonnen & Ludewig, 2016; Zarei *et al.*, 2017). Although GLYR1 was shown to be more efficient in its glyoxylate reductase activity, it can also convert succinic semialdehyde to γ -hydroxybutyrate in γ -aminobutyrate (GABA) metabolism (Hoover *et al.*, 2007; Zarei *et al.*, 2017). During abiotic stress, the expression of both *GLYR1* and *GLYR2* is upregulated, presumably to detoxify the accumulated succinic semialdehyde in plants (Allan *et al.*, 2008; Mekonnen & Ludewig, 2016; Zarei *et al.*, 2017). However, the positive role of succinic semialdehyde reduction during abiotic stress contradicts the rescuing effect of *glyr1* in *hpr1* under high light, and GABA metabolism is not known to be directly linked to

photorespiration. Therefore, the succinic semialdehyde reductase activity of GLYR1 does not seem to be involved in its role related to HPR1 and CAT2.

Since the knockout mutants of GLYR1 are comparable to Col-0 in plant growth and levels of the photorespiratory metabolites, this cytosolic photorespiratory shunt may not be important when the main photorespiratory pathway in the peroxisome is functional, possibly due to the predominant peroxisomal location of glyoxylate. Glyoxylate is highly reactive and can inhibit photosynthesis and other metabolic reactions, thus is toxic to the plant (Mulligan *et al.*, 1983; Cook *et al.*, 1985; Chastain & Ogren, 1989; Campbell & Ogren, 1990; Lu *et al.*, 2014). There are two major glyoxylate metabolic pathways in the peroxisome to maintain its homeostasis: the main photorespiratory pathway in photosynthetic tissue and the glyoxylate cycle in seeds in which glyoxylate is produced and catabolized (Dellero *et al.*, 2016; Pan *et al.*, 2020). Further, the cytosolic GLYR1 and the plastidic/mitochondrial GLYR2 were believed to scavenge the glyoxylate leaked from the peroxisome (Simpson *et al.*, 2008; Dellero *et al.*, 2016). Since cytosolic glyoxylate may become toxic to plants, it is possible that the cytosolic shunt is activated only when the main peroxisomal pathway is defective and under conditions that need very high photorespiratory flux.

We provided evidence that HPR2 is pivotal in converting cytosolic hydroxypyruvate to glycerate in the photorespiratory glyoxylate shunt, as the *glyr1 hpr1 hpr2* triple mutant maintains 86% of the hydroxypyruvate content observed in *hpr1 hpr2* (**Fig. 2.7b**). However, the minor decrease in hydroxypyruvate content, as well as the slightly bigger *glyr1 hpr1 hpr2* rosette size compared to *hpr1 hpr2* after 18 days of high light treatment (**Fig. 2.7a**) suggest the existence of other mechanisms in hydroxypyruvate reduction independent of HPR2. Although the role of HPR3 in reducing hydroxypyruvate is minor, knocking out *HPR3* can further exacerbate the photorespiratory phenotypes of the *hpr1 hpr2* double mutant (Timm *et al.*, 2011). Therefore, HPR3 may be involved in maintaining this photorespiratory shunt in the cytosol when both HPR1 and HPR2 are absent.

We hypothesize that there is a cytosolic aminotransferase with similar activity as the peroxisomal serine:glyoxylate aminotransferase (SGAT). Although SGAT activity was only detected in the peroxisome in previous studies (Liepman & Olsen, 2001, 2004), cytosolic activity may not be detectable unless the cytosolic route is activated. SGAT does not have any apparent homologs in the Arabidopsis genome (Liepman & Olsen, 2004), but substrate promiscuity is

common for aminotransferases (Koper *et al.*, 2022). SGAT is also known as AGT1 because of its alanine:glyoxylate transferase activity; additionally, it can catalyze other amino donor:acceptor combinations such as serine:pyruvate and asparagine:glyoxylate (Liepman & Olsen, 2001; Koper *et al.*, 2022). Human (*Homo sapiens*) AGT2, which localizes to mitochondria and has broad substrate specificity (Koper *et al.*, 2022), has three homologs in Arabidopsis: *AtAGT2*, *AtAGT3*, and *AtPYD4* (pyrimidine 4) (Liepman & Olsen, 2003; Koper *et al.*, 2022). *AtAGT2* was reported to localize to mitochondria and peroxisomes (Carrie *et al.*, 2009). The enzyme activity and localization of *AtAGT3* and *AtPYD4* are unclear, thus may be candidates for the hypothetical cytosolic aminotransferase with SGAT activity.

Some of the metabolic profiles of glycine and serine in this work have complicated patterns, possibly due to their participation in other metabolic pathways. Under ambient (21%) O₂ conditions, 32% of the photorespiratory carbon is thought to leave this pathway as serine (Busch *et al.*, 2018; Fu *et al.*, 2023), indicating that photorespiratory serine may be strongly connected with other metabolisms. Serine has been shown to play a role in the biosynthesis of other amino acids, proteins, and lipids (Ros *et al.*, 2014). While glycine is converted to serine in the mitochondrion during photorespiration, serine can also be converted to glycine in the cytosol and plastid (Rosa-Téllez *et al.*, 2023). This serine-glycine interconversion is an important component in one-carbon metabolism, which is crucial for synthesizing nucleotides and methylated compounds and maintaining nutrient balance (Hanson & Roje, 2001; Rosa-Téllez *et al.*, 2023). Furthermore, it has been reported that excess glycine from photorespiration is used for protein synthesis (Cegelski & Schaefer, 2005) and glutathione accumulation (Noctor *et al.*, 1999). Finally, glycine and serine were found in the vacuole (Riens *et al.*, 1991; Fürtauer *et al.*, 2019), which may represent an inactive pool or have a slow response to environmental changes.

In addition to alternative routes and photorespiratory shunts, post-translational modification of photorespiratory proteins seems to play an important regulatory role in photorespiration. For example, Arabidopsis phosphorylation - mimetic mutant of serine hydroxymethyltransferase 1 (SHMT1) exhibited compromised performance under salt or drought stress (Liu *et al.*, 2019), indicating that phosphorylation of photorespiratory components is important in stress response. Although the specific function of these modifications needs further investigation, phosphorylation also plays important roles in maintaining enzymatic activity and cofactor binding in GOXs (Jossier *et al.*, 2020) and HPR1 (Liu *et al.*, 2020), and thioredoxins in

mitochondria can modify the redox status of the L-protein of glycine decarboxylase complex (GDC) (Reinholdt *et al.*, 2019; da Fonseca-Pereira *et al.*, 2020). Furthermore, many potential sites for phosphorylation, ubiquitination, acetylation, and redox modifications have been identified in photorespiratory enzymes (Hodges, 2022; Aroca *et al.*, 2023), suggesting the possible involvement of additional post-translational modifications in regulating photorespiration. For example, HPR2 may be regulated by post-translational modifications to increase its enzymatic activity when the cytosolic shunt is activated.

Our work has provided evidence for the important role of an alternative photorespiratory route in the cytosol under high light conditions when the major photorespiratory pathway is defective, supporting the metabolic flexibility of photorespiration and substantiating the contribution of photorespiration to stress response. Further investigations are needed to obtain a more comprehensive understanding of the regulation of photorespiration, which may ultimately help to generate new crop varieties with high productivity without compromising their stress tolerance.

2.4 Methods

2.4.1 Plant materials and growth conditions

Wild-type and mutant lines of *Arabidopsis thaliana* used in the study are all from the ecotype Col-0. T-DNA insertion mutants were obtained from the Arabidopsis Biological Resource Center (ABRC, Ohio State University, USA) and confirmed by PCR-based genotyping. Previously characterized mutants are *hpr1-1* (SALK_067724) (Timm *et al.*, 2008), *cat2-1* (SALK_076998) (Queval *et al.*, 2007), *plgg1-1* (SALK_053469) (Pick *et al.*, 2013), and *glyr1-1* (SALK_057410) (Zarei *et al.*, 2017). Previously uncharacterized mutants used in this study are *glyr1-2* (SALK_202680C), *glyr1-3* (SALK_203580C), and *hpr2-3* (SALK_105876). Primers used for genotyping are listed in Table A1.

Arabidopsis seeds were sown on plates containing half-strength Linsmaier and Skoog basal salt (1/2 LS, Caisson Labs), 1% sucrose and 0.8% agar (Phytoblend, Caisson Labs). After seed stratification in the dark at 4 °C for 3 to 7 days, plates were placed in the Percival Intellus Environmental Controller under normal lights ($\sim 100 \mu\text{mol m}^{-2} \text{s}^{-1}$ white light), 21 °C, and 12h/12h light/dark cycle. At ~ 1.5 weeks old, seedlings were transplanted into the soil and moved to the growth chambers with the same growth conditions. For high light treatment, 2-week-old plants were transferred to a chamber with $\sim 700 \mu\text{mol m}^{-2} \text{s}^{-1}$ white light, and the same

temperature and photoperiod as those for NL growth. Plants grown under high CO₂ were directly sown in the soil and grown under 2,000 ppm CO₂, with the same settings for other parameters.

For the glyoxylate and serine feeding experiments, glyoxylate or serine was filter-sterilized and added to the autoclaved medium to a final concentration of 0.4 mM and 0.1 mM, respectively. Plates were placed in the normal light Percival and high light growth chamber, respectively, at the same time.

2.4.2 Suppressor screening and mapping

Seeds of *hpr1-1* were treated with ethyl methanesulfonate (EMS) to induce random mutations. M₁ plants were self-pollinated and M₂ seeds were harvested. The M₂ generation was grown under high light for suppressor screening, and individuals that grew bigger or greener than *hpr1-1* were selected. Candidates with persistent suppressor phenotypes in the M₃ generation were backcrossed to *hpr1-1*. Plants displaying the suppression phenotypes in the BC₁F₂ generation were used for additional backcrosses.

In the BC₃F₂ generation of the *shpr7* suppressor, 80 individuals with the suppression phenotypes were selected. Genomic DNA from these plants was extracted by Wizard Genomic DNA Purification Kit (Promega) and pooled together as one sample, which was used for DNBSEQ PE150 whole genome sequencing with 80X coverage. To minimize the influence of unrelated background mutations, 29 individuals from *hpr1-1* were also sequenced with 30X coverage. Sequencing and bioinformatic analysis were performed by BGI Genomics (<https://www.bgi.com>). Selfed progenies from BC₃F₂ plants exhibiting suppression phenotypes were used for follow-up experiments.

2.4.3 Generation of transgenic lines and RT-PCR

The *35S::FLAG-GLYR1* construct was generated by Gateway cloning according to manufacturer's instructions (ThermoFisher). Briefly, the coding sequence (CDS) of *GLYR1* was amplified from cDNA and cloned into the entry vector pDONR207 through the BP reaction. Next, *GLYR1* was inserted into the destination vector pEarleyGate202 through the LR reaction. Entry and expression constructs were confirmed by Sanger sequencing. The construct was transformed into *Agrobacterium tumefaciens* strain GV3101 by electroporation, and Arabidopsis lines were transformed by *Agrobacteria* using floral dipping. Positive transformants were selected on 1/2 LS plates containing 1% sucrose and 10 µg/ml glufosinate ammonium.

For RT-PCR analysis, RNA was extracted from the leaf tissue using NucleoSpin RNA Plant kit (MACHEREY-NAGEL), then reverse transcribed using the High-Capacity cDNA Reverse Transcription Kit (Applied Biosystems). The CDS of the target genes were PCR-amplified from cDNA using the GoTaq Green Master Mix (Promega) and gene-specific primers (Table A1).

2.4.4 Protein preparation and immunoblot analysis

Whole rosettes from 4-week-old plants, which had been grown for 2 weeks under normal light followed by 2-week growth under high light, were collected and ground in liquid nitrogen, after which ~60 mg of the powder was homogenized with 500 μ l Extraction Buffer [150 mM Tris-HCl (pH 6.8), 7.5% β -mercaptoethanol, 3% sodium dodecyl sulfate, and half a cComplete mini protease inhibitor tablet (Roche)]. Samples were centrifuged at 17,000 \times g at 4 $^{\circ}$ C for 10 min, and the supernatants were transferred to new tubes.

A previously described method was used for immunoblotting (Lavell *et al.*, 2021). Specifically, protein samples were combined with 4X Laemmli Buffer and boiled at 95 $^{\circ}$ C for 5 min. 40 μ l samples were loaded onto a 4-20% Mini-PROTEAN TGX pre-cast gel (Bio-Rad) with the Dual Color Protein Ladder (Bio-Rad). After separation on the gel, proteins were transferred to a nitrocellulose membrane using Power Blotter XL System (Invitrogen) at 25V for 7min, which was then blocked with 5% milk in TBST for 1 h. The anti-GLYR1 antibody was developed by PhytoAB Inc. (CA, USA), based on the antigen peptide PAFPLKHQQKDMRLA with an additional C on C-terminus for conjugation. The membranes were incubated in 1:1000 rabbit anti-GLYR1 antiserum in the blocking buffer overnight at 4 $^{\circ}$ C. The membranes were washed multiple times with TBST, then incubated in 1:10,000 goat anti-rabbit IgG HRP secondary antibody (PhytoAB Inc.) in TBST for 2 h, washed again with TBST, and then developed with the SuperSignal West Pico PLUS Chemiluminescent Substrate kit (Thermo Scientific). A replicated protein gel with the same loading and running conditions was used for Coomassie staining.

2.4.5 Metabolite extraction and quantification

Leaf samples were collected in the late afternoon, after ~10 h light treatment. Two to three well-expanded leaves with similar age were taken from plants with similar morphologies. In the cases where the mutants show different morphologies, the whole rosettes were taken. Plant tissue was frozen and ground in liquid nitrogen.

Metabolite extraction was performed using the methanol/chloroform/water method and quantification was conducted by Gas chromatography–mass spectrometry (GC-MS), as described previously (Fu *et al.*, 2023). Specifically, 500 μ l chloroform/methanol (3:7, v/v) was added to the tissue powder, followed by incubation at -20 °C for 2 h with occasional shaking. Then the internal standard adonitol and 400 μ l water were added to the sample, followed by vigorously mixing and centrifugation at 4 °C, 12000 xg for 10 min. The upper phase (methanol in water) was taken, dried in a lyophilizer and stored in -80°C.

Before analysis, samples were derivatized by adding 20 mg/ml methoxyamine hydrochloride dissolved in dry pyridine and incubated at room temperature overnight. Next, the reaction mixture was silylated by N, O-Bis (trimethylsilyl) trifluoroacetamide with 1% trimethylchlorosilane at 60°C overnight. The trimethylsilyl (TMS) derivatives were analyzed by an Agilent 7890A GC system/5975C inert XL Mass Selective Detector with a 30 m VF-5ms column (Agilent). 1 μ l of each sample was injected into the 230°C inlet, where splitless, 10:1 split, or 20:1 split mode was chosen depending on the levels of the metabolites in plant samples. The oven temperature gradient is as follows: 40°C for 1 min, increased to 80°C in 1 min, then further increased by 10°C/min to 240°C followed by 20°C /min to 320°C, and 5 min holding at 320°C. Scan mode of the MS was used to monitor ions with mass to charge ratio (m/z) between 50–600.

Metabolites were identified by m/z values, using retention time in comparison with authentic standards or the NIST Mass Spectral Library. Software MassLynx (Waters) was used for peak extraction and integration. Metabolites were quantified against the internal standard.

2.4.5 Photosynthetic measurement

Using a previously reported method (Li *et al.*, 2019a), the Dynamic Environment Photosynthesis Imager (DEPI) (Cruz *et al.*, 2016) was used to measure photosystem II quantum efficiency (Φ_{II}) of two-week-old seedlings grown in soil under regular normal light growth conditions as mentioned above. Φ_{II} was calculated from $(F_m' - F_s)/F_m'$, where F_s is the chlorophyll fluorescence emission from light-adapted leaf at steady state and F_m' is the maximum fluorescence from light-adapted leaf during a saturating pulse of light. Custom software (Visual Phenomics) was used to process the fluorescence images (Tessmer *et al.*, 2013), and heatmaps were generated with OLIVER (<https://caapp-msu.bitbucket.io/projects/oliver/index.html>).

2.4.6 Tobacco infiltration and confocal microscopy (performed by Dr. Amanda Koenig and Joy Li)

GLYR1 was N-terminally tagged with eYFP using the Gateway LR Clonase II Enzyme mix (ThermoFisher) by combining entry vector pENTR223-GLYR1 (ABRC, G82382) and pEarleyGate104, according to the manufacturer's instructions. The expression vector (eYFP-GLYR1) was confirmed by Sanger sequencing and transformed into GV3101 *Agrobacterium tumefaciens* cells by electroporation.

5 ml *Agrobacterium* containing the peroxisome marker (mScarlet-SRL in pGWB2)(Koenig *et al.*, 2023) and eYFP-GLYR1 were grown in Luria broth (LB, Rif₂₅/Gent₁₀/Kan₅₀) with 225 rpm shaking at 28 °C overnight. Separate flasks containing 25 ml LB (Rif₂₅/Gent₁₀/Kan₅₀) with 100 µM acetosyringone were inoculated with 1 ml of the overnight cultures and grown at 28 °C to OD₆₀₀ between 0.6 and 0.8. The cells were harvested by centrifugation at 3000 xg for 10 min and then resuspended in MMA infiltration buffer (10 mM MES pH 5.7, 10 mM MgCl₂, 100 µM acetosyringone) to adjust the OD₆₀₀ to 0.6. The cell resuspensions were then incubated at room temperature (~22 °C) for 1 h. The peroxisome marker and eYFP-GLYR1 cultures were combined in 1:1 volume and infiltrated into 6-week-old *Nicotiana tabacum* leaves with a 1 ml needleless syringe. Tobacco plants were recovered in a 12h/12h photoperiod chamber for 2 days before imaging.

Infiltrated tobacco leaves were imaged with an Olympus Fluoview 1000 spectral-based confocal laser scanning microscope with a 40X oil objective (NA: 1.30). Images were captured using the following excitation and emission parameters: eYFP-GLYR1 (ex: 515 nm, em: 530-560 nm), mScarlet-SRL (ex: 559 nm, em: 580-615 nm), and chlorophyll autofluorescence (ex: 515 nm, em: 655-755 nm).

2.4.7 Hydroxypyruvate reductase (HPR) activity assay

Using a previously reported method (Gregory *et al.*, 2023), the maximum activity of HPR in plants was determined by NADH or NADPH oxidation. In brief, 50-150 mg leaf samples were frozen in liquid nitrogen, and ground with 1 ml Extraction Buffer on ice using 2 ml glass-to-glass homogenizer. After centrifugation, the supernatant was used for quantifying protein concentration and measuring enzymatic activity. Protein concentration was measured using Quick Start Bradford 1x Dye Reagent (BIO-RAD) and standards of bovine serum albumin (BIO-RAD), according to the manufacturer's instructions. For enzyme activity, a total of 200 µl

reaction in 96-well microplate were measured. 4-8 μl crude protein extract with 188-192 μl reaction buffer were used for NADH-dependent enzyme activity, while 16-20 μl crude protein extract with 176-180 μl reaction buffer were used for NADH-dependent enzyme activity. The reaction was initiated by adding 4 μl 25 mM Na beta-hydroxypyruvate, and the absorbance at 340 nm was monitored for 5 min. The decrease in absorbance per min and the extinction coefficient of NAD(P)H ($6.22 \text{ mM}^{-1} \text{ cm}^{-1}$) were used to calculate HPR activity in plants, which was then normalized to the protein content in the samples.

2.4.8 Statistics and plots

Data analysis is performed using Microsoft Excel and Rstudio. Student's unpaired two-tailed t -test was used for pairwise comparison. One-way ANOVA with Tukey's HSD test was used for multi-comparison. Boxplot center lines show the medians, and the lower and upper hinges correspond to the first and third quartiles. Whiskers extend from the hinges to the largest or smallest values that are no further than 1.5 times of the interquartile range. Data points are represented as individual dots.

Figures

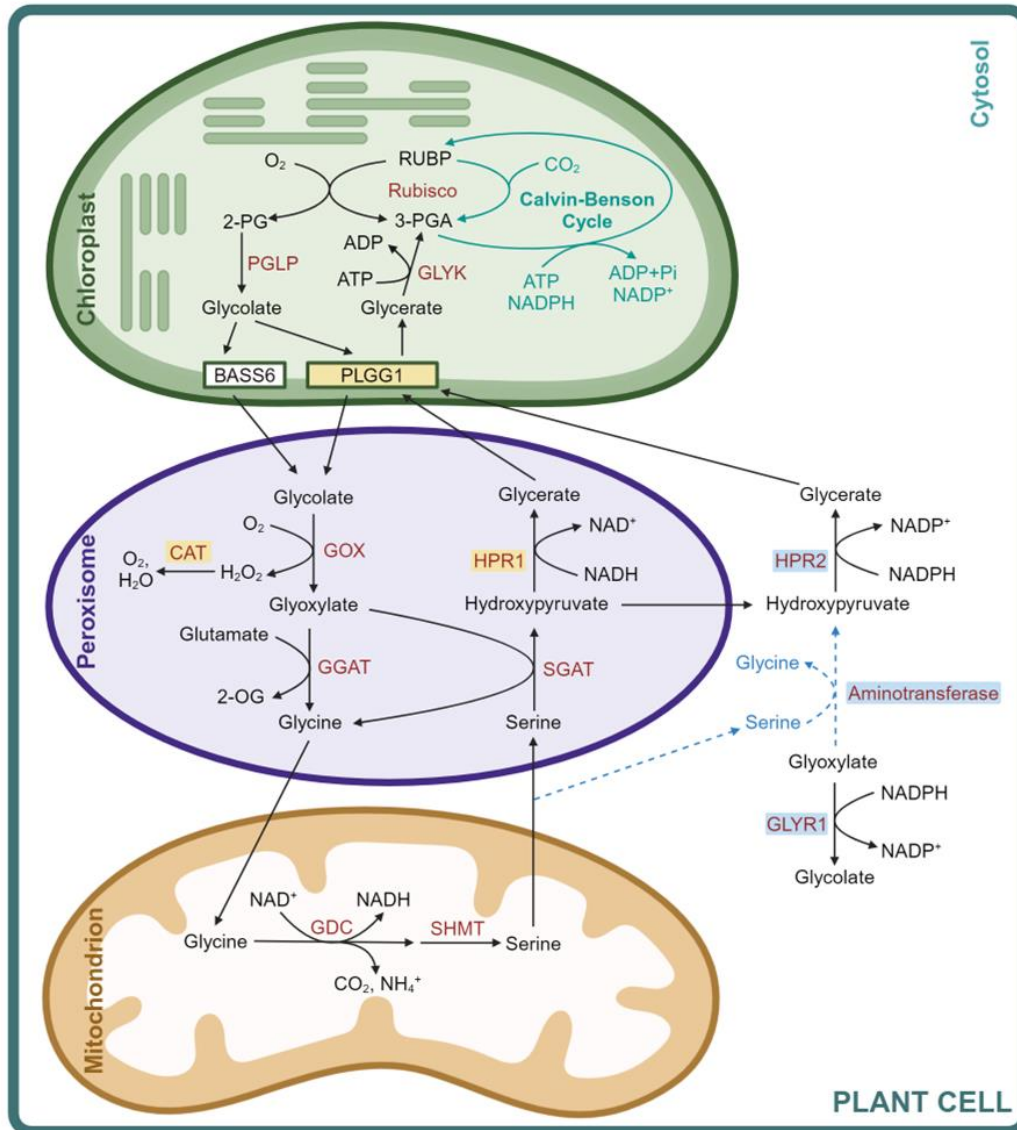


Figure 2.1. The established photorespiration pathway and the cytosolic glyoxylate shunt proposed in this study. Photorespiration involves a series of reactions in the chloroplast, peroxisome, mitochondrion, and cytosol. We propose that defective GLYR1 allows the overly accumulated free glyoxylate in the cytosol to react with serine, catalyzed by an unknown aminotransferase. The hydroxypyruvate produced can be further converted through HPR2 to glycerate, which re-enters the chloroplast. Abbreviations: 2-OG, 2-oxoglutarate; 2-PG, 2-phosphoglycolate; 3-PGA, 3-phosphoglycerate; BASS6, bile acid sodium symporter 6; CAT, catalase; GDC, glycine decarboxylase complex; GGAT, glutamate:glyoxylate aminotransferase; GLYK, glycerate kinase; GLYR1, glyoxylate reductase 1; GOX, glycolate oxidase; HPR, hydroxypyruvate reductase; PGLP, 2-PG phosphatase; PLGG1, plastidial glycolate/glycerate transporter 1; Rubisco, RuBP carboxylase/oxygenase; RuBP, ribulose-1,5-bisphosphate; SGAT, serine:glyoxylate aminotransferase; SHMT, serine hydroxymethyltransferase. Created with BioRender.com.

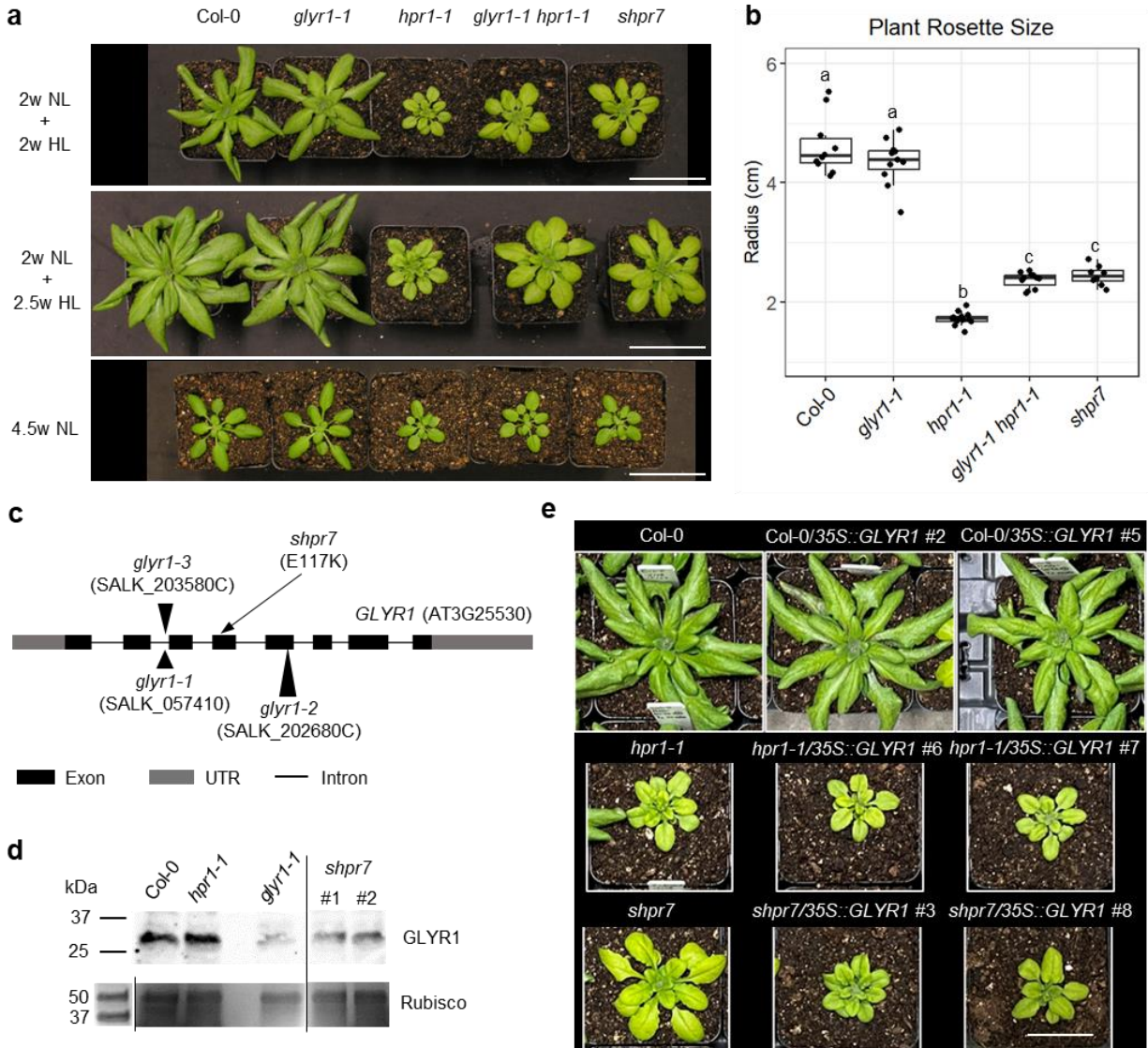


Figure 2.2. Loss of function of GLYR1 partially rescues the growth phenotypes of *hpr1*. (a) Plants grown for 2 weeks (2w) under normal light (NL, $100 \mu\text{mol m}^{-2} \text{s}^{-1}$) followed by 2 or 2.5 weeks of growth under high light (HL, $700 \mu\text{mol m}^{-2} \text{s}^{-1}$), or constantly grown under normal light for 4.5 weeks. Scale bars = 5 cm. (b) Radius measurements of the total rosette of 4-week-old plants grown under 2w normal light + 2w high light. Different letters indicate statistically significant differences ($p < 0.05$), which were determined by One-way ANOVA with Tukey's HSD test. Biological replicates: $n=10$ for Col-0, $n=11$ for *glyr1-1* and *glyr1-1 hpr1-1*, $n=13$ for *hpr1-1*, and $n=8$ for *shpr7*. (c) Schematic depiction of the *GLYR1* gene and positions of the mutations in various alleles. (d) Immunoblot analysis of the GLYR1 protein from different genotypes. The GLYR1 protein was detected by an anti-GLYR1 peptide antibody (top). Rubisco stained by Coomassie Blue in the SDS-PAGE gel was used as a loading control (bottom). (e) Overexpressing *GLYR1* reverts the suppression phenotype back to the *hpr1* mutant phenotype. Plants were grown under 2-week normal light followed by 2.5-week high light. Scale bars = 3 cm.

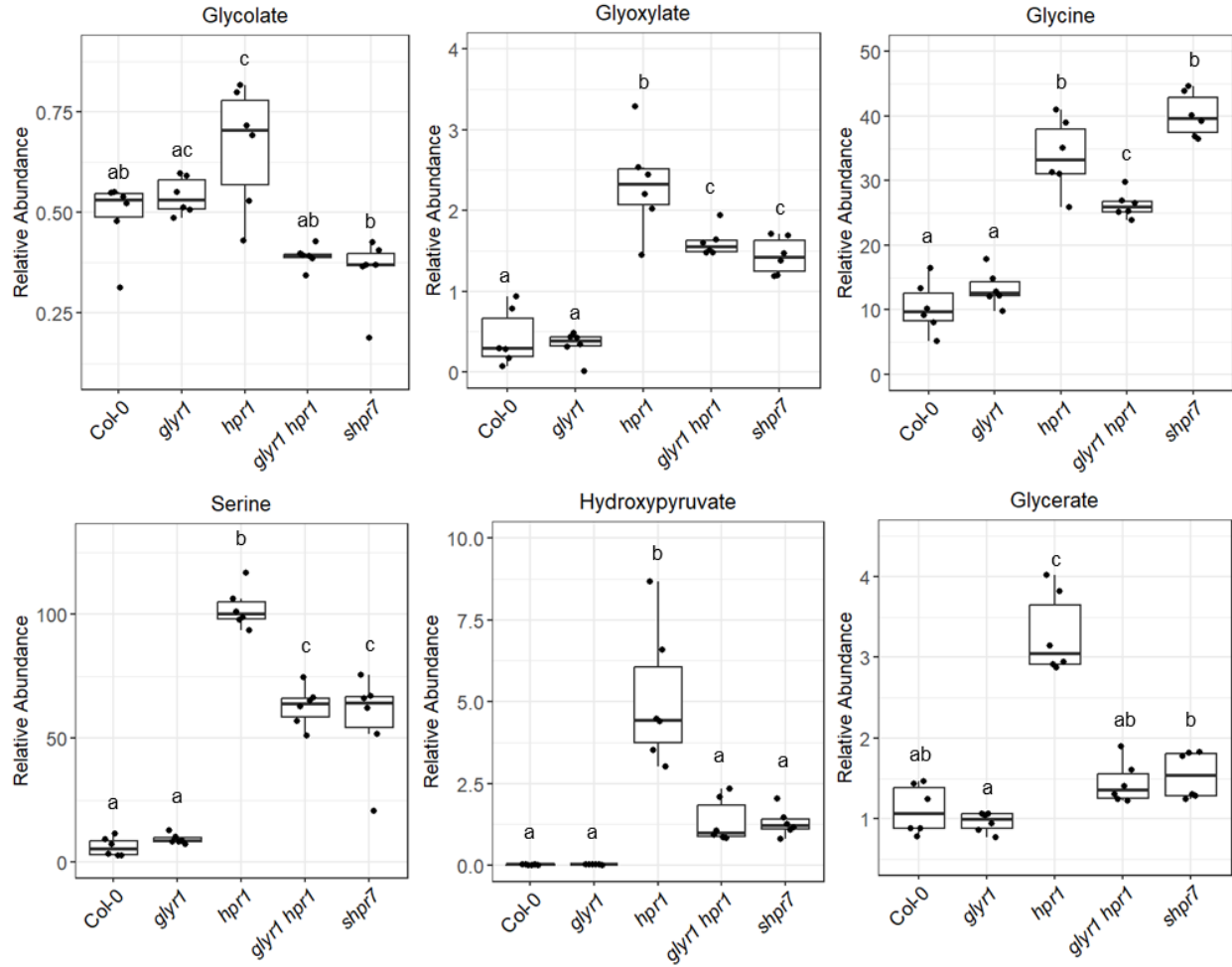


Figure 2.3. Profiling of stable photorespiratory metabolites in 4-week-old high light-treated plants. Plants were grown under 2-week normal light followed by 2-week high light. Different letters indicate statistically significant differences ($p < 0.05$), which were determined by One-way ANOVA with Tukey's HSD test. Biological replicates: $n = 6$.

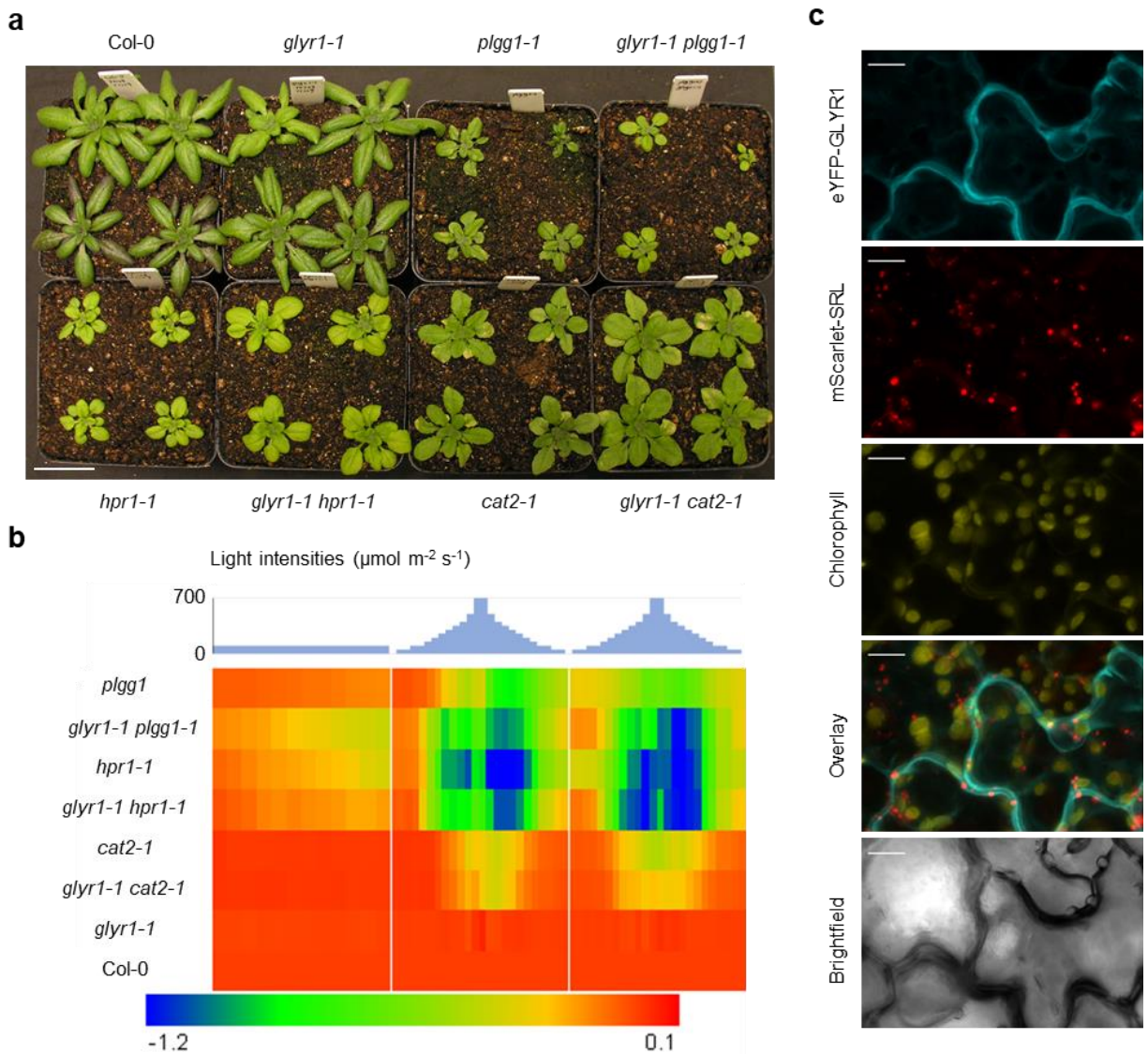


Figure 2.4. Analysis of the impact of defective GLYR1 on other photorespiratory mutants and GLYR1 protein localization. (a) Plants grown under 2-week normal light followed by 2-week high light. Scale bars = 3 cm. (b) Heatmap of photosystem II quantum efficiency for 2-week-old plants under dynamic and high light conditions. Values for the mutants were normalized to that of the wild-type Col-0. Biological replicates: n=12 for Col-0, *cat2-1*, *glyr1-1 cat2-1*, *glyr1-1 hpr1-1*, and *plgg1-1*, n=11 for *glyr1-1* and *hpr1-1*, and n=13 for *plgg1-1*. (c) Maximum intensity Z-projection of confocal images spanning 30 μm of tobacco leaf tissue co-expressing eYFP-GLYR1 (cyan) and mScarlet-I-SRL (peroxisomes, red). Chloroplast signals are from chlorophyll autofluorescence (yellow). Scale bar = 10 μm . Images in (c) were generated by Amanda Koenig.

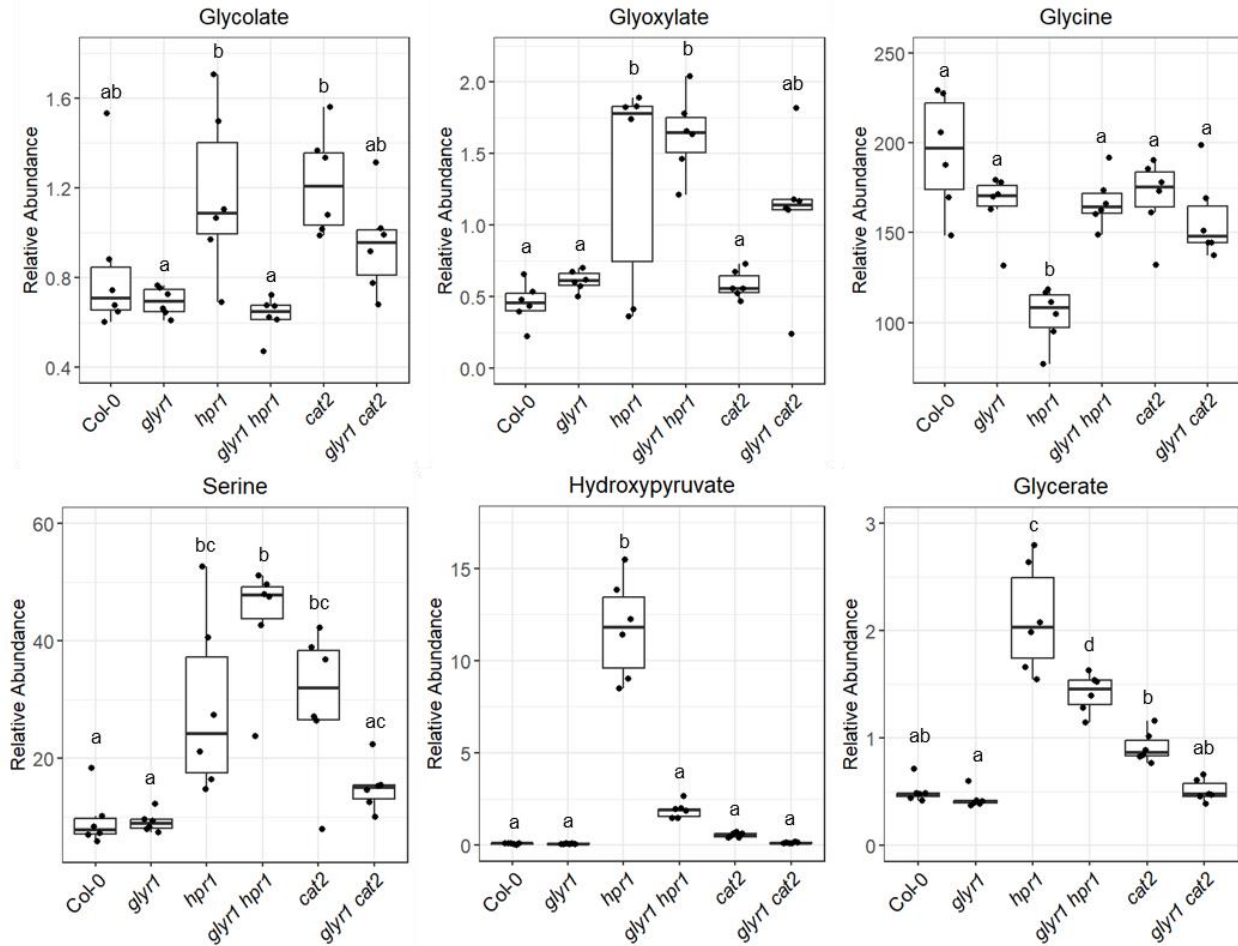


Figure 2.5. Profiling of transitional photorespiratory metabolites in plants transferred to the photorespiratory environment. Plants were grown under 3 weeks of high CO₂ and normal light, and then transferred to ambient CO₂ and high light before lights were turned on. Leaf tissue was sampled after ~10 h. Different letters indicate statistically significant differences (p < 0.05), which were determined by One-way ANOVA with Tukey's HSD test. Biological replicates: n=6.

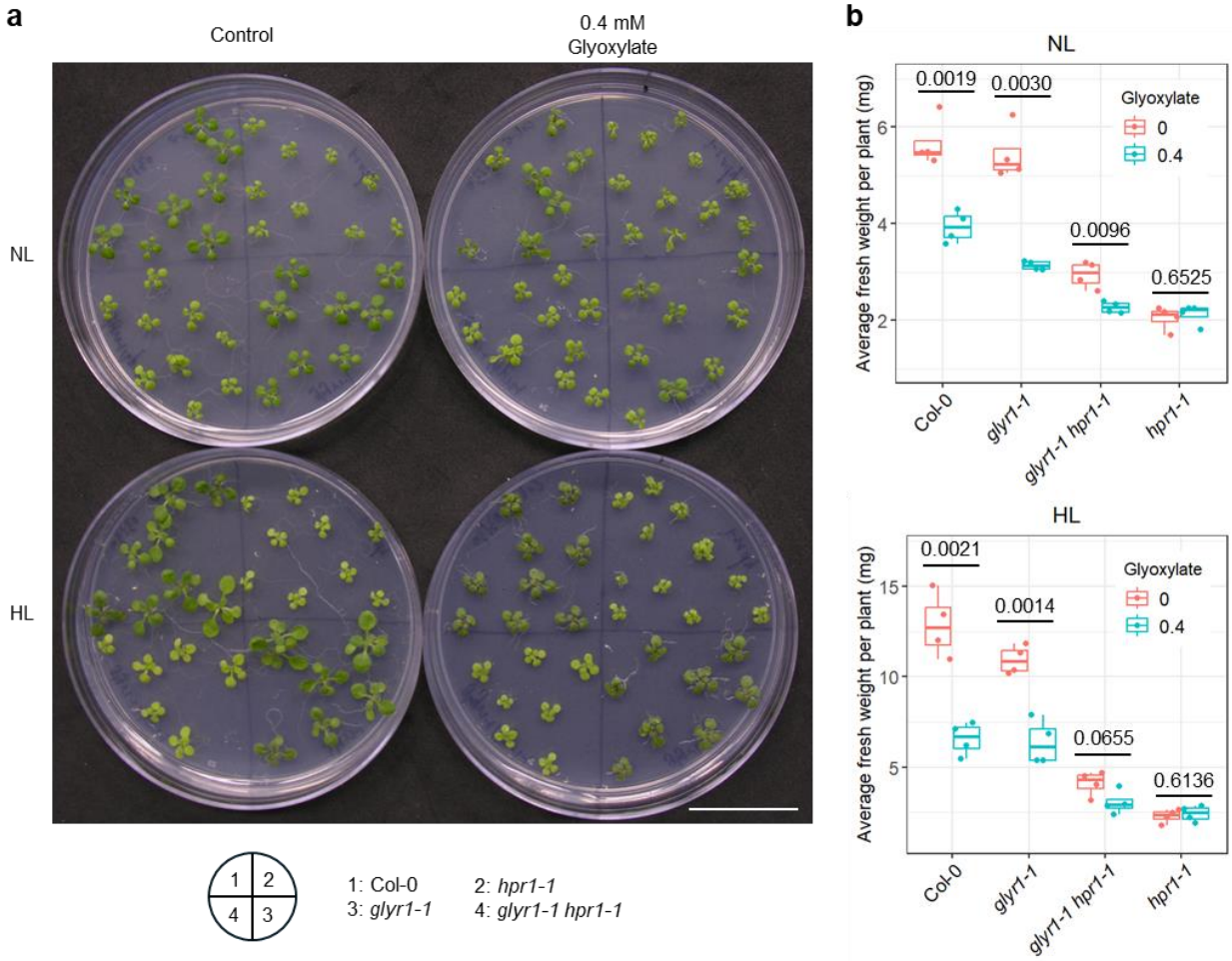


Figure 2.6. Plant growth after feeding with glyoxylate. Growth phenotype (a) and fresh weight (b) of 12-day-old seedlings on plates with or without glyoxylate under normal light (NL) or high light (HL) are recorded. The *p* values determined by Student's unpaired two-tailed *t*-test were labeled on the plot. Seedlings grown on the same plate were treated as a biological replicate. Biological replicates: *n*=4. Scale bars = 3 cm.

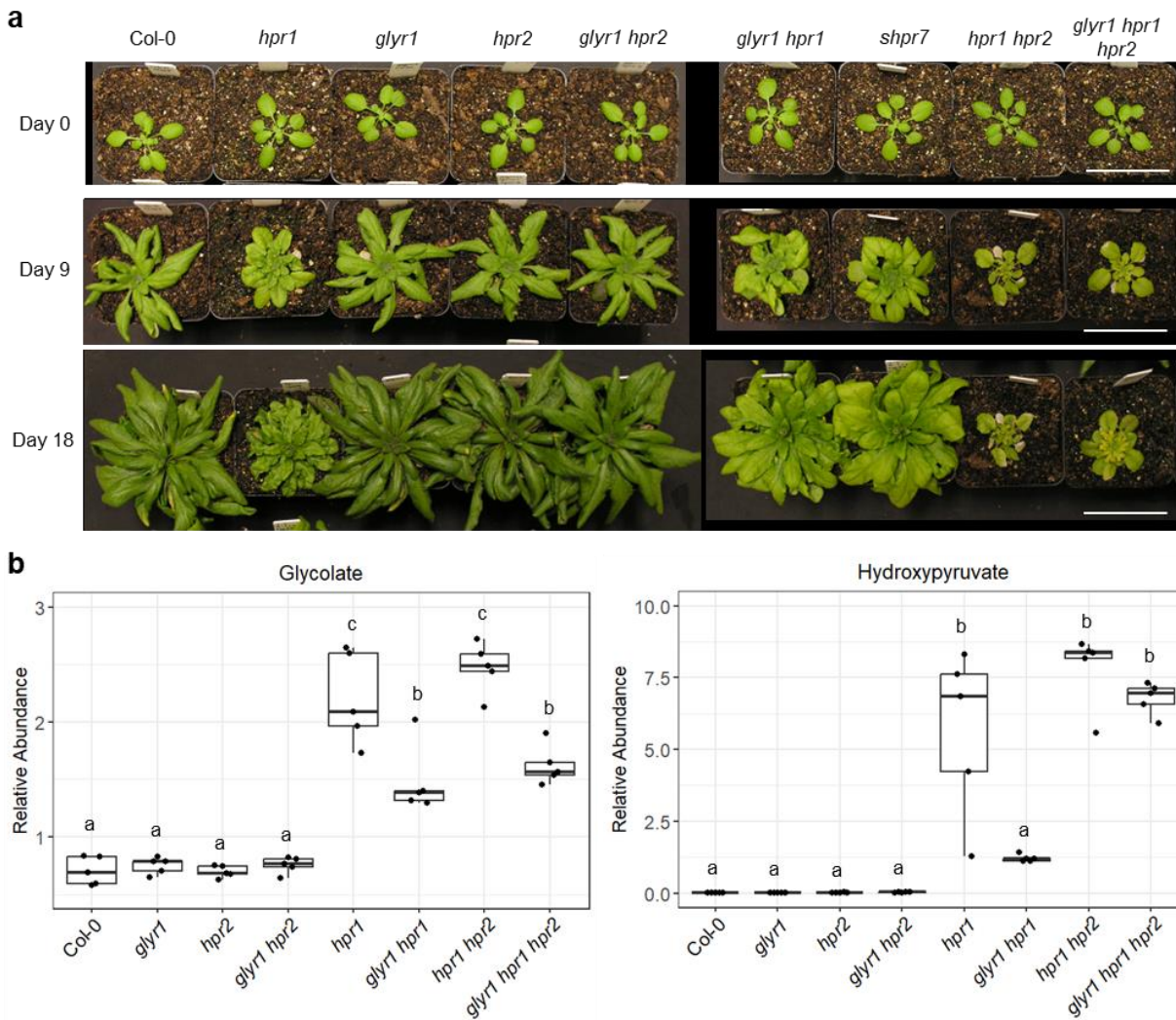


Figure 2.7. The role of *glyr1* is partially dependent on HPR2. (a) Plants grown under 3 weeks of high CO₂ and normal light before being transferred to ambient CO₂ and high light on Day 0. Scale bars = 5 cm. (b) Glycolate and hydroxypyruvate levels at the transitional stage. Plants were grown under 3 weeks of high CO₂ and normal light, and then transferred to ambient CO₂ and high light before the lights were on. Leaf tissue was sampled after ~10 h. Different letters indicate statistically significant differences ($p < 0.05$), which were determined by One-way ANOVA with Tukey's HSD test. Biological replicates: $n = 5$.

CHAPTER 3*. Defective GLYR1 largely reverts the broad transcriptional reprogramming of the *hpr1* mutant under high light conditions

3.1 Introduction

In Chapter 2, under high light, deficiency in GLYR1 was shown to partially rescue the phenotypes of the photorespiration mutants *hpr1* and *cat2* but not those of *plgg1*. Further genetic, physiological and metabolic analyses supported a novel photorespiratory glyoxylate shunt in the cytosol that allows more photorespiratory carbon to be recycled back to the Calvin-Benson cycle. However, it is also important to obtain a comprehensive view of how defects in GLYR1 impact the transcriptome and cell functions globally.

To this end, I performed RNA-seq analysis to analyze the transcriptome of Col-0, *hpr1-1*, *glyr1-1*, *glyr1-1 hpr1-1*, and *shpr7*. Since transcriptomic data obtained from plants under prolonged photorespiratory conditions may not reflect transcriptional changes directly caused by the imposed conditions, we chose to focus on the effects of defective GLYR1 under short-term photorespiratory conditions to reduce secondary effects. Plants were grown for 3 weeks under normal light and high CO₂ (2,000 ppm CO₂), where photorespiration is largely inhibited. At the end of the dark period, plants were transferred to ambient air with high light conditions to induce photorespiration. Leaf samples harvested after 3 h and 10 h of the treatment were used for RNA-seq.

3.2 Results

3.2.1 Defective GLYR1 has little influence on the transcriptome of Col-0 but extensive impact on that of *hpr1*

Principal component analysis (PCA) was first employed to visualize the variations in the RNA-seq data (**Fig. 3.1**). At both 3 h and 10 h, Col-0 and *glyr1-1*, and *glyr1-1 hpr1-1* and *shpr7*, were respectively clustered together, with both clusters clearly separated from *hpr1-1*. This clustering pattern is consistent with the growth phenotypes of these lines, validating the high quality of the RNA-seq data and clear, reproducible transcriptomic response of the mutants.

Analysis of differentially expressed genes (DEGs) revealed 10,139 and 16,104 DEGs at 3 h and 10 h respectively, between *hpr1-1* and Col-0, demonstrating the remarkable transcriptional reprogramming in *hpr1-1* (**Fig. 3.2**). Interestingly, while *glyr1-1* itself had relatively few DEGs

* Some results in this chapter have been submitted for publication. The analyses of RNA-seq data were mostly performed by Nicholas Panchy.

(59 at 3 h and 12 at 10 h), this mutation dramatically altered gene expression in the *hpr1-1* background. At 10 h in particular, the number of DEGs in *glyr1-1 hpr1-1* (15,955) or *shpr7* (15,795) compared to *hpr1-1* was very close to that in *hpr1-1* compared to Col-0, highlighting the strong impact of GLYR1 loss of/reduced function in *hpr1-1*.

Current understanding of the potential function of GLYR1 under stress conditions is mainly from its enzymatic activities as GLYR and succinic semialdehyde reductase, with little known about the downstream components. To elucidate the genes and pathways affected by the loss of function of GLYR1, I chose the top 5 DEGs, which have large fold changes (>2 fold) and small *p-values*, in *glyr1-1* compared to Col-0 from both time points. Gene expression data in all genotype comparisons at both 3 and 10 h (**Table 3.1**, first 5 genes) and the gene descriptions (**Table 3.2**, first 5 genes) of these DEGs were collected. Interestingly, the expression patterns of these 5 DEGs in *shpr7* vs. *hpr1* or *glyr1 hpr1* vs. *hpr1* comparisons were mostly different from *glyr1-1* vs. Col-0 (**Table 3.1**), suggesting that these DEGs have little function in the *glyr1*-induced transcriptional reprogramming in *hpr1-1*. For example, *AT2G43820*, which encodes a glycosyltransferase, was up-regulated in all pairwise comparisons at 3 h, showing a consistent effect of *glyr1* in Col-0 and *hpr1-1* background (**Table 3.1 and 3.2**). However, while this gene has a comparable expression level in *glyr1-1* as in Col-0 at 10 h, *glyr1* induced a repression of this gene in the *hpr1-1* background. *AT3G06325*, another gene that is predicted to generate an antisense RNA, was up-regulated in both *glyr1-1* and *hpr1-1* at 10 h, but defective GLYR1 in *hpr1-1* down-regulated this gene (**Table 3.1 and 3.2**). The functions of these 5 DEGs and their connections with GLYR1 are largely unknown (**Table 3.2**). Further investigations are needed to fully understand the role of GLYR1 under high light and other stress conditions.

Among the top 5 DEGs, *AT5G19880*, a gene belonging to the peroxidase superfamily, had high and similar expressions in *hpr1-1*, *glyr1-1 hpr1-1* and *shpr7* at 3 h, which is inconsistent with the general rescuing trend of *glyr1* in *hpr1* (**Table 3.1 and 3.2**). To further determine the pattern for changes in gene expression, I chose 5 additional DEGs from the top in *hpr1-1* for analysis (**Table 3.1 and 3.2**, last 5 genes). The expression levels of these DEGs were similar in *glyr1-1* and Col-0, but their altered expressions in *hpr1-1* were all at least partially reverted in *glyr1-1 hpr1-1* and *shpr7* (**Table 3.1**), which supports the strong impact of defective GLYR1 in *hpr1-1*. The functions of the last 4 DEGs (#6-#10) are all related to stress (**Table 3.2**), indicating that the stressful cellular environment in *hpr1-1* can be alleviated by *glyr1*. The

expression of *AT2G26400*, which is predicted to encode an acireductone dioxygenase family protein (**Table 3.2**), was highly repressed in *hpr1-1*, but this repression was totally rescued in *glyr1-1 hpr1-1* and *shpr7* (**Table 3.1**), making this unknown protein a good candidate for an important player in the *glyr1*-induced rescue of *hpr1*.

Overall, few DEGs were found between *glyr1-1* and Col-0, but there were huge numbers of DEGs between *glyr1-1 hpr1-1* or *shpr7* and *hpr1-1*. The DEGs induced by the deficiency of GLYR1 in Col-0 do not seem to play important roles in *hpr1*, suggesting that *glyr1* and *hpr1* mutations together activate a distinct mechanism for *hpr1* rescue.

3.2.2 Defective GLYR1 largely reverts the broad transcriptional reprogramming in *hpr1*

To further determine the impact of *glyr1* on the transcriptome of *hpr1*, the DEGs that have a more than 4-fold change in *hpr1-1* compared to Col-0 at 10 h were selected to generate a heatmap (**Fig. 3.3**). Almost all these DEGs showed reversion to some extent in *glyr1-1 hpr1-1* and *shpr7*; the majority of them even had comparable or nearly comparable levels of genes expression in *glyr1-1 hpr1-1*, *shpr7* and Col-0. This data indicates that *glyr1* can effectively revert the transcriptional reprogramming in *hpr1*.

To decipher the biological pathways affected, we employed weighted gene co-expression network analysis (WGCNA) to identify co-expression modules. Using the soft threshold of 30 (**Fig. 3.4a**), a total of 17 co-expression modules, whose sizes ranged from 11 to 4,680 genes, were constructed (**Fig. 3.4b and c, Table 3.3**). Generally, the modules that were associated with 3 h were different from those for 10 h (**Fig. 3.4c**), indicating that the transcriptome is being remodeled along with the increased exposure to high light. Most modules were correlated with *hpr1-1* but rarely with the other lines, suggesting the large rescuing effects of defective GLYR1 in *hpr1-1*. One exception is the lightcyan module, which had positive correlations with Col-0 and *glyr1-1* at 10 h but no other lines (**Fig. 3.4c**). Gene Ontology (GO) enrichment analysis of this module showed enrichment of the biosynthetic process for anthocyanin-containing compounds (**Fig. 3.4d**), which is consistent with the reduced anthocyanin phenotype in *hpr1-1*, *glyr1-1 hpr1-1* and *shpr7* as shown in Chapter 2.

The top modules that comprise large numbers of genes, including turquoise (4,680 genes), blue (3,886 genes), brown (3,047 genes), yellow (2,310 genes), green (2,144 genes) and red (1,815 genes), were all closely associated with *hpr1-1* but rarely with the other lines (**Fig. 3.4c, Table 3.4**). Among these, the yellow and red modules were positively and negatively

associated with *hpr1-1*, respectively, at 3 h (**Fig. 3.4c**). GO enrichment analysis showed that, at 3 h, stress response was activated in *hpr1-1* whereas protein translation-related processes were repressed (**Fig. 3.5**), suggesting that the cell environment in *hpr1-1* at 3 h became stressful and started to disrupt housekeeping activities. The other 4 modules were associated with *hpr1-1* at 10 h, with blue and green modules positively associated and turquoise and brown modules negatively associated. The blue, green and turquoise/brown modules were enriched in protein degradation (**Fig. 3.6a**), nuclear proteins (**Fig. 3.6b**), and chloroplast-related proteins (**Fig. 3.6c and d**), respectively. These results suggest that the stressful cell environment in *hpr1-1* may accelerate protein damage and degradation, especially for chloroplast proteins, and that the transcription machinery is highly activated to cope with this adversary. These data are also consistent with the accumulation of photorespiratory intermediates in *hpr1-1* (see Chapter 2), which likely induces a stressful environment that interferes with broad cellular functions. Defective GLYR1 partially rescues this metabolic accumulation in *hpr1-1*, which helps to prevent the unfavorable cell environment and consequently largely reverts the transcriptional reprogramming in *hpr1-1*.

3.2.3 Photorespiratory and photosynthetic genes are largely suppressed in *hpr1* and rescued by *glyr1* at 10 h

To determine the relationship between GLYR1 and photorespiration or photosynthesis, the expression data for genes in these two pathways were extracted from the RNA-seq data (**Fig. 3.7**). Most of the photorespiratory and photosynthetic genes showed a small shift in expression between 3 and 10 h, suggesting that photorespiration and photosynthesis are dynamic in early high light response. All lines showed similar expression patterns in these genes at 3 h, but at 10 h *hpr1-1* displayed a unique pattern of most decreased expression of these genes, indicating that photorespiration and photosynthesis were generally suppressed in *hpr1-1*, a pattern that got reverted by *glyr1*.

The top 4 genes in the expression heatmap of photorespiration showed a different pattern from the other genes because they were highly up-regulated in *hpr1-1* at 10 h (**Fig. 3.7a**). None of these genes encode major components in photorespiration (**Table 3.4**), thus their upregulation in *hpr1-1* may be due to their function in other biological pathways.

To obtain more information about the photorespiratory glyoxylate shunt in the cytosol proposed in Chapter 2, gene expression data of candidate aminotransferases, AGT2, AGT3 and

PYD4, was gathered along with HPR2 in all genotype comparisons at both 3 and 10 h (**Table 3.5**). The expression of *AGT2* only had small changes in the mutants, but it was repressed in *hpr1-1* at 10 h and rescued by defective GLYR1, similar to that of *HPR2* and most of the photorespiratory genes. In contrast, at 10 h, *AGT3* and *PYD4* were up-regulated in *hpr1-1*, which was reverted by GLYR1 defects. Among the three candidates, *PYD4* is the only gene that differentially expressed in *hpr1-1* at 3 h and had the biggest alternations of expression among genotypes. However, the expression patterns of these three candidate aminotransferases did not provide directive clues about their involvement in the glyoxylate shunt, considering their potential functions in other pathways and the possible regulations on the enzymatic level. Therefore, investigations on the localizations and enzymatic activities of these candidates are still the key to determining the aminotransferase involved in the cytosolic glyoxylate shunt.

Taken together, the expression of genes related to photorespiration and photosynthesis was largely suppressed in *hpr1* at 10 h, a pattern that was mostly rescued by *glyr1*. It is likely that photorespiration and photosynthesis are disrupted by the stressful environment in *hpr1*.

3.3 Discussions

In this work, I have shown that while *glyr1-1* itself did not cause many transcriptional changes in the wild-type background, defects in GLYR1 significantly rescued the *hpr1-1* mutant at the transcriptome level under high light conditions. The top DEGs in *glyr1-1* may be the key to understanding the function of GLYR1 in Col-0, but these genes do not seem to play important roles in the *hpr1-1* background, suggesting that lacking the function of both GLYR1 and HPR1 activates a distinct mechanism which otherwise has minimal influence in the *glyr1-1* single mutant.

Broad and high-level transcriptional reprogramming was found in *hpr1*, probably because of the accumulation of photorespiratory metabolites. Due to the impaired main photorespiratory pathway in the peroxisome in *hpr1*, the photorespiratory intermediates gradually accumulate in the cell as plants are moved to high light conditions, causing an unfavorable environment that disrupts regular biological processes. The lack of GLYR1 in *hpr1* can activate the cytosolic glyoxylate shunt proposed in Chapter 2, which helps to recycle more carbon back to the Calvin-Benson cycle and therefore partially prevents the formation of a stressful cell environment. Photorespiratory and photosynthetic genes were generally suppressed in *hpr1* at 10 h, and this

suppression was largely rescued by *glyr1*. This pattern may be similar to the genes in other primary cellular processes in a stressful environment.

These results support the existence of the photorespiratory glyoxylate shunt in the cytosol, but other possible mechanisms for how *glyr1* rescues *hpr1* also exist. The genes that are differentially expressed in *hpr1-1* and fully reverted in *glyr1-1* and *shpr7* at 3 h may be good candidates for the key regulators in this rescue.

3.4 Methods

3.4.1 Plant growth and RNA extraction

Arabidopsis lines used in this Chapter were described in Chapter 2. Seeds were directly sown to soil in pots and stratified in the dark at 4 °C for 3 to 7 days. Then the pots were moved to high CO₂ (2,000 ppm) conditions, ~100 μmol m⁻² s⁻¹ white light, 21 °C, and 12h/12h light/dark cycle for growth. After growing under high CO₂ for 3 weeks, plants were moved to ambient air condition at the end of the dark period, followed by 3 h or 10 h of high light treatment at ~700 μmol m⁻² s⁻¹.

Five biological replicates each for Col-0, *hpr1-1*, *glyr1-1*, *glyr1-1 hpr1-1*, and *shpr7* were used, and 2-3 well-expanded leaves of similar age were sampled on each plant. Plant tissue was frozen and ground in liquid nitrogen. Total RNA was isolated using the NucleoSpin RNA Plant kit (MACHEREY-NAGEL), after which DNA was further depleted using the TURBO DNA-free Kit (Invitrogen).

3.4.2 RNA sequencing and data analysis

RNA-seq was performed by the MSU Genomics Core, who prepared mRNA libraries with the KAPA mRNA HyperPrep Kit (Roche) and pooled them together with samples from other researchers onto one S4 lane of Illumina NovaSeq 6000. The sequencing yielded 2x150 bp paired end reads with ~20M read pairs per sample.

Analysis of the RNA-seq data was mainly performed by Nicholas Panchy (MSU Bioinformatics Core), who used the nf-core/rnaseq v3.10.1 pipeline (<https://zenodo.org/records/7505987>) built with Nextflow v22.10.4 (Di Tommaso *et al.*, 2017) to process and quantify transcriptomic reads using the standard defaults unless otherwise specified. Briefly, Salmon v1.9.0 (Patro *et al.*, 2017) and the fq v0.9.1 (<https://github.com/stjude-rust-labs/fq>) were used to sub-sample FastQ files and auto-infer read strandedness. Adapter and quality trimming were performed using Trim Galore! v0.6.7

(<https://zenodo.org/records/5127899>) with Cutadapt v3.4 (Martin, 2011). STAR v2.7.9a was used to map the raw FastQ reads to the reference genome and project the alignments onto the transcriptome (Dobin *et al.*, 2013). The alignments were sorted and indexed using SAMtools v1.16.1 (Li *et al.*, 2009), and downstream BAM-level transcript quantification was performed with Salmon v1.9.0 with the --seqBias --gcBias tags (Patro *et al.*, 2017).

Reads were mapped to the TAIR 10.1 version of the *A. thaliana* genome (GCA_000001735). Genes with missing transcript IDs were filtered from the GTF file, which is a known issue with some GTF files (see <https://github.com/nf-core/rnaseq/issues/1086>).

DESeq2 v1.38.3 was used to perform differential expression analysis for 3-h and 10-h samples separately (Love *et al.*, 2014). Tximport v1.26.1 was used to import transcript abundances and construct a gene-level DESeqDataSet object from Salmon quant.sf files (Soneson *et al.*, 2016). Genes were filtered for those with a count of at least 10 in 5 samples.

The fgsea v1.24.0 was used for pre-ranked gene set enrichment analysis (GSEA), and the genes were ranked by the Wald statistic (Korotkevich *et al.*, 2021). Gene ontology enrichments were performed using the TAIR annotation file for *A. thaliana* downloaded from <http://current.geneontology.org/products/pages/downloads.html> from the 2024-04-24 release.

Heatmaps of differentially expressed, photosynthetic, and photorespiration genes were generated using the pheatmap v1.0.12 package (<https://github.com/raivokolde/pheatmap>). Genes (rows) were clustered using row scaled, Euclidean distance and the ward.D clustering approach.

Weighted Gene Co-expression Network Analysis (WGCNA), including network construction, module trait correlations, and intramodular connectivity was performed with the WGCNA v1.72-5 package (Langfelder & Horvath, 2008, 2012), incorporating samples from the 3 and 10 h samples for best results. Genes were filtered as in differential gene expression analysis and count data was normalized using the getVarianceStabilizedData function from the DESeq2 package. A soft power threshold of 30 was used by applying the elbow criterion to scale independence and mean connectivity. For module trait correlation analysis, the different combinations of time and genotype were discretized into presence (1)/ absence (0) values.

Enrichment of gene ontology for WGCNA modules was done using the same sources for GO annotations, but with a hypergeometric test using the phyper function. However, fgsea v1.24.0 was also used to test the enrichment of differentially expressed genes in modules using the previous ranking approach for DEGs.

Figures

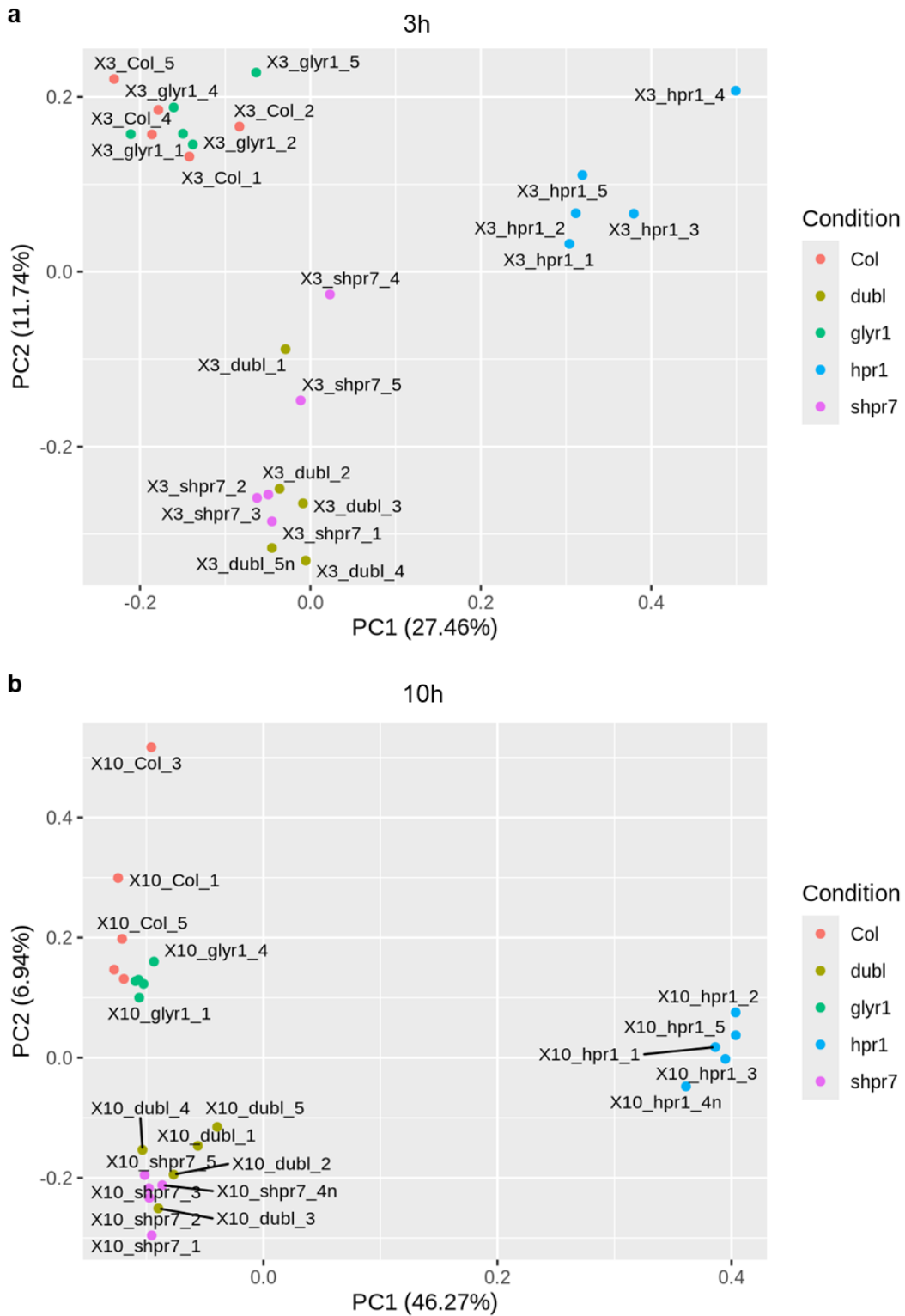


Figure 3.1. Principal Component Analysis plots of RNA-seq samples. All 5 biological replications of each line at 3 h (a) and 10 h (b) time points were plotted. dubl, the *glyr1-1 hpr1-1* double mutant.

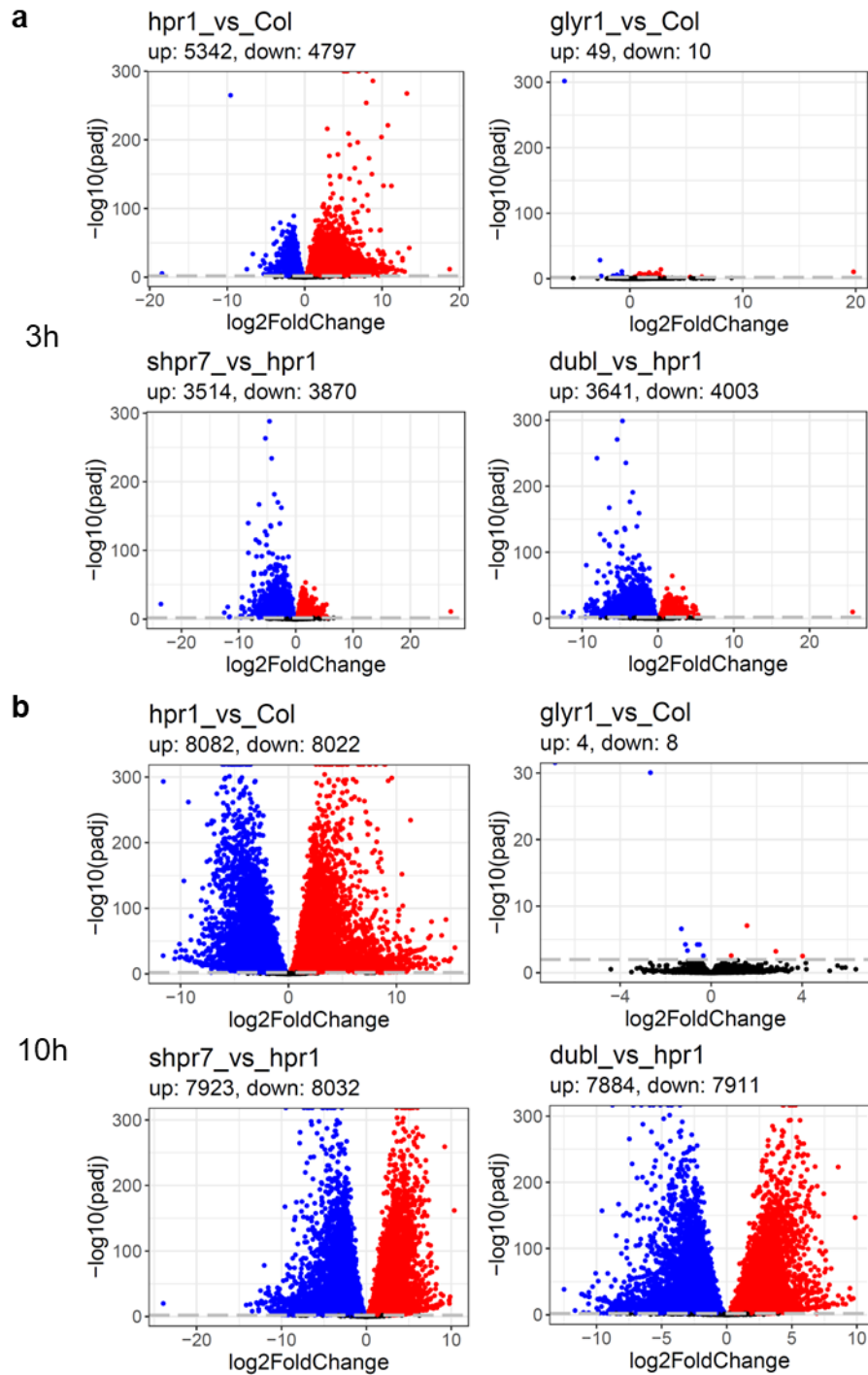


Figure 3.2. Volcano plots to display differentially expressed genes (DEGs). Four pairwise comparisons: *hpr1-1* vs. Col-0, *glyr1-1* vs. Col-0, *shpr7* vs. *hpr1-1*, and *glyr1-1 hpr1-1* vs. *hpr1-1* at 3 h (a) and 10 h (b) are shown. Genes that have an adjusted *p*-value of < 0.01 are considered DEGs and shown above the gray dashed line. Blue, red, and black dots represent the down-regulated, up-regulated, and unchanged genes, respectively.

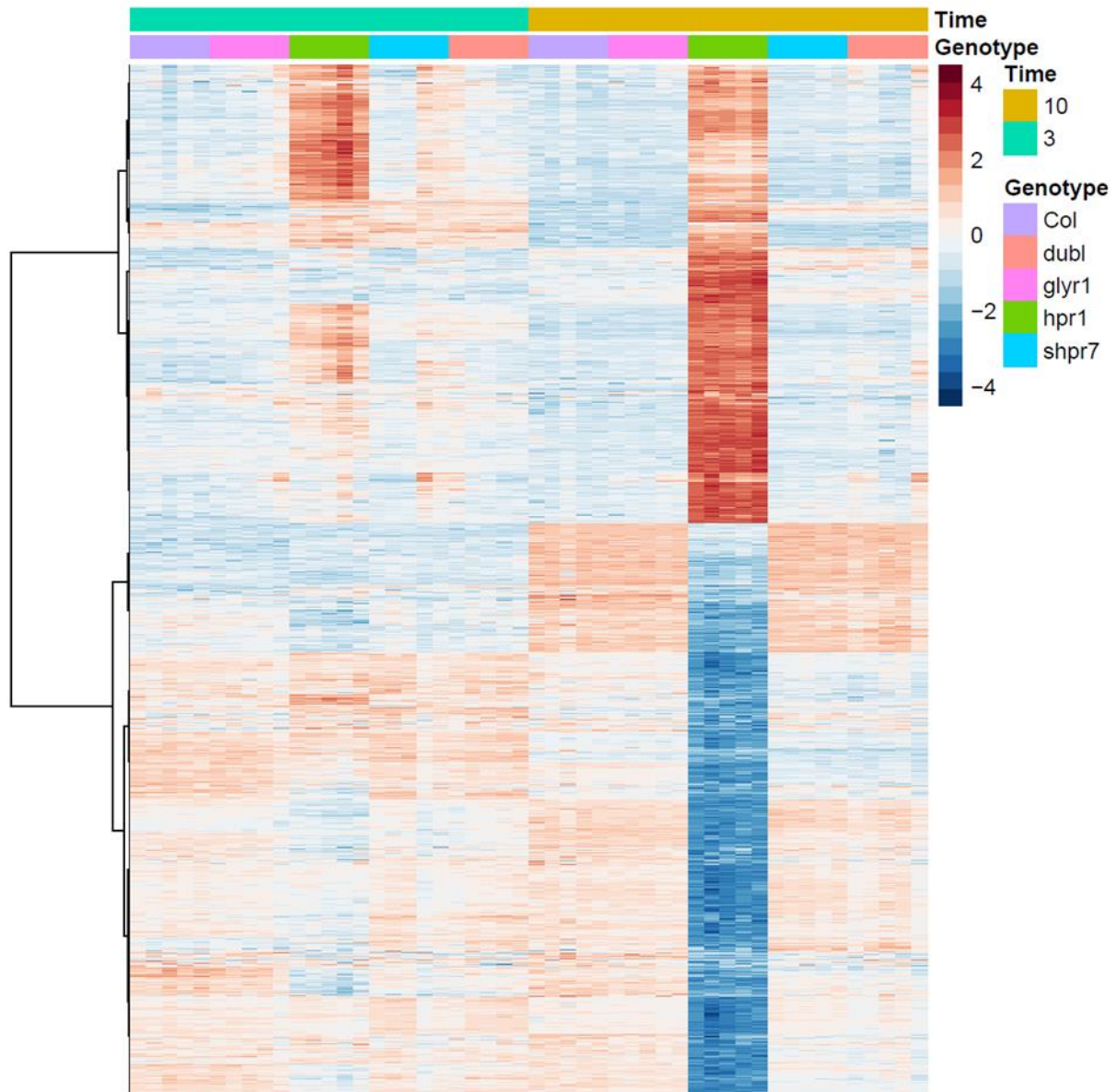


Figure 3.3. Heatmap of the expression of selective DEGs. DEGs in *hpr1-1* at 10 h that have an absolute \log_2 fold ratio >2 and an adjusted *p-value* of < 0.01 were selected. Gene expression was normalized to have an average value of 0 and indicated by the color legend.

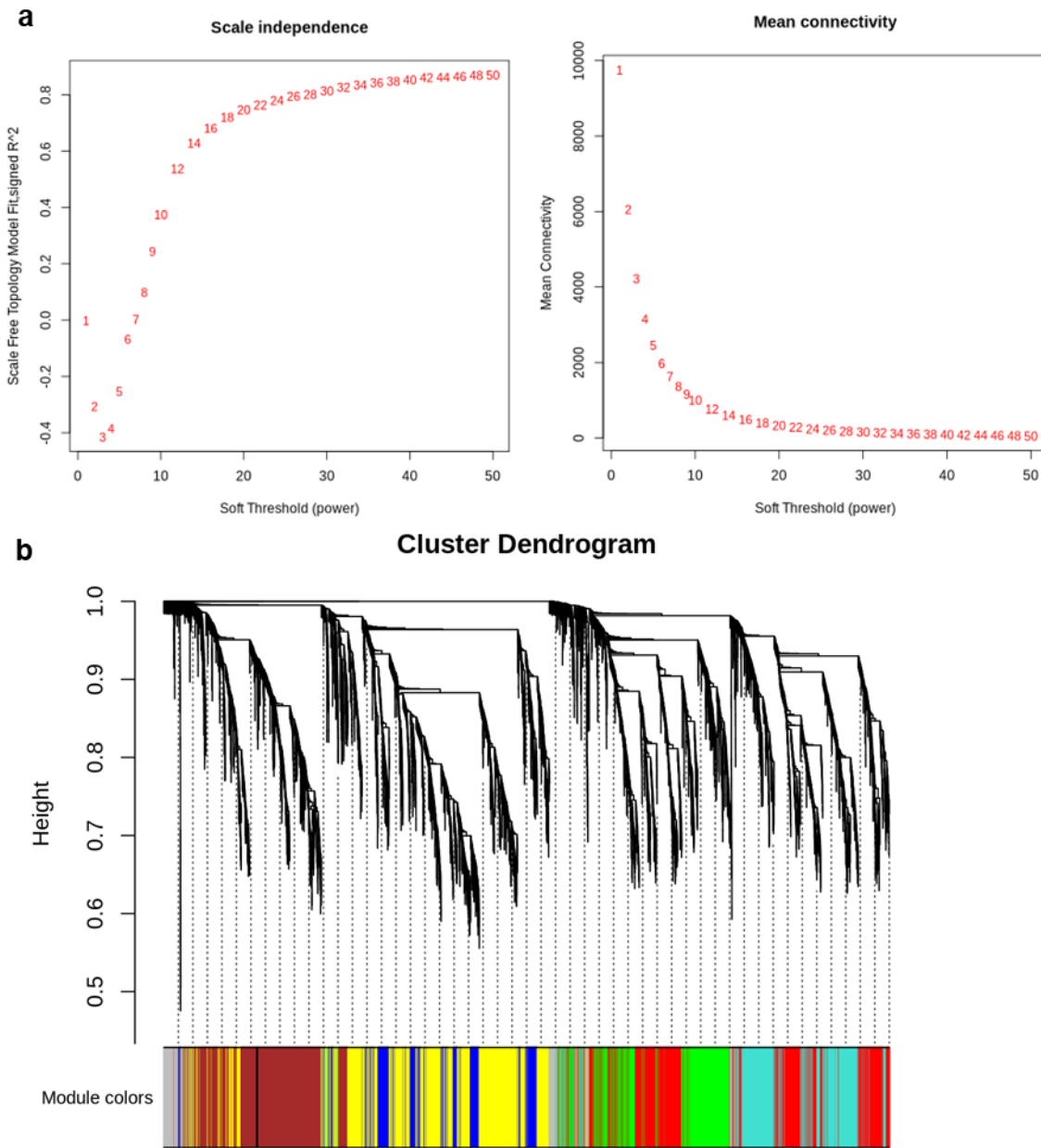
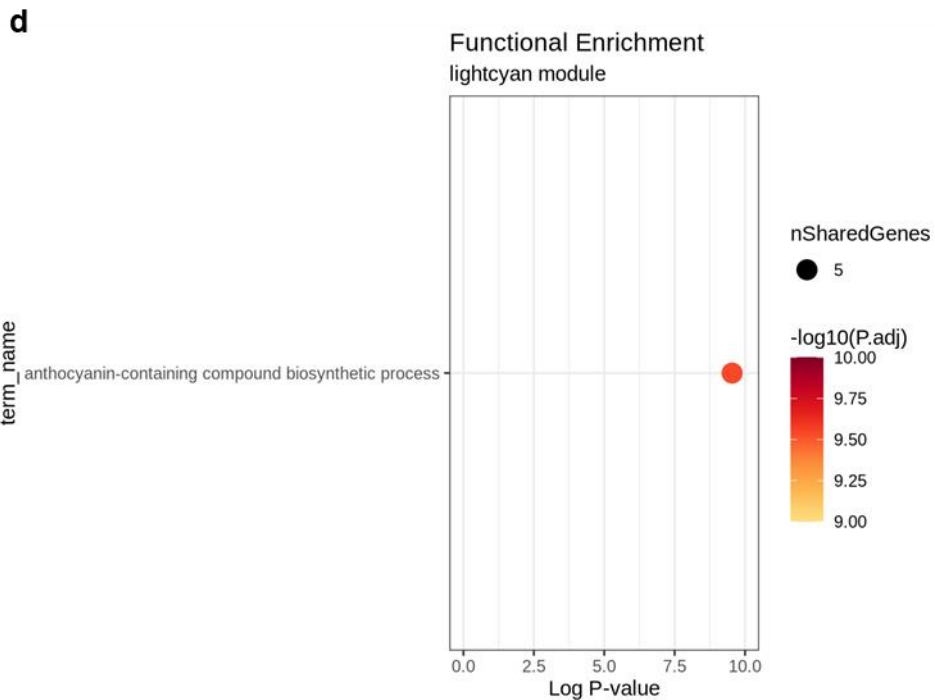
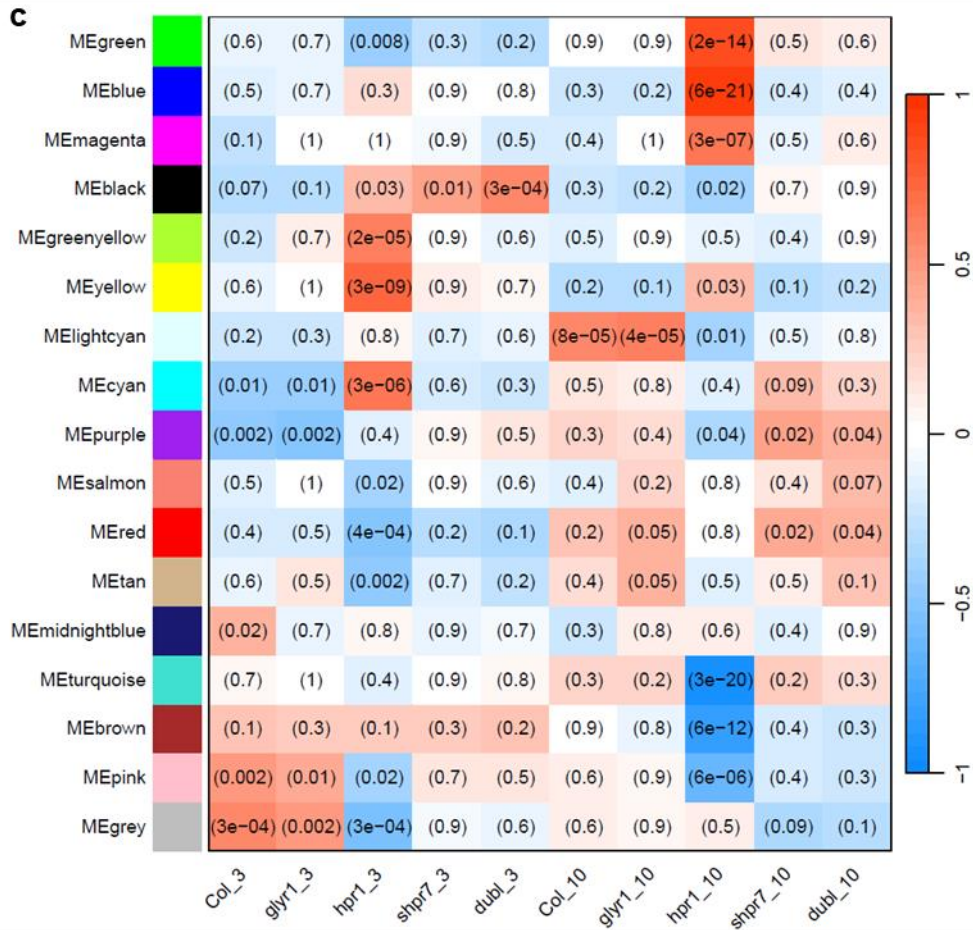


Figure 3.4. Construction of co-expression networks by weighted gene co-expression network analysis (WGCNA). (a) Plots showing the relationships between soft threshold and scale independence (left) and between soft threshold and mean connectivity (right). Soft threshold is determined by the elbow criterion. (b) A hierarchical cluster tree showing co-expression modules identified by WGCNA. Different colors represent different gene modules. The grey module includes genes that failed to be assigned. (c) Heap map of correlations between gene modules and plant genotypes at both time points. The correlation value is indicated by the color legend, and the number in parenthesis in each cell represents the adjusted p-value of the correlation. *dubl*, the *glyr1-1 hpr1-1* double mutant. (d) Gene Ontology (GO) enrichment analysis in the lightcyan module.

Figure 3.4 (cont'd)



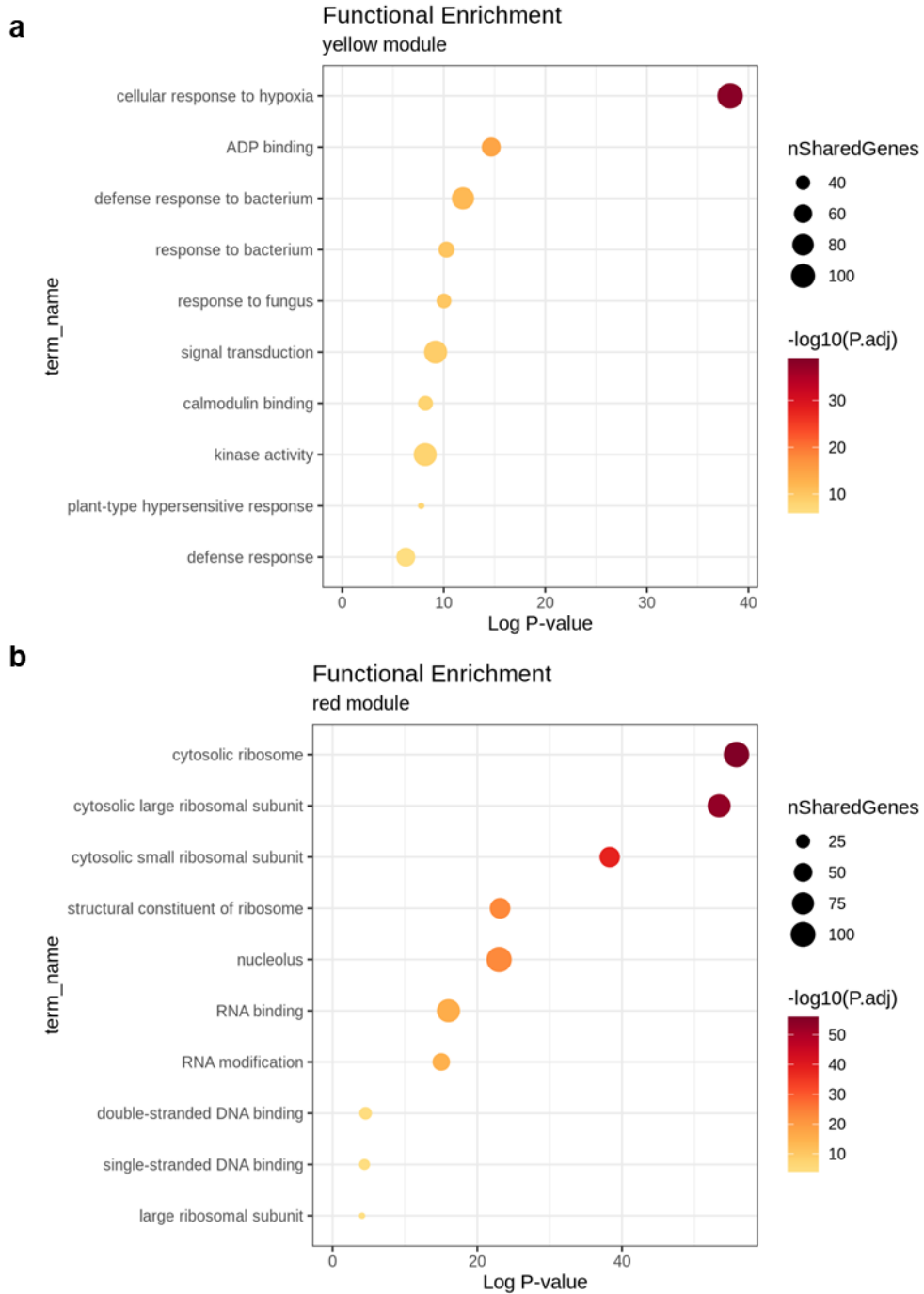


Figure 3.5. Gene Ontology (GO) enrichment analysis of modules closely connected to *hpr1* at 3 h. The top 10 enriched terms in the yellow (a) and red (b) modules are shown.

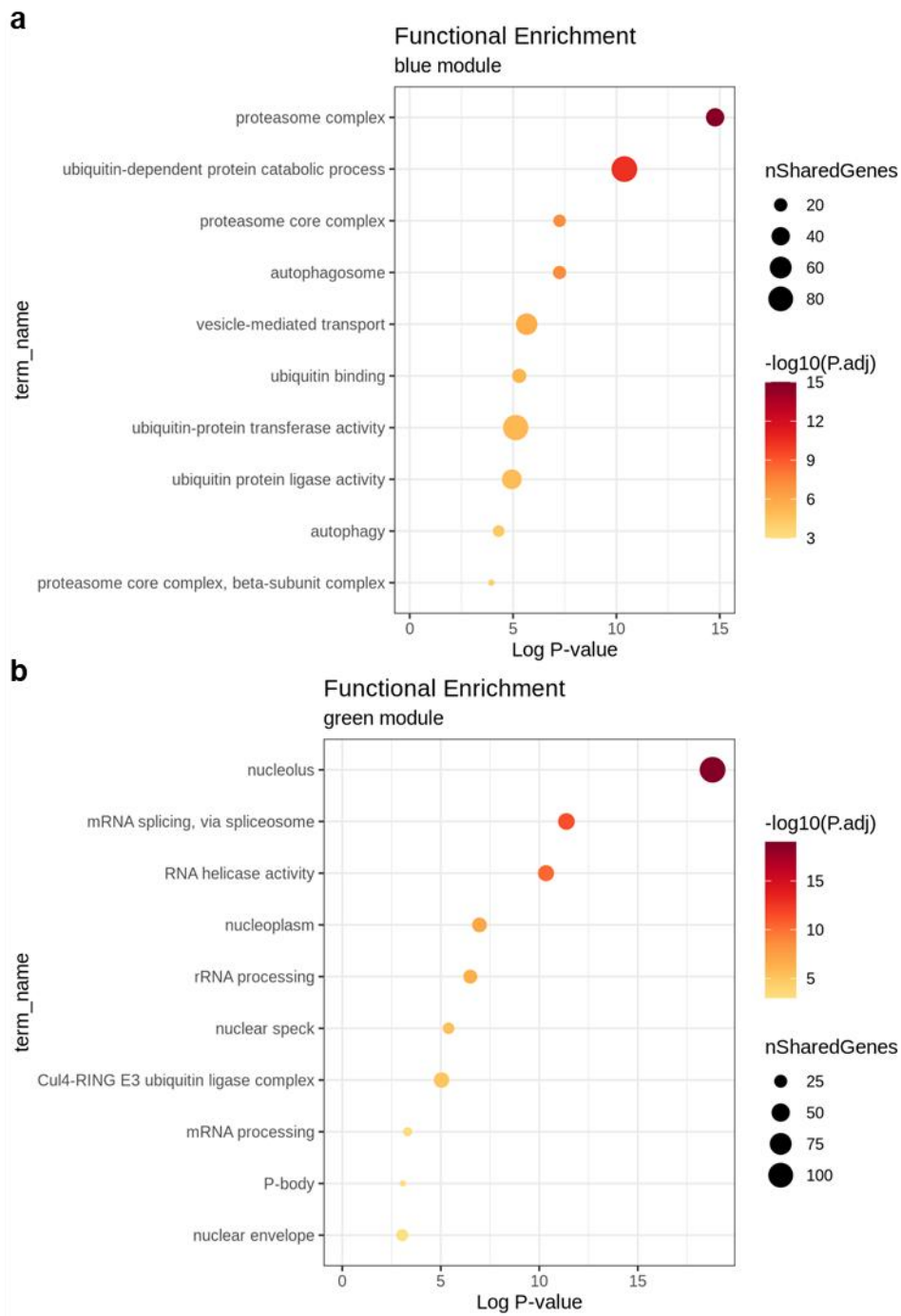
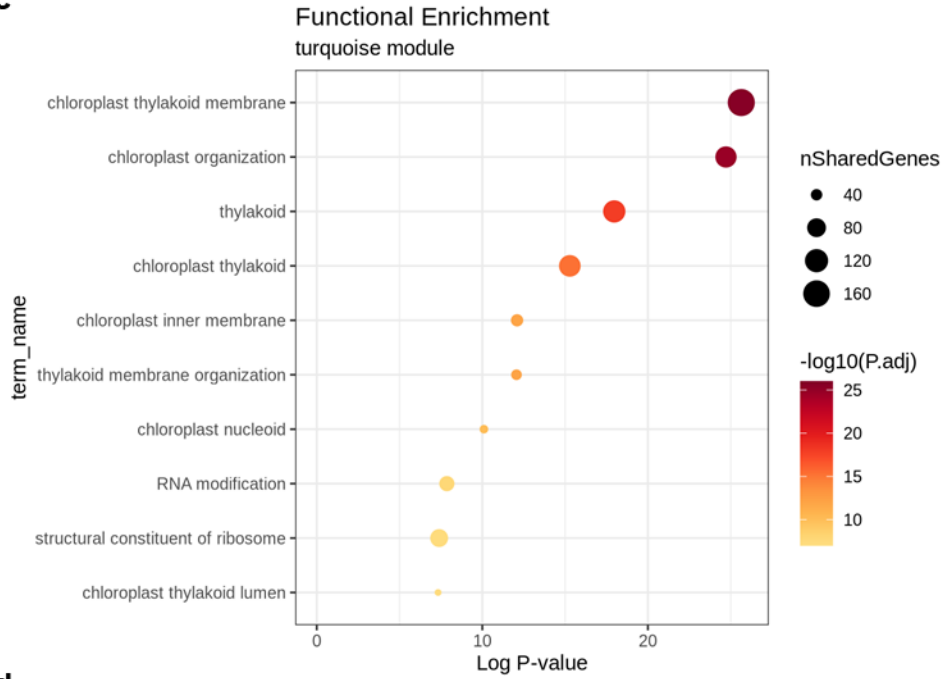


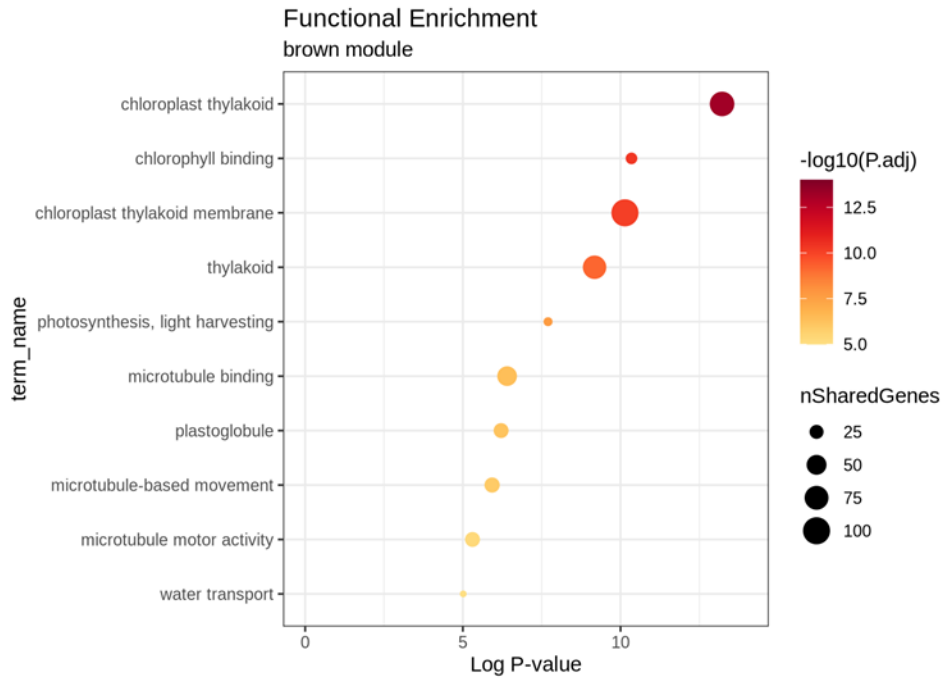
Figure 3.6. Gene Ontology (GO) enrichment analysis of modules closely connected to *hpr1* at 10 h. The top 10 enriched terms in the blue (a), green (b), turquoise (c) and brown (d) modules are shown.

Figure 3.6 (cont'd)

c



d



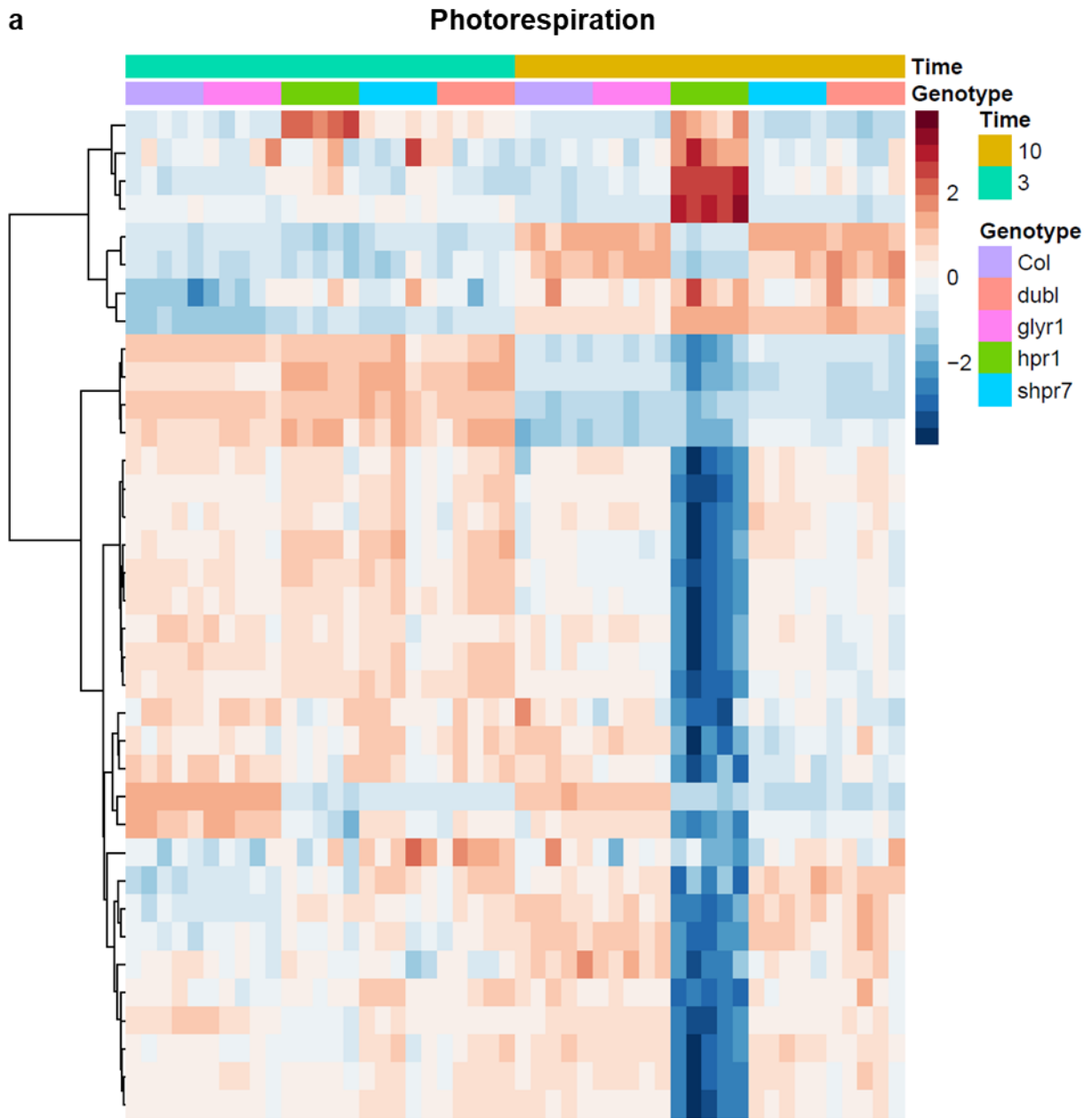
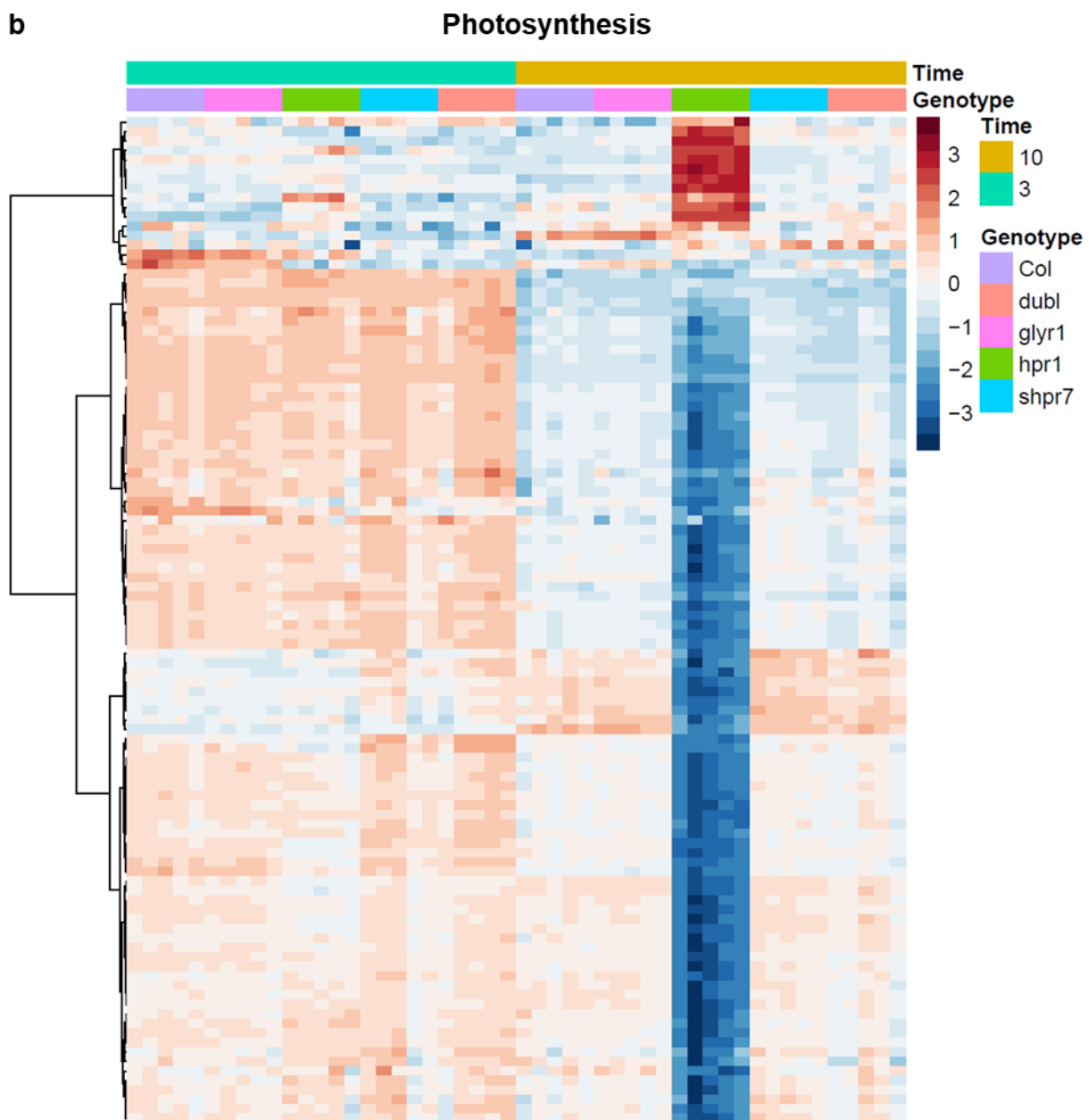


Figure 3.7. Heatmap of the expression of photorespiratory and photosynthetic genes. Expression of photorespiration (**a**) and photosynthesis (**b**) genes were normalized to have an average of 0 and indicated by the color legend.

Figure 3.7 (cont'd)



Tables

Table 3.1. Expression of selected top DEGs.

	Gene ID	3h				10h			
		<i>glyr1</i> vs. Col-0	<i>hpr1</i> vs. Col-0	<i>shpr7</i> vs. <i>hpr1</i>	<i>dubl</i> vs. <i>hpr1</i>	<i>glyr1</i> vs. Col-0	<i>hpr1</i> vs. Col-0	<i>shpr7</i> vs. <i>hpr1</i>	<i>dubl</i> vs. <i>hpr1</i>
log ₂ Fold Change									
1	AT1G20390	-2.64	-1.74	/	/	-2.67	/	-1.67	-2.43
2	AT5G19880	19.81	18.71	/	/	/	6.32	-4.66	/
3	AT2G43820	2.74	4.73	1.18	1.25	/	8.88	-5.17	-4.84
4	AT2G05380	/	3.24	/	/	1.57	4.96	/	/
5	AT3G06325	/	/	/	/	4.02	7.78	-5.75	-5.21
6	AT2G26400	/	-18.42	27.11	25.67	/	/	/	/
7	AT2G36790	/	7.98	-5.31	-5.39	/	5.42	-4.2	-3.31
8	AT1G05680	/	13.2	-4.61	-4.71	/	14.19	-5.77	-5.19
9	AT5G43450	/	7.02	-4.35	-4.34	/	5.51	-3.24	-2.53
10	AT2G41730	/	8.81	-6.42	-6.44	/	6.38	-4.75	-3.48
P _{adjust}									
1	AT1G20390	6.25 E ⁻²⁹	7.78 E ⁻¹⁵	n.s.	n.s.	8.78 E ⁻³¹	n.s.	4.13 E ⁻¹⁵	1.25 E ⁻²⁷
2	AT5G19880	4.72 E ⁻¹¹	2.28 E ⁻¹²	n.s.	n.s.	n.s.	4.68 E ⁻⁰⁴	7.73 E ⁻⁰³	n.s.
3	AT2G43820	1.01 E ⁻¹⁴	4.25 E ⁻⁵⁰	3.46 E ⁻⁰⁴	1.48 E ⁻⁰⁴	n.s.	0	0	1.1 E ⁻²⁹⁶
4	AT2G05380	n.s.	1.09 E ⁻²¹	n.s.	n.s.	8.55 E ⁻⁰⁸	9 E ⁻¹⁰⁰	n.s.	n.s.
5	AT3G06325	n.s.	n.s.	n.s.	n.s.	3.16 E ⁻⁰³	1.37 E ⁻²⁰	4.51 E ⁻²⁰	8.72 E ⁻¹⁸
6	AT2G26400	n.s.	4.29 E ⁻⁰⁶	1.03 E ⁻¹¹	1.19 E ⁻¹⁰	n.s.	n.s.	n.s.	n.s.
7	AT2G36790	n.s.	0	4.7 E ⁻²⁶⁴	2.1 E ⁻²⁷¹	n.s.	9.5 E ⁻¹¹⁰	2.72 E ⁻⁶⁹	3.04 E ⁻⁴⁴
8	AT1G05680	n.s.	3.3 E ⁻²⁶⁸	1.37 E ⁻⁷⁴	1.68 E ⁻⁷⁷	n.s.	2.9 E ⁻⁵⁹	1.63 E ⁻¹²	2.3 E ⁻¹⁰
9	AT5G43450	n.s.	0	1.8 E ⁻¹³⁵	5.5 E ⁻¹³⁵	n.s.	1.9 E ⁻⁵⁶	1.23 E ⁻²⁰	4.15 E ⁻¹³
10	AT2G41730	n.s.	1.7 E ⁻²⁸⁶	9.7 E ⁻¹⁶⁸	3.4 E ⁻¹⁶⁸	n.s.	7.5 E ⁻¹³⁴	3.02 E ⁻⁷⁸	3.91 E ⁻⁴³

Table 3.2. Functional description of selected top DEGs.

	Gene ID	Gene description
1	AT1G20390	Transposable_element_gene; gypsy-like retrotransposon family.
2	AT5G19880	Peroxidase superfamily protein.
3	AT2G43820	UDP-GLUCOSYLTRANSFERASE 74F2 (UGT74F2); ARABIDOPSIS THALIANA SALICYLIC ACID GLUCOSYLTRANSFERASE 1 (ATSAGT1); UDP-GLUCOSE:SALICYLIC ACID GLUCOSYLTRANSFERASE 1 (SGT1); Encodes a nicotinate-O-glycosyltransferase. Induced by Salicylic acid; virus; fungus and bacteria. Also involved in the tryptophan synthesis pathway. Independent of NPR1 for their induction by salicylic acid.
4	AT2G05380	Glycine-rich protein 3 short isoform (GRP3S) mRNA; the mRNA is cell-to-cell mobile.
5	AT3G06325	Natural antisense transcript overlaps with AT3G41762.
6	AT2G26400	Encodes a protein predicted to belong to the acireductone dioxygenase family.
7	AT2G36790	UDP-GLUCOSYL TRANSFERASE 73C6 (UGT73C6); encodes a UDP-glucose:flavonol-3-O-glycoside-7-O-glycosyltransferase attaching a glucosyl residue to the 7-O-position of the flavonols kaempferol, quercetin and their 3-O-glycoside derivatives.
8	AT1G05680	URIDINE DIPHOSPHATE GLYCOSYLTRANSFERASE 74E2 (UGT74E2); Encodes a UDP-glucosyltransferase that acts on IBA (indole-3-butyric acid) and affects auxin homeostasis. The transcript and protein levels of this enzyme are strongly induced by H ₂ O ₂ and may allow integration of ROS (reactive oxygen species) and auxin signaling.
9	AT5G43450	Encodes a protein whose sequence is similar to ACC oxidase.
10	AT2G41730	HRG1; H ₂ O ₂ response gene; sensor/responder of H ₂ O ₂ ; involved in maintaining embryonic root meristem activity. Expression in rosette leaves is activated by high concentration of boron.

Table 3.3. Number of genes in each co-expression module determined by WGCNA.

moduleColors	nGenes
black	148
blue	3886
brown	3047
cyan	36
green	2144
greenyellow	90
grey	843
lightcyan	11
magenta	121
midnightblue	17
pink	127
purple	91
red	1815
salmon	38
tan	76
turquoise	4680
yellow	2310

Table 3.4. The first 4 photorespiratory genes in the expression heatmap shown in Fig. 3.7a.

Gene ID	Gene name
AT1G36370	MORE SULPHUR ACCUMULATION1 (MSA1); SERINE HYDROXYMETHYLTRANSFERASE 7 (SHM7)
AT4G13890	SERINE HYDROXYMETHYLTRANSFERASE 5 (SHM5); EMBRYO SAC DEVELOPMENT ARREST 36 (EDA36); EMBRYO SAC DEVELOPMENT ARREST 37 (EDA37)
AT3G17240	LIPOAMIDE DEHYDROGENASE 2 (mtLPD2)
AT1G22020	SERINE HYDROXYMETHYLTRANSFERASE 6 (SHM6)

Table 3.5. Expression of candidates for the hypothetical cytosolic aminotransferase proposed in Chapter 2.

Gene ID	Gene name	3h				10h			
		<i>glyr1</i> vs. Col-0	<i>hpr1</i> vs. Col-0	<i>shpr7</i> vs. <i>hpr1</i>	<i>dubl</i> vs. <i>hpr1</i>	<i>glyr1</i> vs. Col-0	<i>hpr1</i> vs. Col-0	<i>shpr7</i> vs. <i>hpr1</i>	<i>dubl</i> vs. <i>hpr1</i>
AT1G79870	HPR2	/	/	/	/	/	-1.6	1.41	1.5
AT4G39660	AGT2	/	/	/	/	/	-0.78	0.61	0.71
AT2G38400	AGT3	/	/	/	/	/	1.44	-1	-1.09
AT3G08860	PYD4	/	3.87	/	/	/	4.24	-7.97	-4.49

CHAPTER 4. The role of photorespiration in plant immunity

4.1 Introduction

Plants have developed a sophisticated immune system during their co-evolution with pathogens in nature, which include two interacting and connected layers: pattern-triggered immunity (PTI) and effector-triggered immunity (ETI) (Dodds & Rathjen, 2010; Yuan *et al.*, 2021). PTI is triggered by the elicitors from pathogens, like the peptide flg22, which comes from the conserved domain of the bacterial flagellin (Yu *et al.*, 2017). During PTI, intracellular signaling, transcriptional reprogramming, and other physiological responses such as reactive oxygen species (ROS) burst, callose deposition, and biosynthesis of phytohormones salicylic acid (SA) and jasmonate (JA), limit pathogen growth (Yu *et al.*, 2017). ETI is activated by the recognition of virulent effectors that are secreted from pathogens into the plant cell (Cui *et al.*, 2015). ETI responses are similar to PTI but stronger, and often lead to local programmed cell death called hypersensitive response (HR) (Cui *et al.*, 2015).

As introduced in detail in Chapter 1, evidence for the role of photorespiration in plant immunity is emerging. Studies of the roles of photorespiration in plant-pathogen interaction have focused on H₂O₂ since photorespiration is considered as a major source of H₂O₂ in photosynthetic cells (Foyer *et al.*, 2009). In the photorespiratory pathway, glycolate is converted to glyoxylate by glycolate oxidases (GOXs) in the peroxisome, producing H₂O₂ that is then scavenged by catalases (CATs). Defects in GOXs generally induce depressed immune response and susceptible disease phenotypes in Arabidopsis, tobacco and tomato (Rojas *et al.*, 2012; Ahammed *et al.*, 2018), suggesting that the H₂O₂ produced by GOXs is important to immunity. In *cat* mutants, H₂O₂ accumulation along with SA-dependent defense phenotypes was found under normal conditions without pathogen infection (Takahashi *et al.*, 1997; Chamnongpol *et al.*, 1998; Mittler *et al.*, 1999; Chaouch *et al.*, 2010; Chaouch & Noctor, 2010), and Arabidopsis CAT2 has been shown to coordinate defense signaling (Giri *et al.*, 2017; Yuan *et al.*, 2017; Lv *et al.*, 2019), highlighting the crucial role of CAT-mediated H₂O₂ in immune response. It has also been reported that CAT and GOX can act together to regulate H₂O₂ homeostasis in defense response (Zhang *et al.*, 2016; Williams *et al.*, 2018). Additionally, the glycine decarboxylase complex (GDC) (Navarre & Wolpert, 1995; Yao *et al.*, 2002; Cristina Palmieri *et al.*, 2010; Gilbert & Wolpert, 2013), serine hydroxymethyltransferase (SHMT) (Fu *et al.*, 2022), and

glutamate:glyoxylate aminotransferase (GGAT) (González-lópez *et al.*, 2021) have been shown to involve in ROS homeostasis in immunity.

Photorespiratory metabolites also contribute to plant immunity. A soybean cytosolic SHMT, which has impaired tetrahydrofolate (THF) binding, was identified to confer resistance to the soybean cyst nematode (Liu *et al.*, 2012; Kandoth *et al.*, 2017; Korasick *et al.*, 2020), suggesting the connection between folate metabolism and immunity. In soybean, HPR was also found to interact with P34, the receptor for the *P. syringae* elicitor syringolide, and applying glycerate and 3-PGA to the plant was able to restrain syringolide-induced HR (Okinaka *et al.*, 2002). Additionally, photorespiration-associated amino acids have been shown to induce disease resistance in plants (Kadotani *et al.*, 2016; Yang *et al.*, 2017; Toyota *et al.*, 2018).

Other photorespiratory enzymes, including serine:glyoxylate aminotransferase (SGAT) (Taler *et al.*, 2004; Ahammed *et al.*, 2018) and glycerate kinase (GLYK) (Gao *et al.*, 2020), were also reported to play roles in plant-pathogen interaction, but the underlying mechanisms are unclear.

Although studies have shown that photorespiration impacts plant immune response through multiple processes, our current understanding of the underlying mechanism is still largely fragmentary. To further investigate the interaction between the photorespiratory pathway and plant immune system, I employed two strategies using the model plant *Arabidopsis thaliana* and the bacterial pathogen *Pseudomonas syringae* pv. *tomato* strain DC3000 (*Pst* DC3000). To test the hypothesis that photorespiration plays a positive role in plant immunity, I first assessed disease phenotypes of photorespiratory mutants and found that the peroxisomal photorespiratory enzyme HPR1 and the chloroplastic glycolate/glycerate transporter PLGG1 contribute to plant immune response via the photorespiratory pathway. Additionally, I quantified photorespiration under pathogen infection using the gas exchange experiment, but did not find evidence for the upregulation of photorespiration that had been reported by previous studies.

4.2 Results

4.2.1 Null mutants of *HPR1* and *PLGG1* show defects in immune response

To understand whether components of the photorespiratory pathway influence the warfare between the plant and pathogen, I tested a collection of *Arabidopsis* photorespiratory mutants, including those deficient in enzymes or transporters. Among the mutants, *hpr1* and *plgg1* consistently showed increased disease susceptibility.

Consistent with previous reports of the growth phenotypes of photorespiratory mutants (Timm *et al.*, 2008; Yang *et al.*, 2012), both *hpr1-1* and *plgg1-1* plants grown in ambient air exhibited small rosettes; in addition, *plgg1-1* also had lesions on leaves (**Fig. 4.1a**). When infiltrated with *Pst* DC3000, at 2 dpi (2 days post infiltration), both knockout lines of *HPR1* (*hpr1-1* and *hpr1-2*) and the null *PLGG1* allele showed a higher level of bacterial growth in plants compared with the wild-type (**Fig. 4.1b**). Consistently, the infected leaves of the *hpr1* mutants also exhibited more severe water-soaking symptoms (**Fig. 4.1c**), the symptoms that describe the pathogen-driven establishment of an aqueous apoplastic environment favoring infection (Xin *et al.*, 2016). Therefore, defective HPR1 or PLGG1 seems to compromise plant immune response.

To get a better understanding of the role of HPR1 and PLGG1 in plant immunity, the two main layers of the immune system, PTI and ETI, were tested in the mutants. PTI was induced by pre-treatment of 100 nM of flg22 followed by *Pst* DC3000 infiltration into the plants 22-24 h after flg22 inoculation, called the flg22 protection assay. At 2 dpi, the *hpr1-1* and *plgg1-1* mutants with flg22 pretreatment showed significantly higher levels of bacterial populations and more obvious water-soaking symptoms than Col-0 in the same group (**Fig. 4.1d and e**), indicating that the PTI response in *hpr1-1* and *plgg1-1* is compromised. To induce the ETI response, *Pst* DC3000 (*avrPpt2*), an avirulent strain carrying the effector protein AvrRpt2, was inoculated into the plants. AvrRpt2-induced ETI requires the activation of the receptor protein RPS2 (Spoel & Dong, 2012), whose null mutant *rps2-101c* (Mackey *et al.*, 2003) exhibited severe disease symptoms such as massive bacterial growth, necrosis and chlorosis in the leaves at 3 dpi (**Fig. 4.1f and g**). The disease symptoms in *hpr1-1* and *plgg1-1* were weaker than those in *rps2-101c* but apparently stronger than in Col-0 (**Fig. 4.1f and g**), suggesting impaired ETI response in these two photorespiratory mutants.

Other than bacterial growth inside the plants, more aspects of the PTI response were investigated in *hpr1-1* and *plgg1-1*. In response to flg22 treatment, comparable apoplastic ROS burst, a hallmark of early PTI response (Yu *et al.*, 2017), was observed in *hpr1-1*, *plgg1-1* and Col-0 (**Fig. 4.2a**), suggesting that HPR1 or PLGG1 defect does not impact apoplastic ROS burst. Late PTI response, including callose deposition as a physical barrier against pathogens (Yu *et al.*, 2017) and expression of the SA signaling marker gene *PR1* (Pieterse *et al.*, 2012), were also tested. Callose deposition was induced by flg22 application in both Col-0 and *plgg1-1* plants at 8

h post infiltration (8 hpi), but with clearly fewer induced callose deposits in *plgg1-1* (**Fig. 4.2b and c**). Although flg22 triggered *PR1* expression in all three lines at 24 hpi, *hpr1-1* and *plgg1-1* displayed much reduced upregulation compared with Col-0 (**Fig. 4.2d**). The weaker callose deposition and *PR1* gene expression in *hpr1-1* and *plgg1-1* are consistent with their susceptible disease phenotypes in the flg22 protection assay (**Fig. 4.1d and e**), indicating compromised PTI in *hpr1-1* and *plgg1-1*.

Taken together, results from bacterial growth, callose deposition and *PR1* gene expression analyses support the conclusion that defects in HPR1 and PLGG1 impair both PTI and ETI responses.

4.2.2 The growth and disease phenotypes of *hpr1* and *plgg1* can be largely rescued by high CO₂ conditions

To determine whether the function of HPR1 and PLGG1 in plant immunity is dependent on photorespiration specifically, and not a pleiotropic effect, mutant plants were grown under high CO₂ (2,000 ppm), where photorespiration is largely inhibited. As expected, the *hpr1-1* and *plgg1-1* mutants grown under high CO₂ had similar morphologies as Col-0 (**Fig. 4.3a**). To rule out the direct influence of high CO₂ on pathogens, *Pst* DC3000 and *Pst* DC3000 (*avrPpt2*) were grown on plates under ambient air or high CO₂. Results showed that these two strains had comparable growth irrespective of the environmental CO₂ concentrations (**Fig. 4.3b**).

The flg22 protection assay and *Pst* DC3000 (*avrPpt2*) infiltration were performed again on high CO₂-grown mutants to evaluate the function of HPR1 and PLGG1 in both PTI and ETI responses. With flg22 or mock treatments, the *hpr1-1* and *plgg1-1* mutants grown under high CO₂ exhibited comparable bacterial growth and water-soaking symptoms as Col-0 at 2 dpi (**Fig. 4.4a-d**). The null allele of *RPS2* grown under high CO₂ still showed susceptibility to *Pst* DC3000 (*avrRpt2*) at 3 dpi, but the disease phenotypes in *hpr1-1* and *plgg1-1* were similar to those in Col-0 (**Fig. 4.4e and f**). These results revealed that the compromised immune response in *hpr1-1* and *plgg1-1* can be largely rescued by high CO₂, prompting the conclusion that the effects of HPR1 and PLGG1 in plant immunity are dependent on the photorespiratory pathway.

4.2.3 Photorespiration rate is unchanged during plant interaction with *Pst* DC3000 and flg22 in Arabidopsis

As described in Chapter 1, various parameters, including the difference of net CO₂ assimilation rate between 2% and 21% O₂, photorespiratory CO₂ compensation point (Γ^*) and

the ratio of glycine to serine (Gly/Ser), have been used to estimate photorespiration rate. Using these methods, previous studies reported increased photorespiration rate in tomato upon *Pst* DC3000 infection (Ahammed *et al.*, 2018), in banana seedlings inoculated with *Fusarium oxysporum* f. sp. *cucumerinum* (FOC) (Dong *et al.*, 2016), and in nitrate-induced FOC-resistant cucumber plants (Sun *et al.*, 2021), suggesting that photorespiration may be actively regulated by plants as a strategy in defense. To further determine how photorespiration is regulated during defense, I performed gas exchange experiments to test whether an increased photorespiration rate can be seen in the Arabidopsis-*Pst* DC3000 model system used in my studies.

First, I used a moderate concentration of *Pst* DC3000 ($\sim 1 \times 10^6$ CFU ml⁻¹) to inoculate the plant and measured photorespiration rate in plants before and at 14-18 hpi of *Pst* DC3000 infiltration. *Pst* DC3000-treated plants had similar rubisco oxygenation rates (v_o) to mock-treated plants, suggesting that the photorespiration rate does not change under this condition (**Fig. 4.5a**). Photosynthesis-related parameters, including net CO₂ assimilation rate (A), rubisco carboxylation rate (v_c) and quantum efficiency of photosystem II (Φ_{II}), were also found to be comparable between the two groups of plants (**Fig. 4.5a**).

Next, I reasoned that the potential regulation of photorespiration may be restricted to a certain stage during plant-pathogen interaction instead of throughout the whole process, and therefore used a higher concentration of *Pst* DC3000 ($\sim 1 \times 10^7$ CFU ml⁻¹) and a late time point (23-25 hpi). Plants after *Pst* DC3000 infiltration showed a much lower v_o than those treated with mock (**Fig. 4.5b**), which was opposite to what I had expected. A, v_c and Φ_{II} were also found to decrease in *Pst* DC3000-treated plants at this time point, raising the possibility of cell damage that disrupts normal biological processes including photorespiration.

To avoid the difficulties in finding a perfect time point after *Pst* DC3000 infiltration, I switched to flg22 treatment to obtain a strong immune response without cell death. However, no obvious changes in v_o , A, v_c or Φ_{II} were found at 20-24 hpi with a high concentration of flg22 (500 nM) (**Fig. 4.6**), suggesting that neither photorespiration nor photosynthesis is influenced by PTI response at this time point.

Overall, using Arabidopsis with *Pst* DC3000 or flg22 treatment, I have not been able to reproduce the increased photorespiration rate reported previously. More investigations are needed to reach a clear conclusion on if and how photorespiration changes during plant-pathogen interaction.

4.3 Discussion and future directions

To elucidate the role of photorespiration in immunity, I tested the disease phenotypes of photorespiratory mutants and measured photorespiration rate on plants with pathogen treatments. I found that defects in Arabidopsis HPR1 and PLGG1 proteins compromise the immune response in both PTI and ETI, and the susceptible phenotypes shown in the *hpr1-1* and *plgg1-1* mutants can be reverted by high CO₂. These findings provide additional evidence for the important role of photorespiration in defense response. Based on these results and the literature on these two photorespiratory proteins, I hypothesize that the connections between HPR1/PLGG1 and defense response might be changes in ROS homeostasis or photorespiratory intermediates.

As discussed in detail in Chapter 1, in photosynthetic cells, photorespiration is a major source of H₂O₂ (Foyer *et al.*, 2009), a crucial signaling molecule during plant-pathogen interaction. Current evidence shows that the regulation of photorespiratory ROS is not limited to the H₂O₂-producing enzyme GOX and the H₂O₂-scavenging enzyme CAT, but involves other photorespiratory enzymes such as GDC, SHMT1 and GGAT1 (see Chapter 1 for details). Therefore, although neither HPR1 nor PLGG1 directly participates in producing or scavenging H₂O₂, the disruptions of photorespiratory metabolism in *hpr1-1* and *plgg1-1* may still influence ROS homeostasis. Although *hpr1-1* and *plgg1-1* had similar apoplastic ROS burst as Col-0, HPR1, which is in the peroxisomal matrix, and PLGG1, which is on the chloroplast inner envelope, are more likely to influence the homeostasis of intracellular, instead of extracellular, ROS (**Fig. 4.2a**). To test if *hpr1-1* and *plgg1-1* have decreased levels of intracellular ROS, compromised ROS signaling, or disordered ROS response, I have generated transgenic lines of these two mutants expressing the peroxisomal H₂O₂ reporter HyPer (Costa *et al.*, 2010) to monitor the dynamics of ROS inside peroxisomes, and started to test the expressions of ROS-responsive genes such as *OXII* (oxidative signal-inducible 1) (Rentel *et al.*, 2004; Petersen *et al.*, 2009), *GSTU24* (glutathione S-transferase tau 24) and *APX1* (ascorbate peroxidase 1) (Chaouch & Noctor, 2010), during defense.

As detailed in Chapter 1, photorespiratory metabolites have been shown to play a role in immunity. The deficiency of either HPR1 or PLGG1 was found in previous publications (Timm *et al.*, 2008; Pick *et al.*, 2013) and my work (Chapter 2) to cause increases in photorespiratory intermediates, including glycolate, glyoxylate, glycine, serine, hydroxypyruvate, and glycerate, under ambient air conditions. One or more of these accumulated photorespiratory intermediates

may be involved in the susceptible disease phenotypes in *hpr1-1* and *plgg1-1*. Since the application of glycerate inhibits HR in soybean (Okinaka *et al.*, 2002), glycerate may be a good candidate. To test this hypothesis, photorespiratory metabolites in the pathogen-treated mutants and Col-0 can be measured by GC-MS to identify candidate metabolites whose level changes correlate to immune response. These metabolites together with pathogens can then be applied to plants to validate their function.

I also measured photorespiration rate in *Arabidopsis* treated with *Pst* DC3000 or flg22, but failed to confirm the previously reported up-regulation of photorespiration. The low-throughput of gas exchange measurements by Li-COR might be a reason, as plants usually have big individual variations and it is difficult to capture small changes in photorespiration or investigate a series of time points with the current techniques. It is also possible that the regulation of photorespiration is highly dynamic or restricted to specific stages of the immune response, even specific plant-pathogen systems. Lastly, photorespiration is not a closed cycle (Fu *et al.*, 2023) The measured v_o only represents the rate of the initial step of photorespiration but not necessarily the whole process. If the activity of a photorespiratory enzyme or the concentration of a photorespiratory metabolite is regulated during plant-pathogen interaction after the initial stage, it may not alter v_o .

In summary, both the photorespiratory pathway and the immune response are complex processes. Large-scale and systematic approaches involving simultaneous measurements of photorespiration and immune response may be required, in order to obtain a comprehensive view of the interplay between these two systems under different conditions.

4.4 Methods

4.4.1 Plant and pathogen materials and growth conditions

Wild-type and mutant lines of *Arabidopsis thaliana* used in the study are all from the ecotype Col-0. Mutants *hpr1-1* (SALK_067724) and *plgg1-1* (SALK_053469) were the same lines as those used in Chapter 2. The *hpr1-2* mutant (SALK_143584) was characterized previously (Timm *et al.*, 2008) and used in a previous study in my lab (Li *et al.*, 2019a). The *rps2-101c* mutant was characterized before (Mindrinos *et al.*, 1994) and was kindly provided by Dr. Brad Day.

Arabidopsis seeds were directly sown in the soil in pots. After seed stratification in the dark at 4 °C for 3 to 7 days, pots were moved to growth chambers with ~100 $\mu\text{mol m}^{-2} \text{s}^{-1}$ white light, 21 °C, and 12 h/12 h light/dark cycle for plant growth.

Pseudomonas syringae pv. *tomato* strain DC3000 (*Pst* DC3000), strain *Pst* DC3000 (*avrPpt2*) and peptide flg22 were kindly provided by Drs. Sheng Yang He and Brad Day. *Pst* DC3000 and *Pst* DC3000 (*avrPpt2*) were grown on Modified Luria-Bertani medium (LM, 10.0 g Bacto tryptone, 6.0 g Bacto yeast extract, 1.5 g K_2HPO_4 , 0.6 g NaCl, 0.4 g $\text{MgSO}_4 \cdot 7\text{H}_2\text{O}$ per liter H_2O) at 28-30 °C with Rif₅₀ and Rif₅₀/Kan₅₀ respectively.

4.4.2 Pathogen infection assays

Bacterial infiltration in Arabidopsis was performed using a previous protocol (Yao *et al.*, 2013). Briefly, 5-week-old Arabidopsis plants were syringe-infiltrated with a bacterial suspension [$\sim 1 \times 10^5$ colony-forming units (CFU) ml^{-1} *Pst* DC3000 or $\sim 1 \times 10^6$ CFU ml^{-1} *Pst* DC3000 (*avrPpt2*) in 0.25 mM MgCl_2 solution]. Plants were dried in the air in the growth chamber and covered with domes to keep high humidity. Two or 3 days after inoculation, i.e., 2 dpi for *Pst* DC3000 and 3 dpi for *Pst* DC3000 (*avrPpt2*), plant tissue was collected and ground, and bacterial populations were determined by serial dilutions.

For flg22 protection assays, plant leaves were syringe-infiltrated with 100 nM flg22 or 0.1% DMSO (mock). After 22–24 h, plants in the growth chamber without domes were infiltrated again with a bacterial suspension [$\sim 1 \times 10^6$ CFU ml^{-1} *Pst* DC3000 in 0.25 mM MgCl_2 solution]. Bacterial populations were quantified at 2 dpi.

4.4.3 Apoplastic ROS burst assay

As described previously (Zhang *et al.*, 2019), 4 mm leaf discs were taken from ~5-week-old plants and kept floating on water (adaxial side up) in 96-well plates overnight. Then water was removed and replaced with 100 μl immune-eliciting solution [34 $\mu\text{g ml}^{-1}$ luminol (Sigma-Aldrich), 20 $\mu\text{g ml}^{-1}$ horseradish peroxidase (Sigma-Aldrich) and 100 nM flg22 (0.1% DMSO for mock) in water]. Luminescence was measured at 470nm with a SpectraMax L microplate reader (Molecular Devices).

4.4.4 Quantification of callose deposits

Five-week-old plants were infiltrated with 100 nM flg22 or 0.1% DMSO on three leaves for each plant. After 8 h, leaves were sampled and stained using a previous protocol (Bach-Pages & Preston, 2018) with modifications. Briefly, leaves were soaked in 100% ethanol overnight to

clear chlorophyll, then fixed with acetic acid/ethanol solution (1:3, v/v) for 2 h. Next, samples were incubated sequentially in 75% ethanol, 50% ethanol and 150 mM K₂HPO₄ (pH 9.5) for 15 min at each step, then stained with 0.01% aniline blue in 150 mM K₂HPO₄ (pH 9.5) solution at 4 °C overnight. Leaves were mounted in 50% glycerol on glass slides and observed with the Axio Imager M1 epi-fluorescence microscope (ZEISS), using the DAPI filter. The number of callose deposits was counted with ImageJ (<https://imagej.net/ij/>).

4.4.5 RNA extraction and qRT-PCR

Five-week-old plants were infiltrated with 100 nM flg22 or 0.1% DMSO. After ~24 h, leaf tissue was sampled and ground in liquid nitrogen. RNA was extracted using the NucleoSpin RNA Plant kit (MACHEREY-NAGEL), then reverse transcribed using the High Capacity cDNA Reverse Transcription Kit (Applied Biosystems). Fast SYBR Green Master Mix (Applied Biosystems) was used with a 7500 Fast Real-Time PCR System (Applied Biosystems) for real-time PCR. The primer pairs are 5'-GGCTAACTACAACACTACGCTG-3' and 5'-TCTCGTTCACATAATTCCCAC-3' for *PR1*; and 5'-GGTTACAAGACAAGGTTCACTC-3' and 5'-CATTCAGGACCAAACACTCTTCAG-3' for the internal control gene *PP2AA3*. Data of each gene was normalized to its averaged gene expression in mock-treated Col-0.

4.4.6 Gas exchange measurements

Mature, fully-expanded leaves from 5- to 5.5-week-old plants were used in gas exchange measurements with LI-6800 (LI-COR Biosciences, Lincoln, Nebraska, USA). During measurements, chamber temperature was maintained at ~25°C and vapor pressure deficit was controlled at 1-1.5 kPa H₂O. Each leaf was measured under a series of light intensities: 800, 100, 50, 45, 40, 35, 30, 25 μmol m⁻² s⁻¹. The same leaf was measured twice, before and after pathogen treatments. Treatments used and corresponding time points are: *Pst* DC3000 (~1 × 10⁶ CFU ml⁻¹) at 14-18 hpi, *Pst* DC3000 (~1 × 10⁷ CFU ml⁻¹) at 23-25 hpi, 500 nM flg22 treatment at 20-24 hpi, and 0.25 mM MgCl₂ solution or 0.1% DMSO as mock treatments.

Net CO₂ assimilation rate (*A*) and quantum efficiency of photosystem II (Φ_{II}) were directly measured with LI-6800, and rubisco carboxylate rate (*v_c*) and oxygenation rate (*v_o*) were estimated based on a previous protocol (Gregory *et al.*, 2023). In brief, the estimation was based on $v_c = (A + R_L) / (1 - \Gamma^*/C_c)$ and $v_o = (v_c - A - R_L) / 0.5$, where the partial pressure of chloroplastic CO₂ (*C_c*) was calculated using $C_c = C_i - (A / g_m)$. Among these parameters, the partial pressure of intercellular CO₂ (*C_i*) was provided by LI-6800, non-photorespiratory CO₂ release in the light

(R_L) was determined using the common intersection method (Walker *et al.*, 2016a). Finally, the partial pressure of CO₂ in the chloroplast at the photorespiratory compensation point (Γ^*) and mesophyll conductance to CO₂ (g_m) were assumed to be 4.88 Pa and 2.23 $\mu\text{mol m}^{-2} \text{s}^{-1} \text{Pa}^{-1}$, respectively, based on previous measurements (Bao *et al.*, 2021).

4.4.7 Statistics and plots

Data analysis and plots were conducted as described in Chapter 2. Student's paired two-tailed *t*-test was used for pairwise comparison. One-way or Two-way ANOVA with Tukey's HSD test was used for multi-comparison.

Figures

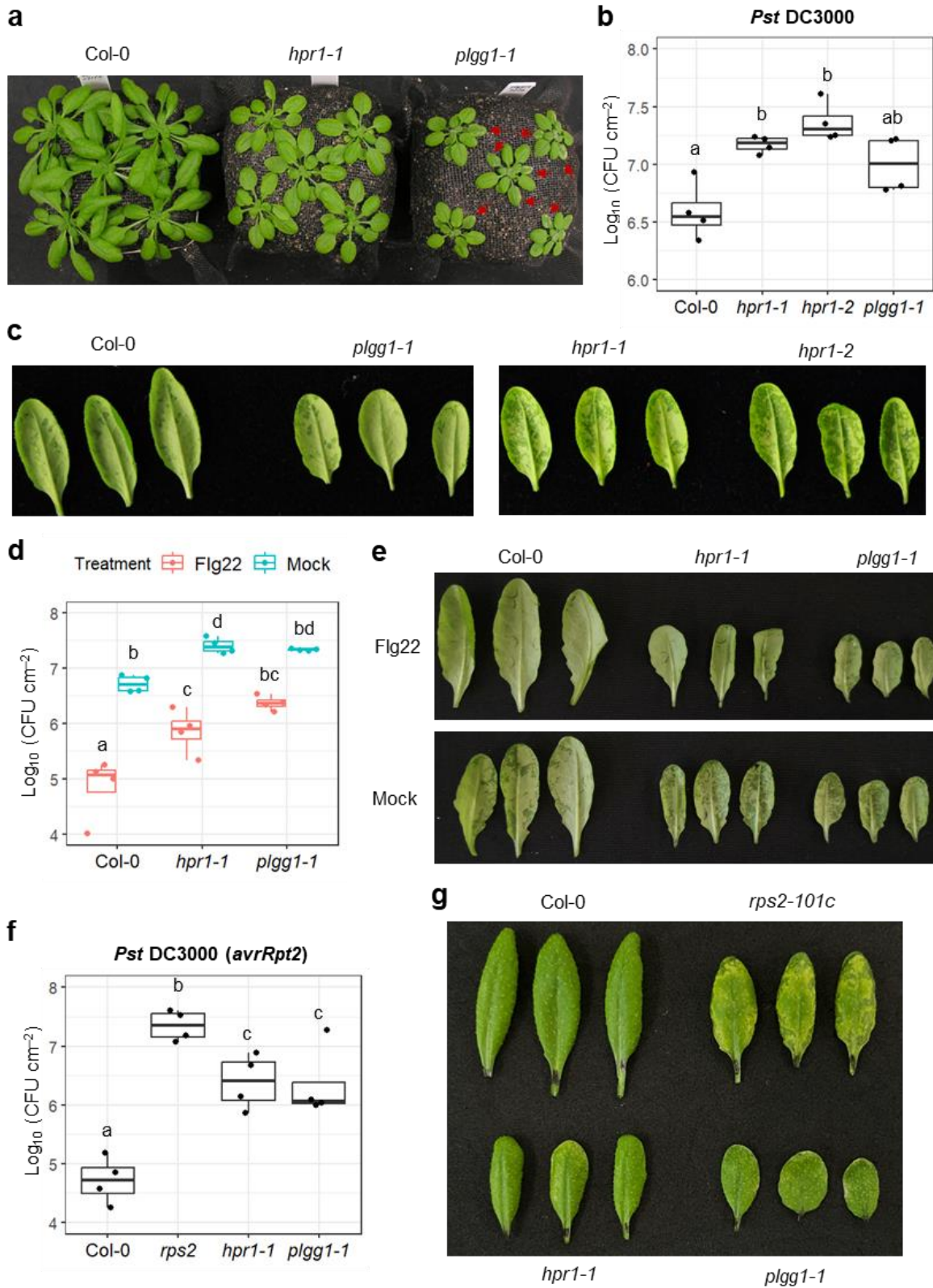


Figure 4.1. Null mutants of *HPR1* and *PLGG1* show defects in growth and immune response.

Figure 4.1 (cont'd)

(a) Five-week-old plants grown under ambient CO₂. Red arrows indicate the yellow lesions in the older leaves of *plgg1-1*. **(b, c)** Quantification of bacterial populations inside the leaves (b) and water-soaking symptoms on the leaves (c) at 2 d post infiltration (2 dpi) with *Pseudomonas syringae* pv. *tomato* DC3000 (*Pst* DC3000) at $\sim 1 \times 10^5$ CFU ml⁻¹. **(d, e)** Quantification of bacterial populations inside the leaves (d) and water-soaking symptoms on the leaves (e) that were pretreated with 100 nM flg22 and then infiltrated 24 h later with *Pst* DC3000 $\sim 1 \times 10^6$ CFU ml⁻¹. Plant leaves were sampled at 2 dpi. **(f, g)** Quantification of bacterial populations inside the plant leaves (f) and disease symptoms on the leaves (g) at 3 dpi with *Pst* DC3000 (*avrRpt2*) at $\sim 1 \times 10^6$ CFU ml⁻¹. Five-week-old plants were used in all experiments. Different letters indicate statistically significant differences ($p < 0.05$), which were determined by One-way (b, f) or Two-way (d) ANOVA with Tukey's HSD test. Biological replicates: n=4.

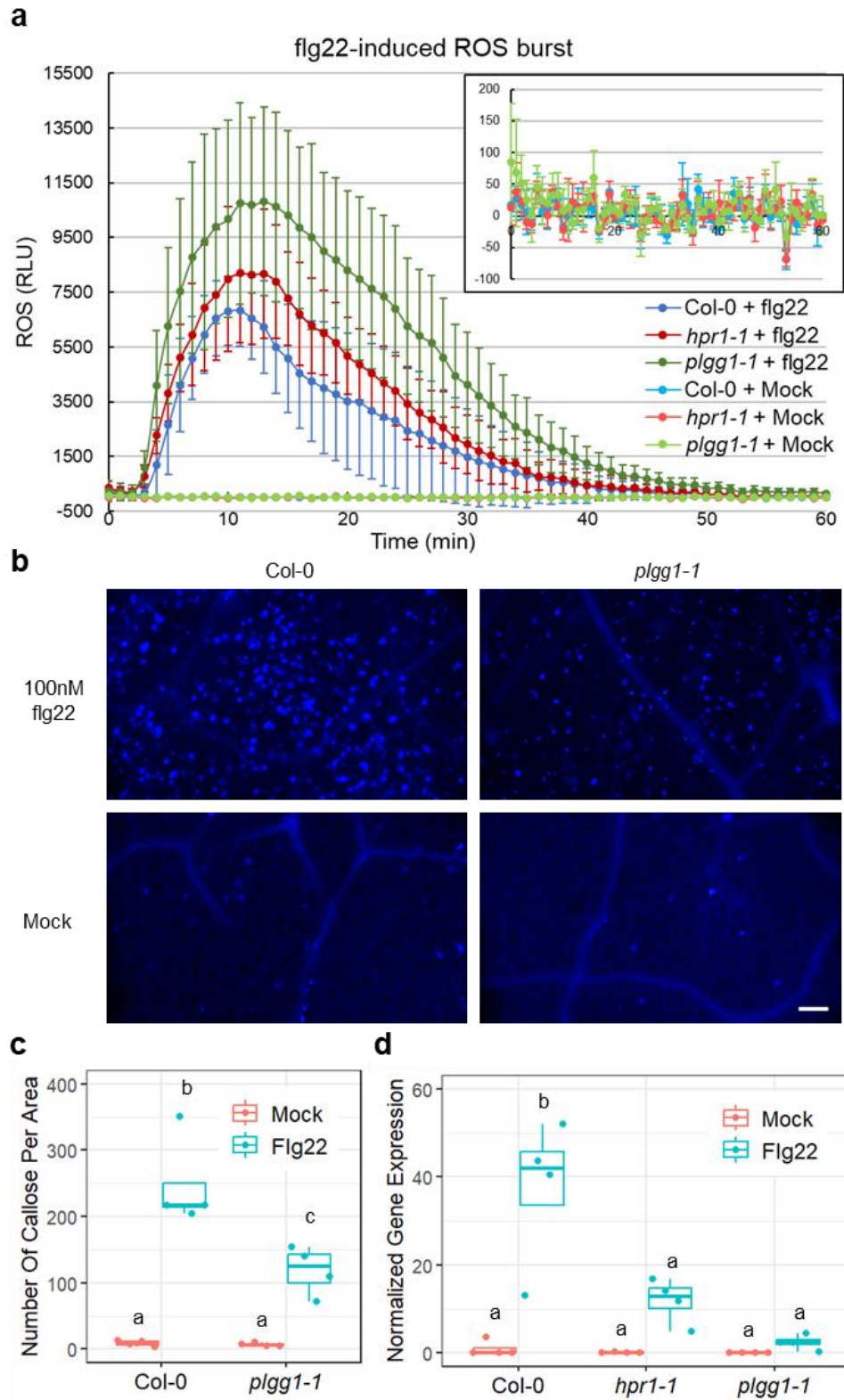


Figure 4.2. PTI response of *hpr1* and *plgg1* in apoplastic ROS burst, callose deposition, and expression of the *PR1* gene.

Figure 4.2 (cont'd)

(a) Apoplastic ROS burst induced by 100 nM flg22. 0.1% DMSO was used as the mock treatment. Results represent the mean \pm SD. Biological replicates: n=6 for mock-treated plants, and n=5 for flg22-treated plants. **(b)** Callose deposits induced by 100 nM flg22 at 8 h post infiltration (hpi). Leaves were stained with 0.1% aniline blue and observed under an epifluorescence microscope using a DAPI filter. Scale bar = 100 μ m. **(c)** Callose deposits quantified using ImageJ. Biological replicates: n=4. **(d)** Expression of *PR1* induced by 100 nM flg22 at 24 hpi. *PP2AA3* was used as the internal control and data was normalized to the average of *PR1* gene expression in mock-treated Col-0. Biological replicates: n=4. Five-week-old plants were used in all experiments. Different letters in (c) and (d) indicate statistically significant differences ($p < 0.05$), which were determined by Two-way ANOVA with Tukey's HSD test.

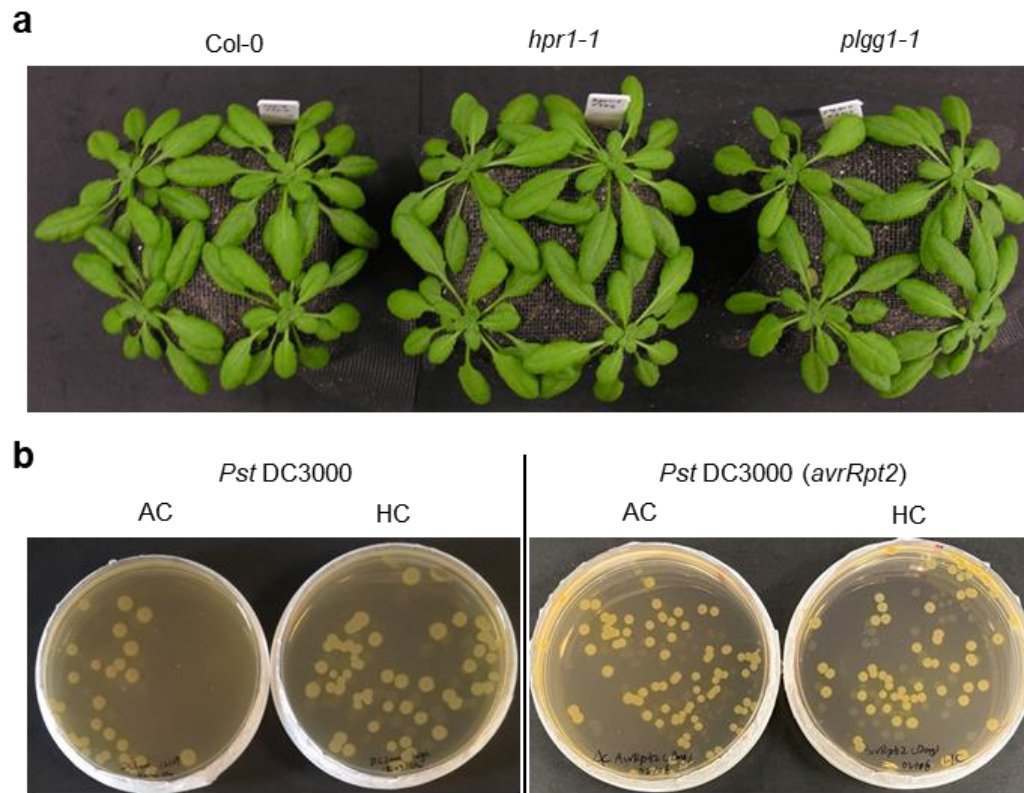


Figure 4.3. Growth phenotypes of plants and pathogens under high CO₂ conditions. (a) Five-week-old plants grown under 2,000 ppm of CO₂. **(b)** *Pst* DC3000 and *Pst* DC3000 (*avrRpt2*) grown in high CO₂ (2,000 ppm, HC) or ambient air (AC) growth chambers for 4 or 3 days.

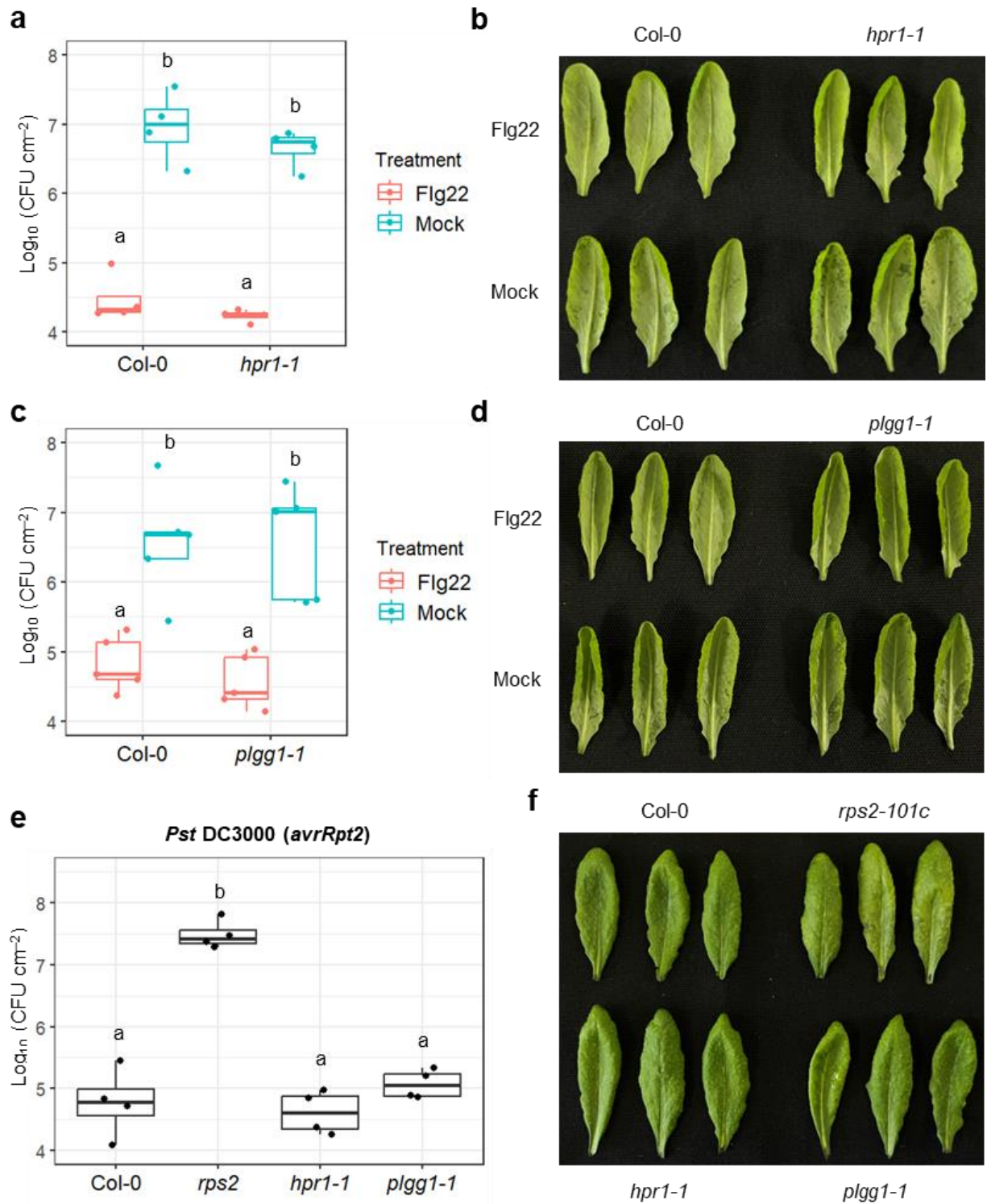


Figure 4.4. Disease phenotypes of *hpr1* and *plgg1* are largely rescued by high CO₂ conditions.

Figure 4.4 (cont'd)

(a, b) Quantification of bacterial population inside the leaves (a) and water-soaking symptoms on the leaves (b) of Col-0 and *hpr1-1* plants that were pretreated with 100 nM flg22, and then infiltrated 24 h later with *Pst* DC3000 at $\sim 1 \times 10^6$ CFU ml⁻¹. Plant leaves were sampled at 2 dpi.

(c, d) The level of bacterial populations inside the leaves (c) and water-soaking symptoms on the leaves (d) of Col-0 and *plgg1-1* plants that were pretreated with 100 nM flg22, and then infiltrated 24 h later with *Pst* DC3000 at $\sim 1 \times 10^6$ CFU ml⁻¹. Plant leaves were sampled at 2 dpi.

(e, f) Quantification of bacterial populations inside the leaves (e) and disease symptoms on the leaves (f) at 3 dpi with *Pst* DC3000 (*avrRpt2*) at $\sim 1 \times 10^6$ CFU ml⁻¹. Five-week-old plants were used in all experiments. Different letters indicate statistically significant differences ($p < 0.05$), which were determined by One-way (e) or Two-way (a, c) ANOVA with Tukey's HSD test. Biological replicates: n=4.

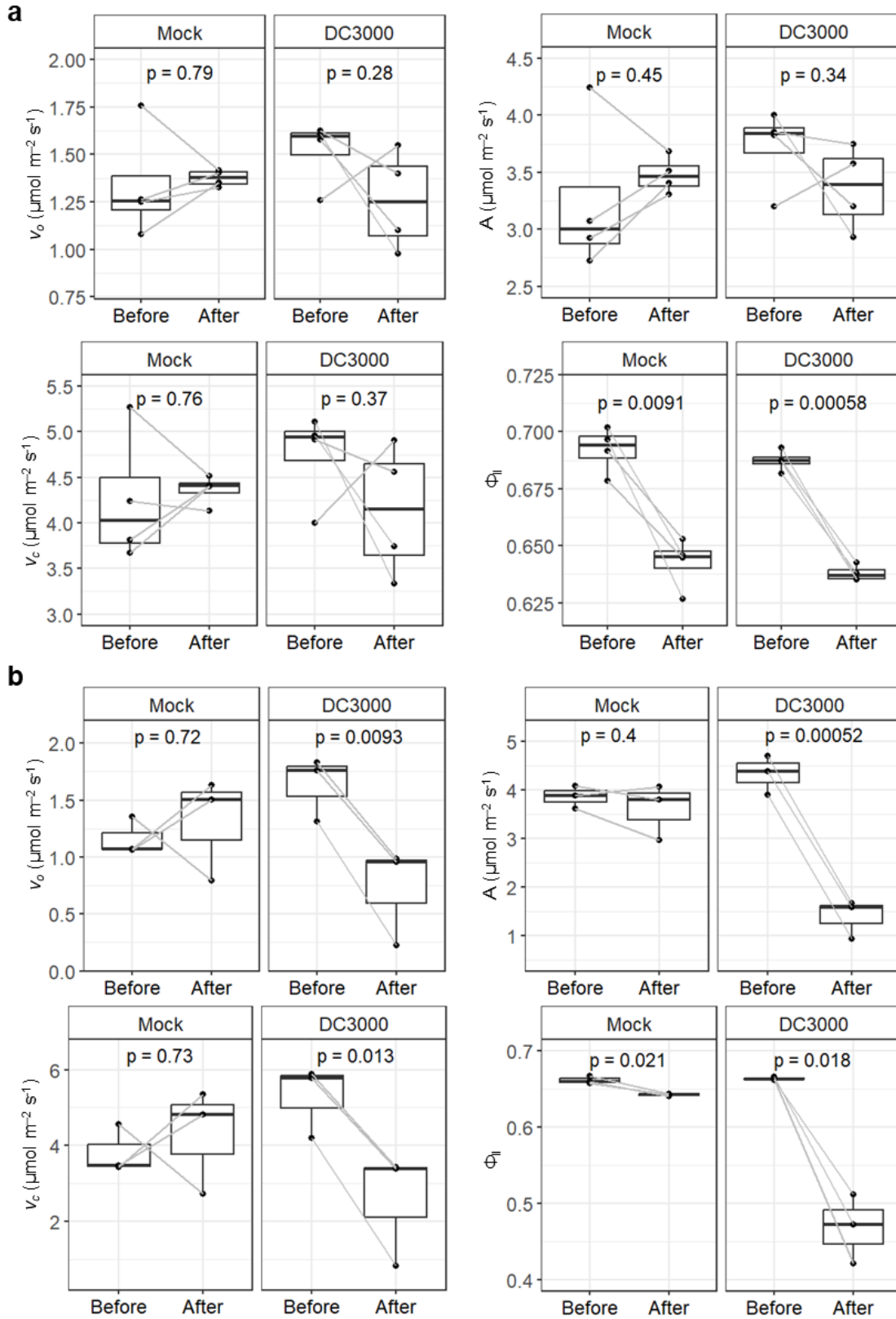


Figure 4.5. Measurement of photorespiration and photosynthesis under normal light conditions on plants treated with *Pst* DC3000.

Figure 4.5 (cont'd)

(a) Rubisco oxygenation rate (v_o), net CO₂ assimilation rate (A), rubisco carboxylation rate (v_c) and quantum efficiency of photosystem II (Φ_{II}) of Col-0 plants before *Pst* DC3000 ($\sim 1 \times 10^6$ CFU ml⁻¹) treatment and at 14-18 hpi. Biological replicates: n=4. **(b)** v_o , A, v_c and Φ_{II} of Col-0 plants before *Pst* DC3000 ($\sim 1 \times 10^7$ CFU ml⁻¹) treatment and at 23-25 hpi. Biological replicates: n=3. MgCl₂ solution (0.25 mM) was used as mock. The p values were determined by Student's paired two-tailed t -test.

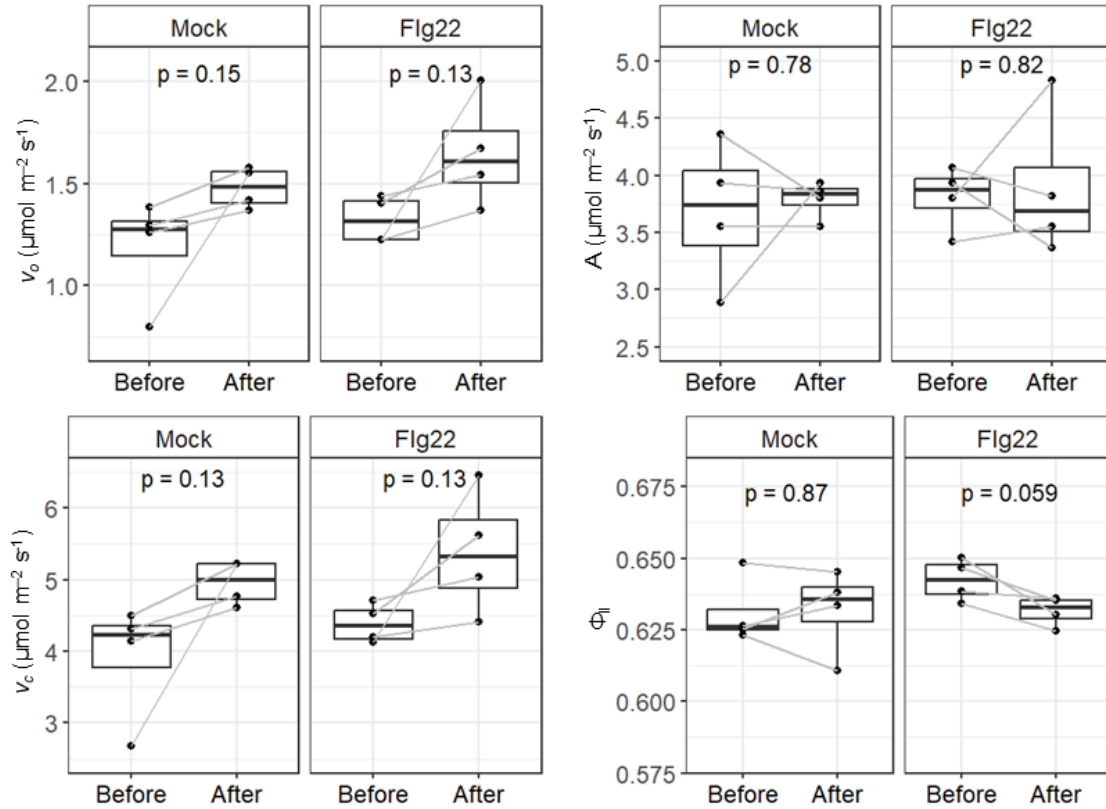


Figure 4.6. Measurements of photorespiration and photosynthesis under normal light conditions on plants treated with flg22. v_o , A , v_c and Φ_{II} of Col-0 plants before 500 nM flg22 treatment and at 20-24 hpi are shown. Biological replicates: $n=4$. DMSO (0.1%) was used as mock. The p values were determined by Student's paired two-tailed t -test.

CHAPTER 5. Summary and future perspectives

My dissertation focuses on the role of photorespiration in plants under stress conditions, high light and pathogen infection in particular. I applied various strategies to dissect the relationships between photorespiration and stress conditions and investigate the underlying mechanisms.

To understand how photorespiration is modulated under high light, I performed a screening for suppressors of the photorespiratory mutant *hpr1*. *GLYR1*, which encodes a cytosolic enzyme that converts glyoxylate to glycolate, was identified as the gene carrying the causal mutation that partially reverts the mutant phenotypes of *hpr1* under high light, including growth, photorespiratory metabolites, and photosynthesis. Defective *GLYR1* can also rescue the phenotypes of the catalase mutant *cat2* under high light, but not the mutant of the *PLGG1*. Further investigations with metabolic and genetic tools suggest the existence of a cytosolic glyoxylate shunt of photorespiration, where glyoxylate and serine can be converted into hydroxypyruvate by an unknown aminotransferase, feeding into the HPR2-mediated reaction. The glycerate produced by HPR2 returns to chloroplast and eventually carbons are recycled to the Calvin-Benson cycle. This cytosolic glyoxylate shunt supports the flexibility of photorespiration, which may be important in plant response to stress conditions like high light when the main photorespiratory pathway is deficient as in the cases of *hpr1* and *cat2*.

To further investigate the function of *GLYR1*, I performed RNA-seq for Col-0, *glyr1-1*, *hpr1-1*, *glyr1-1 hpr1-1* and *shpr7*. The *glyr1* mutant only has a small number of differentially expressed genes compared to Col-0, but *glyr1 hpr1* and *shpr7* have a massive number of differentially expressed genes compared to *hpr1*. The transcriptional reprogramming in *hpr1* involves broad biological processes, which can be largely reverted by the lack of a functional *GLYR1*. This RNA-seq data is consistent with the accumulation of photorespiratory metabolites in *hpr1* and its partial rescue by *glyr1*, supporting the cytosolic glyoxylate shunt proposed in Chapter 2.

To investigate the role of photorespiration in plant immunity, I treated photorespiratory mutants with pathogens and found two photorespiratory mutants, *hpr1* and *plgg1*, showing susceptible phenotypes under pathogen infections. High CO₂ conditions can rescue the susceptible phenotypes of these two mutants, indicating that the role of HPR1 and PLGG1 in plant immunity is dependent on photorespiration. Although further investigations are needed to

elucidate the underlying mechanisms, my current results suggest the positive role of photorespiration in plant immunity.

My work provides evidence to the important role of photorespiration in plant stress response, a key area where our understanding is still fragmentary. Photorespiration is a complex process that involves a series of reactions with multiple enzymes and metabolites across chloroplasts, peroxisomes, mitochondria and the cytosol, therefore large-scale experiments that simultaneously assay for different aspects of the pathway during stress response are required to obtain a full understanding of the role of photorespiration in plant stress response. In addition, my work and previous work from my lab showed that HPR1 and PLGG1 play positive roles in both high light and immunity, suggesting that photorespiration may contribute to abiotic and biotic stresses using similar mechanisms. Hence, it will also be interesting to expand this line of research to compare photorespiration under different stresses. Lastly, knowledge gained on the role of photorespiration in stress response may guide future breeding and engineering efforts for the simultaneous improvement of yield and resilience in crop plants.

REFERENCES

- Ahammed GJ, Li X, Zhang G, Zhang H, Shi J, Pan C, Yu J, Shi K. 2018.** Tomato photorespiratory glycolate-oxidase-derived H₂O₂ production contributes to basal defence against *Pseudomonas syringae*. *Plant Cell and Environment* **41**: 1126–1138.
- Allan WL, Simpson JP, Clark SM, Shelp BJ. 2008.** γ -Hydroxybutyrate accumulation in Arabidopsis and tobacco plants is a general response to abiotic stress: Putative regulation by redox balance and glyoxylate reductase isoforms. *Journal of Experimental Botany* **59**: 2555–2564.
- Aroca A, García-Díaz I, García-Calderón M, Gotor C, Márquez AJ, Betti M. 2023.** Photorespiration: regulation and new insights on the potential role of persulfidation. *Journal of Experimental Botany* **74**: 6023–6039.
- Bach-Pages M, Preston GM. 2018.** Methods to quantify biotic-induced stress in plants. In: Medina C, López-Baena FJ, eds. Host-Pathogen Interactions: Methods and Protocols. New York, NY: Springer New York, 241–255.
- Bao H, Morency M, Rianti W, Saeheng S, Roje S, Weber APM, Walker BJ. 2021.** Catalase protects against nonenzymatic decarboxylations during photorespiration in *Arabidopsis thaliana*. *Plant Direct* **5**: 1–13.
- Bassi R, Dall’osto L. 2021.** Dissipation of light energy absorbed in excess: the molecular mechanisms. *Annu. Rev. Plant Biol.* **2021** **72**: 47–76.
- Benjamin I, Kenigsbuch D, Galperin M, Abrameto JA, Cohen Y. 2009.** Cisgenic melons over expressing glyoxylate-aminotransferase are resistant to downy mildew. *European Journal of Plant Pathology* **125**: 355–365.
- Betti M, Bauwe H, Busch FA, Fernie AR, Keech O, Levey M, Ort DR, Parry MAJ, Sage R, Timm S, *et al.* 2016.** Manipulating photorespiration to increase plant productivity: recent advances and perspectives for crop improvement. *Journal of Experimental Botany* **67**: 2977–2988.
- Brikis CJ, Zarei A, Trobacher CP, Deell JR, Akama K, Mullen RT, Bozzo GG, Shelp BJ. 2017.** Ancient plant glyoxylate/succinic semialdehyde reductases: GLYR1s are cytosolic, whereas GLYR2s are localized to both mitochondria and plastids. *Frontiers in Plant Science* **8**.
- Busch FA, Sage RF, Farquhar GD. 2018.** Plants increase CO₂ uptake by assimilating nitrogen via the photorespiratory pathway. *Nature Plants* **4**: 46–54.
- Camejo D, Guzmán-Cedeño Á, Moreno A. 2016.** Reactive oxygen species, essential molecules, during plant-pathogen interactions. *Plant Physiology and Biochemistry* **103**: 10–23.
- Campbell WJ, Ogren WL. 1990.** Glyoxylate inhibition of ribulosebiphosphate carboxylase/oxygenase activation in intact, lysed, and reconstituted chloroplasts. *Photosynthesis Research* **23**: 257–268.
- Carrie C, Kühn K, Murcha MW, Duncan O, Small ID, O’Toole N, Whelan J. 2009.** Approaches to defining dual-targeted proteins in Arabidopsis. *Plant Journal* **57**: 1128–1139.
- Cegelski L, Schaefer J. 2005.** Glycine metabolism in intact leaves by in vivo ¹³C and ¹⁵N labeling. *Journal of Biological Chemistry* **280**: 39238–39245.

- Chamnongpol S, Willekens H, Moeder W, Langebartels C, Sandermann H, Van Montagu M, Inzé D, Van Camp W. 1998.** Defense activation and enhanced pathogen tolerance induced by H₂O₂ in transgenic tobacco. *Proceedings of the National Academy of Sciences of the United States of America* **95**: 5818–5823.
- Chaouch S, Noctor G. 2010.** Myo-inositol abolishes salicylic acid-dependent cell death and pathogen defence responses triggered by peroxisomal hydrogen peroxide. *New Phytologist* **188**: 711–718.
- Chaouch S, Queval G, Vanderauwera S, Mhamdi A, Vandenabeele M, Langlois-Meurinne M, Van Breusegem F, Saindrenan P, Noctor G. 2010.** Peroxisomal hydrogen peroxide is coupled to biotic defense responses by ISOCHORISMATE SYNTHASE1 in a daylength-Related manner. *Plant Physiology* **153**: 1692–1705.
- Chastain CJ, Ogren WL. 1989.** Glyoxylate inhibition of ribulosebiphosphate carboxylase/oxygenase activation state in vivo. *Plant and Cell Physiology* **30**: 937–944.
- Chaux F, Peltier G, Johnson X. 2015.** A security network in PSI photoprotection: Regulation of photosynthetic control, NPQ and O₂ photoreduction by cyclic electron flow. *Frontiers in Plant Science* **6**.
- Chen Z, Silva H, Klessig DF. 1993.** Active oxygen species in the induction of plant systemic acquired resistance by salicylic acid. *Science* **262**: 1883–1886.
- Chern M, Bai W, Chen X, Canlas PE, Ronald PC. 2013.** Reduced expression of glycolate oxidase leads to enhanced disease resistance in rice. *PeerJ* **2013**: 1–16.
- Ching SLK, Gidda SK, Rochon A, van Cauwenberghe OR, Shelp BJ, Mullen RT. 2012.** Glyoxylate reductase isoform 1 is localized in the cytosol and not peroxisomes in plant cells. *Journal of Integrative Plant Biology* **54**: 152–168.
- Conrath U, Chen Z, Ricigliano JR, Klessig DF. 1995.** Two inducers of plant defense responses, 2,6-dichloroisonicotinic acid and salicylic acid, inhibit catalase activity in tobacco. *Proceedings of the National Academy of Sciences of the United States of America* **92**: 7143–7147.
- Cook CM, Mulligan RM, Tolbert NE. 1985.** Inhibition and stimulation of ribulose-1,5-bisphosphate carboxylase/oxygenase by glyoxylate. *Archives of Biochemistry and Biophysics* **240**: 392–401.
- Costa A, Drago I, Behera S, Zottini M, Pizzo P, Schroeder JI, Pozzan T, Schiavo F Lo. 2010.** H₂O₂ in plant peroxisomes: An in vivo analysis uncovers a Ca²⁺-dependent scavenging system. *Plant Journal* **62**: 760–772.
- Cousins AB, Pracharoenwattana I, Zhou W, Smith SM, Badger MR. 2008.** Peroxisomal malate dehydrogenase is not essential for photorespiration in arabidopsis but its absence causes an increase in the stoichiometry of photorespiratory CO₂ release. *Plant Physiology* **148**: 786–795.
- Cousins AB, Walker BJ, Pracharoenwattana I, Smith SM, Badger MR. 2011.** Peroxisomal hydroxypyruvate reductase is not essential for photorespiration in Arabidopsis but its absence causes an increase in the stoichiometry of photorespiratory CO₂ release. *Photosynthesis Research* **108**: 91–100.

- Crisp PA, Ganguly DR, Smith AB, Murray KD, Estavillo GM, Searle I, Ford E, Bogdanović O, Lister R, Borevitz JO, et al. 2017.** Rapid recovery gene downregulation during excess-light stress and recovery in Arabidopsis. *The Plant Cell* **29**: 1836–1863.
- Cristina Palmieri M, Lindermayr C, Bauwe H, Steinhauser C, Durner J. 2010.** Regulation of plant glycine decarboxylase by S-nitrosylation and glutathionylation. *Plant Physiology* **152**: 1514–1528.
- Cruz JA, Savage LJ, Zegarac R, Hall CC, Satoh-Cruz M, Davis GA, Kovac WK, Chen J, Kramer DM. 2016.** Dynamic environmental photosynthetic imaging reveals emergent phenotypes. *Cell Systems* **2**: 365–377.
- Cui H, Tsuda K, Parker JE. 2015.** Effector-triggered immunity: From pathogen perception to robust defense. *Annual Review of Plant Biology* **66**: 487–511.
- Dellero Y, Jossier M, Schmitz J, Maurino VG, Hodges M. 2016.** Photorespiratory glycolate-glyoxylate metabolism. *Journal of Experimental Botany* **67**: 3041–3052.
- Deslandes L, Rivas S. 2012.** Catch me if you can: Bacterial effectors and plant targets. *Trends in Plant Science* **17**: 644–655.
- Dobin A, Davis CA, Schlesinger F, Drenkow J, Zaleski C, Jha S, Batut P, Chaisson M, Gingeras TR. 2013.** STAR: ultrafast universal RNA-seq aligner. *Bioinformatics* **29**: 15–21.
- Dodds PN, Rathjen JP. 2010.** Plant immunity: towards an integrated view of plant–pathogen interactions. *Nature Reviews Genetics* **11**: 539–548.
- Dong X, Wang M, Ling N, Shen Q, Guo S. 2016.** Potential role of photosynthesis-related factors in banana metabolism and defense against *Fusarium oxysporum* f. sp. *cubense*. *Environmental and Experimental Botany* **129**: 4–12.
- Eisenhut M, Bräutigam A, Timm S, Florian A, Tohge T, Fernie AR, Bauwe H, Weber APM. 2017.** Photorespiration is crucial for dynamic response of photosynthetic metabolism and stomatal movement to altered CO₂ availability. *Molecular Plant* **10**: 47–61.
- Eisenhut M, Roell MS, Weber APM. 2019.** Mechanistic understanding of photorespiration paves the way to a new green revolution. *New Phytologist* **223**: 1762–1769.
- Esser C, Kuhn A, Groth G, Lercher MJ, Maurino VG. 2014.** Plant and animal glycolate oxidases have a common eukaryotic ancestor and convergently duplicated to evolve long-chain 2-hydroxy acid oxidases. *Molecular Biology and Evolution* **31**: 1089–1101.
- da Fonseca-Pereira P, Souza PVL, Hou LY, Schwab S, Geigenberger P, Nunes-Nesi A, Timm S, Fernie AR, Thormählen I, Araújo WL, et al. 2020.** Thioredoxin h2 contributes to the redox regulation of mitochondrial photorespiratory metabolism. *Plant Cell and Environment* **43**: 188–208.
- Foyer CH. 2018.** Reactive oxygen species, oxidative signaling and the regulation of photosynthesis. *Environmental and Experimental Botany* **154**: 134–142.
- Foyer CH, Bloom AJ, Queval G, Noctor G. 2009.** Photorespiratory metabolism: Genes, mutants, energetics, and redox signaling. *Annual Review of Plant Biology* **60**: 455–484.
- Foyer CH, Hanke G. 2022.** ROS production and signalling in chloroplasts: cornerstones and evolving concepts. *The Plant Journal* **111**: 642–661.

- Fu X, Gregory LM, Weise SE, Walker BJ. 2023.** Integrated flux and pool size analysis in plant central metabolism reveals unique roles of glycine and serine during photorespiration. *Nature Plants* **9**: 169–178.
- Fu X, Walker BJ. 2022.** Dynamic response of photorespiration in fluctuating light environments. *Journal of Experimental Botany*.
- Fu S, Wang K, Ma T, Liang Y, Ma Z, Wu J, Xu Y, Zhou X. 2022.** An evolutionarily conserved C4HC3-type E3 ligase regulates plant broad-spectrum resistance against pathogens. *Plant Cell* **34**: 1822–1843.
- Fürtauer L, Küstner L, Weckwerth W, Heyer AG, Nägele T. 2019.** Resolving subcellular plant metabolism. *The Plant Journal* **100**: 438–455.
- Gao C, Xu H, Huang J, Sun B, Zhang F, Savage Z, Duggan C, Yan T, Wu CH, Wang Y, et al. 2020.** Pathogen manipulation of chloroplast function triggers a light-dependent immune recognition. *Proceedings of the National Academy of Sciences of the United States of America* **117**: 9613–9620.
- Gilbert BM, Wolpert TJ. 2013.** Characterization of the LOV1 -Mediated, Victorin-Induced, Cell-Death Response with Virus-Induced Gene Silencing. *Molecular Plant-Microbe Interactions* **26**: 903–917.
- Giraldo – González JJ, de Souza Carvalho FM, Ferro JA, Herai RH, Chaves Bedoya G, Rodas Mendoza EF. 2021.** Transcriptional changes involved in kumquat (*Fortunella* spp) defense response to *Xanthomonas citri* subsp. *citri* in early stages of infection. *Physiological and Molecular Plant Pathology* **116**.
- Giri MK, Singh N, Banday ZZ, Singh V, Ram H, Singh D, Chattopadhyay S, Nandi AK. 2017.** GBF1 differentially regulates CAT2 and PAD4 transcription to promote pathogen defense in *Arabidopsis thaliana*. *Plant Journal* **91**: 802–815.
- Givan C V., Tsutakawa S, Hodgson JM, David N, Randall DD. 1988.** Glyoxylate reductase activity in pea leaf protoplasts nucleotide specificity and subcellular location. *Journal of Plant Physiology* **132**: 593–599.
- González-lópez MDC, Jijón-moreno S, Dautt-castro M, Ovando-vázquez C, Ziv T, Horwitz BA, Casas-flores S. 2021.** Secretome analysis of *arabidopsis*–*trichoderma atroviride* interaction unveils new roles for the plant glutamate:Glyoxylate aminotransferase *ggat1* in plant growth induced by the fungus and resistance against *botrytis cinerea*. *International Journal of Molecular Sciences* **22**: 1–28.
- Gregory LM, Roze L V., Walker BJ. 2023.** Increased activity of core photorespiratory enzymes and CO₂ transfer conductances are associated with higher and more optimal photosynthetic rates under elevated temperatures in the extremophile *Rhazya stricta*. *Plant Cell and Environment* **46**: 3704–3720.
- Hanson AD, Roje S. 2001.** One-carbon metabolism in higher plants. *Annual Review of Plant Physiology and Plant Molecular Biology* **52**: 119–137.
- He L, Jin P, Chen X, Zhang TY, Zhong KL, Liu P, Chen JP, Yang J. 2021.** Comparative proteomic analysis of *Nicotiana benthamiana* plants under Chinese wheat mosaic virus infection. *BMC Plant Biology* **21**: 1–17.

Hodges M. 2022. Photorespiration and improving photosynthesis. In: Lüttge U, Cánovas FM, Risueño M-C, Leuschner C, Pretzsch H, eds. *Progress in Botany Vol. 84*. Cham: Springer Nature Switzerland, 171–219.

Hoover GJ, Van Cauwenberghe OR, Breitskreuz KE, Clark SM, Merrill AR, Shelp BJ. 2007. Characteristics of an Arabidopsis glyoxylate reductase: General biochemical properties and substrate specificity for the recombinant protein, and developmental expression and implications for glyoxylate and succinic semialdehyde metabolism in planta. *Canadian Journal of Botany* **85**: 883–895.

Huang W, Hu H, Zhang SB. 2015. Photorespiration plays an important role in the regulation of photosynthetic electron flow under fluctuating light in tobacco plants grown under full sunlight. *Frontiers in Plant Science* **6**.

Huang W, Yang YJ, Wang JH, Hu H. 2019a. Photorespiration is the major alternative electron sink under high light in alpine evergreen sclerophyllous Rhododendron species. *Plant Science* **289**: 110275.

Huang W, Zhang SB, Hu H. 2014. Sun leaves up-regulate the photorespiratory pathway to maintain a high rate of CO₂ assimilation in tobacco. *Frontiers in Plant Science* **5**.

Huang J, Zhao X, Chory J. 2019b. The Arabidopsis transcriptome responds specifically and dynamically to high light stress. *Cell Reports* **29**: 4186-4199.e3.

Jossier M, Liu Y, Massot S, Hodges M. 2020. Enzymatic properties of recombinant phosphomimetic photorespiratory glycolate oxidases from Arabidopsis thaliana and Zea mays. *Plants* **9**.

Kadotani N, Akagi A, Takatsuji H, Miwa T, Igarashi D. 2016. Exogenous proteinogenic amino acids induce systemic resistance in rice. *BMC Plant Biology* **16**: 1–10.

Kalapos B, Juhász C, Balogh E, Kocsy G, Tóbiás I, Gullner G. 2021. Transcriptome profiling of pepper leaves by RNA-Seq during an incompatible and a compatible pepper-tobamovirus interaction. *Scientific Reports* **11**: 1–19.

Kandath PK, Liu S, Prenger E, Ludwig A, Lakhssassi N, Heinz R, Zhou Z, Howland A, Gunther J, Eidson S, et al. 2017. Systematic mutagenesis of serine hydroxymethyltransferase reveals an essential role in nematode resistance. *Plant Physiology* **175**: 1370–1380.

Kaur N, Li J, Hu J. 2013. Peroxisomes and Photomorphogenesis. In: del Río LA, ed. *Subcellular Biochemistry. Peroxisomes and their Key Role in Cellular Signaling and Metabolism*. Dordrecht: Springer Netherlands, 195–211.

Kleine T, Kindgren P, Benedict C, Hendrickson L, Strand A. 2007. Genome-wide gene expression analysis reveals a critical role for CRYPTOCHROME1 in the response of Arabidopsis to high irradiance. *Plant Physiology* **144**: 1391–1406.

Koenig AM, Liu B, Hu J. 2023. Visualizing the dynamics of plant energy organelles. *Biochemical Society Transactions* **51**: 2029–2040.

Koper K, Han S-W, Casas Pastor D, Yoshikuni Y, Maeda HA. 2022. Evolutionary origin and functional diversification of aminotransferases. *Journal of Biological Chemistry* **298**: 102122.

- Korasick DA, Kandoth PK, Tanner JJ, Mitchum MG, Beamer LJ. 2020.** Impaired folate binding of serine hydroxymethyltransferase 8 from soybean underlies resistance to the soybean cyst nematode. *Journal of Biological Chemistry* **295**: 3708–3718.
- Korotkevich G, Sukhov V, Budin N, Shpak B, Artyomov MN, Sergushichev A. 2021.** Fast gene set enrichment analysis. *bioRxiv*: 060012.
- Krieger-Liszkay A, Shimakawa G. 2022.** Regulation of the generation of reactive oxygen species during photosynthetic electron transport. *Biochemical Society Transactions* **50**: 1025–1034.
- Lakhssassi N, Patil G, Piya S, Zhou Z, Baharlouei A, Kassem MA, Lightfoot DA, Hewezi T, Barakat A, Nguyen HT, et al. 2019.** Genome reorganization of the GmSHMT gene family in soybean showed a lack of functional redundancy in resistance to soybean cyst nematode. *Scientific Reports* **9**: 1–16.
- Langfelder P, Horvath S. 2008.** WGCNA: an R package for weighted correlation network analysis. *BMC Bioinformatics* **9**: 559.
- Langfelder P, Horvath S. 2012.** Fast R Functions for Robust Correlations and Hierarchical Clustering. *Journal of Statistical Software* **46**: 1–17.
- Launay A, Jolivet S, Clément G, Zarattini M, Dello Y, Le Hir R, Jossier M, Hodges M, Expert D, Fagard M. 2022.** DspA/E-Triggered Non-Host Resistance against *E. amylovora* Depends on the Arabidopsis GLYCOLATE OXIDASE 2 Gene. *International Journal of Molecular Sciences* **23**: 4224.
- Lavell A, Smith M, Xu Y, Froehlich JE, De La Mora C, Benning C. 2021.** Proteins associated with the *Arabidopsis thaliana* plastid rhomboid-like protein RBL10. *The Plant Journal* **108**: 1332–1345.
- Laxa M. 2017.** Regulatory cis-elements are located in accessible promoter regions of the CAT2 promoter and affect activating histone modifications in *Arabidopsis thaliana*. *Plant Molecular Biology* **93**: 49–60.
- Laxa M, Fromm S. 2018.** Co-expression and regulation of photorespiratory genes in *Arabidopsis thaliana*: A bioinformatic approach. *Current Plant Biology* **14**: 2–18.
- Laxa M, Müller K, Lange N, Doering L, Pruscha JT, Peterhänsel C. 2016.** The 5'UTR Intron of Arabidopsis GGT1 Aminotransferase Enhances Promoter Activity by Recruiting RNA Polymerase II. *Plant Physiology* **172**: 313–327.
- Lefevre H, Bauters L, Gheysen G. 2020.** Salicylic acid biosynthesis in plants. *Frontiers in Plant Science* **11**: 1–7.
- Levey M, Timm S, Mettler-Altmann T, Borghi GL, Koczor M, Arrivault S, Weber APM, Bauwe H, Gowik U, Westhoff P. 2019.** Efficient 2-phosphoglycolate degradation is required to maintain carbon assimilation and allocation in the C4 plant *Flaveria bidentis*. *Journal of Experimental Botany* **70**: 575–587.
- Li H, Handsaker B, Wysoker A, Fennell T, Ruan J, Homer N, Marth G, Abecasis G, Durbin R, Subgroup 1000 Genome Project Data Processing. 2009.** The sequence alignment/map format and SAMtools. *Bioinformatics* **25**: 2078–2079.

- Li J, Hu J. 2015.** Using co-expression analysis and stress-based screens to uncover Arabidopsis peroxisomal proteins involved in drought response (D Bassham, Ed.). *PLOS ONE* **10**: e0137762.
- Li M, Kim C. 2022.** Chloroplast ROS and stress signaling. *Plant Communications* **3**: 100264.
- Li J, Tietz S, Cruz JA, Strand DD, Xu Y, Chen J, Kramer DM, Hu J. 2019a.** Photometric screens identified Arabidopsis peroxisome proteins that impact photosynthesis under dynamic light conditions. *The Plant Journal* **97**: 460–474.
- Li J, Weraduwege SM, Preiser AL, Tietz S, Weise SE, Strand DD, Froehlich JE, Kramer DM, Hu J, Sharkey TD. 2019b.** A cytosolic bypass and g6p shunt in plants lacking peroxisomal hydroxypyruvate reductase1. *Plant Physiology* **180**: 783–792.
- Liepman AH, Olsen LJ. 2001.** Peroxisomal alanine: Glyoxylate aminotransferase (AGT1) is a photorespiratory enzyme with multiple substrates in Arabidopsis thaliana. *Plant Journal* **25**: 487–498.
- Liepman AH, Olsen LJ. 2003.** Alanine aminotransferase homologs catalyze the glutamate:Glyoxylate aminotransferase reaction in peroxisomes of Arabidopsis. *Plant Physiology* **131**: 215–227.
- Liepman AH, Olsen LJ. 2004.** Genomic analysis of aminotransferases in Arabidopsis thaliana. *Critical Reviews in Plant Sciences* **23**: 73–89.
- Liu Y, Guérard F, Hodges M, Jossier M. 2020.** Phosphomimetic T335D mutation of Hydroxypyruvate Reductase 1 modifies cofactor specificity and impacts Arabidopsis growth in air. *Plant Physiology* **183**: 194–205.
- Liu S, Kandoth PK, Warren SD, Yeckel G, Heinz R, Alden J, Yang C, Jamai A, El-Mellouki T, Juvalle PS, et al. 2012.** A soybean cyst nematode resistance gene points to a new mechanism of plant resistance to pathogens. *Nature* **492**: 256–260.
- Liu Y, Mauve C, Lamothe-Sibold M, Guérard F, Glab N, Hodges M, Jossier M. 2019.** Photorespiratory serine hydroxymethyltransferase 1 activity impacts abiotic stress tolerance and stomatal closure. *Plant Cell and Environment* **42**: 2567–2583.
- Love MI, Huber W, Anders S. 2014.** Moderated estimation of fold change and dispersion for RNA-seq data with DESeq2. *Genome Biology* **15**: 550.
- Lu Y, Li Y, Yang Q, Zhang Z, Chen Y, Zhang S, Peng XX. 2014.** Suppression of glycolate oxidase causes glyoxylate accumulation that inhibits photosynthesis through deactivating Rubisco in rice. *Physiologia Plantarum* **150**: 463–476.
- Lutziger I, Oliver DJ. 2001.** Characterization of Two cDNAs Encoding Mitochondrial Lipoamide Dehydrogenase from Arabidopsis 1. *Plant Physiology* **127**: 615–623.
- Lv T, Li X, Fan T, Luo H, Xie C, Zhou Y, Tian CE. 2019.** The calmodulin-binding protein IQM1 interacts with CATALASE2 to affect pathogen defense. *Plant Physiology* **181**: 1314–1327.
- Ma F, Jazmin LJ, Young JD, Allen DK. 2014.** Isotopically nonstationary ¹³C flux analysis of changes in Arabidopsis thaliana leaf metabolism due to high light acclimation. *Proceedings of the National Academy of Sciences of the United States of America* **111**: 16967–16972.

- Ma Y, Ma X, Gao X, Wu W, Zhou B. 2021.** Light induced regulation pathway of anthocyanin biosynthesis in plants. *International Journal of Molecular Sciences* **22**.
- Ma H, Sheng C, Qiao L, Zhao H, Niu D. 2020.** A comparative proteomic approach to identify defence-related proteins between resistant and susceptible rice cultivars challenged with the fungal pathogen *Rhizoctonia solani*. *Plant Growth Regulation* **90**: 73–88.
- Mackey D, Belkhadir Y, Alonso JM, Ecker JR, Dangl JL. 2003.** Arabidopsis RIN4 is a target of the type III virulence effector AvrRpt2 and modulates RPS2-mediated resistance. *Cell* **112**: 379–389.
- Mano S, Hayashi M, Nishimura M. 1999.** Light regulates alternative splicing of hydroxypyruvate reductase in pumpkin. *Plant Journal* **17**: 309–320.
- Manohar M, Tian M, Moreau M, Park SW, Choi HW, Fei Z, Friso G, Asif M, Manosalva P, Von Dahl CC, et al. 2015.** Identification of multiple salicylic acid-binding proteins using two high throughput screens. *Frontiers in Plant Science* **5**: 1–14.
- Martin M. 2011.** Cutadapt removes adapter sequences from high-throughput sequencing reads. *EMBnet journal* **17**: 10.
- Mathioudakis MM, Veiga RSL, Canto T, Medina V, Mossialos D, Makris AM, Livieratos I. 2013.** Pepino mosaic virus triple gene block protein 1 (TGBp1) interacts with and increases tomato catalase 1 activity to enhance virus accumulation. *Molecular Plant Pathology* **14**: 589–601.
- Mekonnen DW, Ludewig F. 2016.** Phenotypic and chemotypic studies using Arabidopsis and yeast reveal that GHB converts to SSA and induce toxicity. *Plant Molecular Biology* **91**: 429–440.
- Messant M, Timm S, Fantuzzi A, Weckwerth W, Bauwe H, Rutherford AW, Krieger-Liszkay A. 2018.** Glycolate induces redox tuning of photosystem II in vivo: Study of a photorespiration mutant. *Plant Physiology* **177**: 1277–1285.
- Mindrinos M, Katagiri F, Yu G-L, Ausubel FM. 1994.** The *A. thaliana* disease resistance gene RPS2 encodes a protein containing a nucleotide-binding site and leucine-rich repeats. *Cell* **78**: 1089–1099.
- Mishra Y, Johansson Jänkänpää H, Kiss AZ, Funk C, Schröder WP, Jansson S. 2012.** Arabidopsis plants grown in the field and climate chambers significantly differ in leaf morphology and photosystem components. *BMC Plant Biology* **12**.
- Misra BB, de Armas E, Chen S. 2016.** Differential metabolomic responses of PAMP-triggered immunity and effector-triggered immunity in Arabidopsis suspension cells. *Metabolomics* **12**: 1–15.
- Mitsuya Y, Takahashi Y, Berberich T, Miyazaki A, Matsumura H, Takahashi H, Terauchi R, Kusano T. 2009.** Spermine signaling plays a significant role in the defense response of Arabidopsis thaliana to cucumber mosaic virus. *Journal of Plant Physiology* **166**: 626–643.
- Mittler R, Herr EH, Orvar BL, Van Camp W, Willekens H, Inzé D, Ellis BE. 1999.** Transgenic tobacco plants with reduced capability to detoxify reactive oxygen intermediates are hyperresponsive to pathogen infection. *Proceedings of the National Academy of Sciences of the United States of America* **96**: 14165–14170.

- Moreno JI, Martín R, Castresana C. 2005.** Arabidopsis SHMT1, a serine hydroxymethyltransferase that functions in the photorespiratory pathway influences resistance to biotic and abiotic stress. *Plant Journal* **41**: 451–463.
- Mulligan RM, Wilson B, Tolbert NE. 1983.** Effects of glyoxylate on photosynthesis by intact chloroplasts. *Plant Physiology* **72**: 415–419.
- Muraoka H, Tang Y, Terashima I, Koizumi H, Washitani I. 2000.** Contributions of diffusional limitation, photoinhibition and photorespiration to midday depression of photosynthesis in *Arisaema heterophyllum* in natural high light. *Plant, Cell and Environment* **23**: 235–250.
- Murota K, Shimura H, Takeshita M, Masuta C. 2017.** Interaction between Cucumber mosaic virus 2b protein and plant catalase induces a specific necrosis in association with proteasome activity. *Plant Cell Reports* **36**: 37–47.
- Navarre DA, Wolpert TJ. 1995.** Inhibition of the glycine decarboxylase multienzyme complex by the host-selective toxin victorin. *The Plant Cell* **7**: 463–471.
- Ngou BPM, Ahn HK, Ding P, Jones JDG. 2021.** Mutual potentiation of plant immunity by cell-surface and intracellular receptors. *Nature* **592**: 110–115.
- Noctor G, Arisi A-CM, Jouanin L, Foyer CH. 1999.** Photorespiratory glycine enhances glutathione accumulation in both the chloroplastic and cytosolic compartments. *Journal of Experimental Botany* **50**: 1157–1167.
- Okinaka Y, Yang C-H, Herman E, Kinney A, Keen NT. 2002.** The P34 syringolide elicitor receptor interacts with a soybean photorespiration enzyme, NADH-dependent hydroxypyruvate reductase. *Molecular Plant-Microbe Interactions*® **15**: 1213–1218.
- Ort DR. 2001.** When there is too much light. *Plant Physiology* **125**: 29–32.
- Ort DR, Baker NR. 2002.** A photoprotective role for O₂ as an alternative electron sink in photosynthesis? *Current Opinion in Plant Biology* **5**: 193–198.
- Osei-Bonsu I, McClain AM, Walker BJ, Sharkey TD, Kramer DM. 2021.** The roles of photorespiration and alternative electron acceptors in the responses of photosynthesis to elevated temperatures in cowpea. *Plant, Cell & Environment* **44**: 2290–2307.
- Pan R, Liu J, Wang S, Hu J. 2020.** Peroxisomes: versatile organelles with diverse roles in plants. *New Phytologist* **225**: 1410–1427.
- Patro R, Duggal G, Love MI, Irizarry RA, Kingsford C. 2017.** Salmon provides fast and bias-aware quantification of transcript expression. *Nature Methods* **14**: 417–419.
- Pérez-Delgado CM, García-Calderón M, Sánchez DH, Udvardi MK, Kopka J, Márquez AJ, Betti M. 2013.** Transcriptomic and metabolic changes associated with photorespiratory ammonium accumulation in the model legume *Lotus japonicus*. *Plant Physiology* **162**: 1834–1848.
- Petersen LN, Ingle RA, Knight MR, Denby KJ. 2009.** OXI1 protein kinase is required for plant immunity against *Pseudomonas syringae* in arabidopsis. *Journal of Experimental Botany* **60**: 3727–3735.
- Pick TR, Bräutigam A, Schulz MA, Obata T, Fernie AR, Weber APM. 2013.** PLGG1, a plastidic glycolate glycerate transporter, is required for photorespiration and defines a unique

class of metabolite transporters. *Proceedings of the National Academy of Sciences of the United States of America* **110**: 3185–3190.

Pieterse CMJ, Van Der Does D, Zamioudis C, Leon-Reyes A, Van Wees SCM. 2012. Hormonal modulation of plant immunity. *Annual Review of Cell and Developmental Biology* **28**: 489–521.

Pracharoenwattana I, Zhou W, Smith SM. 2010. Fatty acid beta-oxidation in germinating Arabidopsis seeds is supported by peroxisomal hydroxypyruvate reductase when malate dehydrogenase is absent. *Plant Molecular Biology* **72**: 101–109.

Pruitt RN, Locci F, Wanke F, Zhang L, Saile SC, Joe A, Karelina D, Hua C, Fröhlich K, Wan WL, et al. 2021. The EDS1–PAD4–ADR1 node mediates Arabidopsis pattern-triggered immunity. *Nature* **598**: 495–499.

Queval G, Issakidis-Bourguet E, Hoerberichts FA, Vandorpe M, Gakière B, Vanacker H, Migniac-Maslow M, Van Breusegem F, Noctor G. 2007. Conditional oxidative stress responses in the Arabidopsis photorespiratory mutant *cat2* demonstrate that redox state is a key modulator of daylength-dependent gene expression, and define photoperiod as a crucial factor in the regulation of H₂O₂-induced cell death. *Plant Journal* **52**: 640–657.

Reinholdt O, Schwab S, Zhang Y, Reichheld J-P, Fernie AR, Hagemann M, Timm S. 2019. Redox-Regulation of Photorespiration through Mitochondrial Thioredoxin o1. *Plant Physiology* **181**: 442–457.

Rentel MC, Lecourieux D, Ouaked F, Usher SL, Petersen L, Okamoto H, Knight H, Peck SC, Grierson CS, Hirt H, et al. 2004. OXI1 kinase is necessary for oxidative burst-mediated signalling in Arabidopsis. *Nature* **427**: 858–861.

Reumann S, Weber APM. 2006. Plant peroxisomes respire in the light: Some gaps of the photorespiratory C2 cycle have become filled—Others remain. *Biochimica et Biophysica Acta (BBA) - Molecular Cell Research* **1763**: 1496–1510.

Riens B, Lohaus G, Heineke D, Heldt HW. 1991. Amino acid and sucrose content determined in the cytosolic, chloroplastic, and vacuolar compartments and in the phloem sap of spinach leaves. *Plant Physiology* **97**: 227–233.

Roach T, Krieger-Liszkay A. 2014. Regulation of photosynthetic electron transport and photoinhibition. *Current Protein & Peptide Science* **15**: 351–362.

Rojas CM, Mysore KS. 2012. Glycolate oxidase is an alternative source for H₂O₂ production during plant defense responses and functions independently from NADPH oxidase. *Plant Signaling and Behavior* **7**: 752–755.

Rojas CM, Senthil-Kumar M, Wang K, Ryu C-M, Kaundal A, Mysore KS. 2012. Glycolate oxidase modulates reactive oxygen species-mediated signal transduction during nonhost resistance in *Nicotiana benthamiana* and Arabidopsis. *The Plant Cell* **24**: 336–352.

Ros R, Muñoz-Bertomeu J, Krueger S. 2014. Serine in plants: Biosynthesis, metabolism, and functions. *Trends in Plant Science* **19**: 564–569.

Rosa-Téllez S, Alcántara-Enguíanos A, Martínez-Seidel F, Casatejada-Anchel R, Saeheng S, Bailes CL, Erban A, Barbosa-Medeiros D, Alepúz P, Matus JT, et al. 2023. The serine–

glycine–one-carbon metabolic network orchestrates changes in nitrogen and sulfur metabolism and shapes plant development. *The Plant Cell*: 1–23.

Rossel JB, Wilson IW, Pogson BJ. 2002. Global changes in gene expression in response to high light in Arabidopsis. *Plant Physiology* **130**: 1109–1120.

Ruban A V. 2016. Nonphotochemical chlorophyll fluorescence quenching: Mechanism and effectiveness in protecting plants from photodamage. *Plant Physiology* **170**: 1903–1916.

Saji S, Bathula S, Kubo A, Tamaoki M, Aono M, Sano T, Tobe K, Timm S, Bauwe H, Nakajima N, et al. 2017. Ozone-sensitive arabidopsis mutants with deficiencies in photorespiratory enzymes. *Plant and Cell Physiology* **58**: 914–924.

Sánchez-Casas P, Klessig DF. 1994. A salicylic acid-binding activity and a salicylic acid-inhibitable catalase activity are present in a variety of plant species. *Plant Physiology* **106**: 1675–1679.

Segarra G, Casanova E, Bellido D, Odena MA, Oliveira E, Trillas I. 2007. Proteome, salicylic acid, and jasmonic acid changes in cucumber plants inoculated with *Trichoderma asperellum* strain T34. *Proteomics* **7**: 3943–3952.

Selinski J, Scheibe R. 2019. Malate valves: old shuttles with new perspectives. *Plant Biology* **21**: 21–30.

Sharma N, Nagar S, Thakur M, Suriyakumar P, Kataria S, Shanker AK, Landi M, Anand A. 2023. Photosystems under high light stress: throwing light on mechanism and adaptation. *Photosynthetica* **61**: 250–263.

Shi X, Bloom A. 2021. Photorespiration: the futile cycle? *Plants* **10**: 908.

Shi Y, Ke X, Yang X, Liu Y, Hou X. 2022a. Plants response to light stress. *Journal of Genetics and Genomics* **49**: 735–747.

Shi Q, Sun H, Timm S, Zhang S, Huang W. 2022b. Photorespiration alleviates photoinhibition of Photosystem I under fluctuating light in tomato. *Plants* **11**.

Shikanai T. 2007. Cyclic Electron Transport Around Photosystem I: Genetic Approaches. *Annual Review of Plant Biology* **58**: 199–217.

Silva BN, Picanço BBM, Martins SCV, Rodrigues FA. 2023. Impairment of the photorespiratory pathway on tomato leaves during the infection process of *Septoria lycopersici*. *Physiological and Molecular Plant Pathology* **125**.

Simpson JP, Di Leo R, Dhanoa PK, Allan WL, Makhmoudova A, Clark SM, Hoover GJ, Mullen RT, Shelp BJ. 2008. Identification and characterization of a plastid-localized Arabidopsis glyoxylate reductase isoform: Comparison with a cytosolic isoform and implications for cellular redox homeostasis and aldehyde detoxification. *Journal of Experimental Botany* **59**: 2545–2554.

Smith K, Strand DD, Kramer DM, Walker BJ. 2023. The role of photorespiration in preventing feedback regulation via ATP synthase in *Nicotiana tabacum*. *Plant Cell and Environment*.

Soneson C, Love MI, Robinson MD. 2016. Differential analyses for RNA-seq: transcript-level estimates improve gene-level inferences. *F1000Research* **2016 4:1521** **4**: 1521.

- Sørhagen K, Laxa M, Peterhänsel C, Reumann S. 2013.** The emerging role of photorespiration and non-photorespiratory peroxisomal metabolism in pathogen defence (A Weber, Ed.). *Plant Biology* **15**: 723–736.
- South PF, Cavanagh AP, Lopez-calcagno PE, Raines CA, Ort DR. 2018.** Optimizing photorespiration for improved crop productivity. *Journal of Integrative Plant Biology* **60**: 1217–1230.
- Spoel SH, Dong X. 2012.** How do plants achieve immunity? Defence without specialized immune cells. *Nature Reviews Immunology* **12**: 89–100.
- Sun Y, Li P, Deng M, Shen D, Dai G, Yao N, Lu Y. 2017.** The *Ralstonia solanacearum* effector RipAK suppresses plant hypersensitive response by inhibiting the activity of host catalases. *Cellular Microbiology* **19**.
- Sun Y, Li Y, Li Y, Wang M, Mur LAJ, Shen Q, Guo S. 2021.** Nitrate mediated resistance against *Fusarium* infection in cucumber plants acts via photorespiration. *Plant Cell and Environment* **44**: 3412–3431.
- Sunil B, Saini D, Bapatla RB, Aswani V, Raghavendra AS. 2019.** Photorespiration is complemented by cyclic electron flow and the alternative oxidase pathway to optimize photosynthesis and protect against abiotic stress. *Photosynthesis Research* **139**: 67–79.
- Suzuki N, Devireddy AR, Inupakutika MA, Baxter A, Miller G, Song L, Shulaev E, Azad RK, Shulaev V, Mittler R. 2015.** Ultra-fast alterations in mRNA levels uncover multiple players in light stress acclimation in plants. *The Plant Journal* **84**: 760–772.
- Szymańska R, Ślesak I, Orzechowska A, Kruk J. 2017.** Physiological and biochemical responses to high light and temperature stress in plants. *Environmental and Experimental Botany* **139**: 165–177.
- Takahashi S, Badger MR. 2011.** Photoprotection in plants: a new light on photosystem II damage. *Trends in Plant Science* **16**.
- Takahashi S, Bauwe H, Badger M. 2007.** Impairment of the photorespiratory pathway accelerates photoinhibition of photosystem II by suppression of repair but not acceleration of damage processes in *Arabidopsis*. *Plant Physiology* **144**: 487–494.
- Takahashi H, Chen Z, Du H, Liu Y, Klessig DF. 1997.** Development of necrosis and activation of disease resistance in transgenic tobacco plants with severely reduced catalase levels. *Plant Journal* **11**: 993–1005.
- Taler D, Galperin M, Benjamin I, Cohen Y, Kenigsbuch D. 2004.** Plant eR genes that encode photorespiratory enzymes confer resistance against disease. *Plant Cell* **16**: 172–184.
- Tessmer OL, Jiao Y, Cruz JA, Kramer DM, Chen J. 2013.** Functional approach to high-throughput plant growth analysis. *BMC Systems Biology* **7**.
- Timm S. 2020.** The impact of photorespiration on plant primary metabolism through metabolic and redox regulation. *Biochemical Society Transactions* **48**: 2495–2504.
- Timm S, Bauwe H. 2013.** The variety of photorespiratory phenotypes - employing the current status for future research directions on photorespiration. *Plant Biology* **15**: 737–747.

- Timm S, Florian A, Fernie AR, Bauwe H. 2016.** The regulatory interplay between photorespiration and photosynthesis. *Journal of Experimental Botany* **67**: 2923–2929.
- Timm S, Florian A, Jahnke K, Nunes-Nesi A, Fernie AR, Bauwe H. 2011.** The hydroxypyruvate-reducing system in Arabidopsis: Multiple enzymes for the same end. *Plant Physiology* **155**: 694–705.
- Timm S, Florian A, Wittmiß M, Jahnke K, Hagemann M, Fernie AR, Bauwe H. 2013.** Serine acts as a metabolic signal for the transcriptional control of photorespiration-related genes in Arabidopsis. *Plant Physiology* **162**: 379–389.
- Timm S, Hagemann M. 2020.** Photorespiration-how is it regulated and how does it regulate overall plant metabolism? *Journal of Experimental Botany* **71**: 3955–3965.
- Timm S, Mielewczik M, Florian A, Frankenbach S, Dreissen A, Hocken N, Fernie AR, Walter A, Bauwe H. 2012.** High-to-low CO₂ acclimation reveals plasticity of the photorespiratory pathway and indicates regulatory links to cellular metabolism of Arabidopsis. *PLoS ONE* **7**.
- Timm S, Nunes-Nesi A, Florian A, Eisenhut M, Morgenthal K, Wirtz M, Hell R, Weckwerth W, Hagemann M, Fernie AR, et al. 2021.** Metabolite profiling in Arabidopsis thaliana with moderately impaired photorespiration reveals novel metabolic links and compensatory mechanisms of photorespiration. *Metabolites* **2021, Vol. 11, Page 391** **11**: 391.
- Timm S, Nunes-Nesi A, Pärnik T, Morgenthal K, Wienkoop S, Keerberg O, Weckwerth W, Kleczkowski LA, Fernie AR, Bauwe H, et al. 2008.** A cytosolic pathway for the conversion of hydroxypyruvate to glycerate during photorespiration in Arabidopsis. *Plant Cell* **20**: 2848–2859.
- Di Tommaso P, Chatzou M, Floden EW, Barja PP, Palumbo E, Notredame C. 2017.** Nextflow enables reproducible computational workflows. *Nature Biotechnology* **35**: 316–319.
- Toyota M, Spencer D, Sawai-Toyota S, Jiaqi W, Zhang T, Koo AJ, Howe GA, Gilroy S. 2018.** Glutamate triggers long-distance, calcium-based plant defense signaling. *Science* **361**: 1112–1115.
- Voss I, Sunil B, Scheibe R, Raghavendra AS. 2013.** Emerging concept for the role of photorespiration as an important part of abiotic stress response. *Plant Biology* **15**: 713–722.
- Wada M. 2013.** Chloroplast movement. *Plant Science* **210**: 177–182.
- Walker BJ, Skabelund DC, Busch FA, Ort DR. 2016a.** An improved approach for measuring the impact of multiple CO₂ conductances on the apparent photorespiratory CO₂ compensation point through slope-intercept regression. *Plant Cell and Environment* **39**: 1198–1203.
- Walker BJ, VanLoocke A, Bernacchi CJ, Ort DR. 2016b.** The Costs of Photorespiration to Food Production Now and in the Future. *Annual Review of Plant Biology* **67**: 107–129.
- Wang A, Shu X, Jing X, Jiao C, Chen L, Zhang J, Ma L, Jiang Y, Yamamoto N, Li S, et al. 2021.** Identification of rice (*Oryza sativa* L.) genes involved in sheath blight resistance via a genome-wide association study. *Plant Biotechnology Journal* **19**: 1553–1566.
- Wang Z, Wang Y, Wang Y, Li H, Wen Z, Hou X. 2022.** HPR1 is required for high light intensity induced photorespiration in Arabidopsis thaliana. *International Journal of Molecular Sciences* **23**: 1–17.

- Wasternack C, Song S. 2017.** Jasmonates: Biosynthesis, metabolism, and signaling by proteins activating and repressing transcription. *Journal of Experimental Botany* **68**: 1303–1321.
- Williams A, Pétriacq P, Schwarzenbacher RE, Beerling DJ, Ton J. 2018.** Mechanisms of glacial-to-future atmospheric CO₂ effects on plant immunity. *New Phytologist* **218**: 752–761.
- Wiludda C, Schulze S, Gowik U, Engelmann S, Koczor M, Streubel M, Bauwe H, Westhoff P. 2012.** Regulation of the photorespiratory *GLDPA* gene in *C4 Flaveria* : An intricate interplay of transcriptional and posttranscriptional processes. *The Plant Cell* **24**: 137–151.
- Wingler A, Lea PJ, Quick WP, Leegood RC. 2000.** Photorespiration: metabolic pathways and their role in stress protection. *Philosophical Transactions of the Royal Society of London. Series B, Biological Sciences* **355**: 1517–1529.
- Wingler A, Quick WP, Bungard RA, Bailey KJ, Lea PJ, Leegood RC. 1999.** The role of photorespiration during drought stress: An analysis utilizing barley mutants with reduced activities of photorespiratory enzymes. *Plant, Cell and Environment* **22**: 361–373.
- Xin XF, Nomura K, Aung K, Velásquez AC, Yao J, Boutrot F, Chang JH, Zipfel C, He SY. 2016.** Bacteria establish an aqueous living space in plants crucial for virulence. *Nature* **539**: 524–529.
- Xu JJ, Fang X, Li CY, Zhao Q, Martin C, Chen XY, Yang L. 2018a.** Characterization of arabidopsis thaliana hydroxyphenylpyruvate reductases in the tyrosine conversion pathway. *Frontiers in Plant Science* **9**: 1–13.
- Xu YP, Yang J, Cai XZ. 2018b.** Glycolate oxidase gene family in *Nicotiana benthamiana*: Genomewide identification and functional analyses in disease resistance. *Scientific Reports* **8**: 1–11.
- Yang Y, Jin H, Chen Y, Lin W, Wang C, Chen Z, Han N, Bian H, Zhu M, Wang J. 2012.** A chloroplast envelope membrane protein containing a putative LrgB domain related to the control of bacterial death and lysis is required for chloroplast development in *Arabidopsis thaliana*. *New Phytologist* **193**: 81–95.
- Yang J, Sun C, Fu D, Yu T. 2017.** Test for L-glutamate inhibition of growth of *Alternaria alternata* by inducing resistance in tomato fruit. *Food Chemistry* **230**: 145–153.
- Yao N, Tada Y, Sakamoto M, Nakayashiki H, Park P, Tosa Y, Mayama S. 2002.** Mitochondrial oxidative burst involved in apoptotic response in oats. *Plant Journal* **30**: 567–579.
- Yao J, Withers J, He SY. 2013.** *Pseudomonas syringae* infection assays in *Arabidopsis*. In: Goossens A, Pauwels L, eds. *Jasmonate Signaling: Methods and Protocols*. Totowa, NJ: Humana Press, 63–81.
- Yu X, Feng B, He P, Shan L. 2017.** From chaos to harmony: responses and signaling upon microbial pattern recognition. *Annual Review of Phytopathology* **55**: 109–137.
- Yuan HM, Liu WC, Lu YT. 2017.** CATALASE2 coordinates SA-mediated repression of both auxin accumulation and JA biosynthesis in plant defenses. *Cell Host and Microbe* **21**: 143–155.
- Yuan M, Ngou BPM, Ding P, Xin XF. 2021.** PTI-ETI crosstalk: an integrative view of plant immunity. *Current Opinion in Plant Biology* **62**: 102030.

- Yue H, Huang LP, Lu DYH, Zhang ZH, Zhang Z, Zhang DY, Zheng LM, Gao Y, Tan XQ, Zhou XG, et al. 2021.** Integrated Analysis of microRNA and mRNA Transcriptome Reveals the Molecular Mechanism of *Solanum lycopersicum* Response to *Bemisia tabaci* and Tomato chlorosis virus. *Frontiers in Microbiology* **12**: 1–17.
- Zabala M de T, Littlejohn G, Jayaraman S, Studholme D, Bailey T, Lawson T, Tillich M, Licht D, Bölter B, Delfino L, et al. 2015.** Chloroplasts play a central role in plant defence and are targeted by pathogen effectors. *Nature Plants* **1**: 1–14.
- Zarei A, Brikis CJ, Bajwa VS, Chiu GZ, Simpson JP, DeEll JR, Bozzo GG, Shelp BJ. 2017.** Plant glyoxylate/succinic semialdehyde reductases: Comparative biochemical properties, function during chilling stress, and subcellular localization. *Frontiers in Plant Science* **8**: 1–13.
- Zelitch I, Schultes NP, Peterson RB, Brown P, Brutnell TP. 2009.** High glycolate oxidase activity is required for survival of maize in normal air. *Plant Physiology* **149**: 195–204.
- Zhang M, Li Q, Liu T, Liu L, Shen D, Zhu Y, Liu P, Zhou JM, Dou D. 2015.** Two cytoplasmic effectors of *Phytophthora sojae* regulate plant cell death via interactions with plant catalases. *Plant Physiology* **167**: 164–175.
- Zhang L, Paasch BC, Chen J, Day B, He SY. 2019.** An important role of l-fucose biosynthesis and protein fucosylation genes in *Arabidopsis* immunity. *New Phytologist* **222**: 981–994.
- Zhang Y, Song R, Yuan H, Li T, Wang L, Lu K, Guo J, Liu W. 2021.** Overexpressing the N-terminus of CATALASE2 enhances plant jasmonic acid biosynthesis and resistance to necrotrophic pathogen *Botrytis cinerea* B05.10. *Molecular Plant Pathology* **22**: 1226–1238.
- Zhang Z, Xu Y, Xie Z, Li X, He ZH, Peng XX. 2016.** Association-dissociation of glycolate oxidase with catalase in rice: A potential switch to modulate intracellular H₂O₂ levels. *Molecular Plant* **9**: 737–748.
- Zhao H, Lou Y, Sun H, Li L, Wang L, Dong L, Gao Z. 2016.** Transcriptome and comparative gene expression analysis of *Phyllostachys edulis* in response to high light. *BMC Plant Biology* **16**.
- Zhao J, Sun Q, Quentin M, Ling J, Abad P, Zhang X, Li Y, Yang Y, Favery B, Mao Z, et al. 2021.** A Meloidogyne incognita C-type lectin effector targets plant catalases to promote parasitism. *New Phytologist* **232**: 2124–2137.
- Zhao J, Zhang Y, Bian X, Lei J, Sun J, Guo N, Gai J, Xing H. 2013.** A comparative proteomics analysis of soybean leaves under biotic and abiotic treatments. *Molecular Biology Reports* **40**: 1553–1562.
- Zheng XT, Yu ZC, Tang JW, Cai ML, Chen YL, Yang CW, Chow WS, Peng CL. 2021.** The major photoprotective role of anthocyanins in leaves of *Arabidopsis thaliana* under long-term high light treatment: antioxidant or light attenuator? *Photosynthesis Research* **149**: 25–40.

APPENDIX

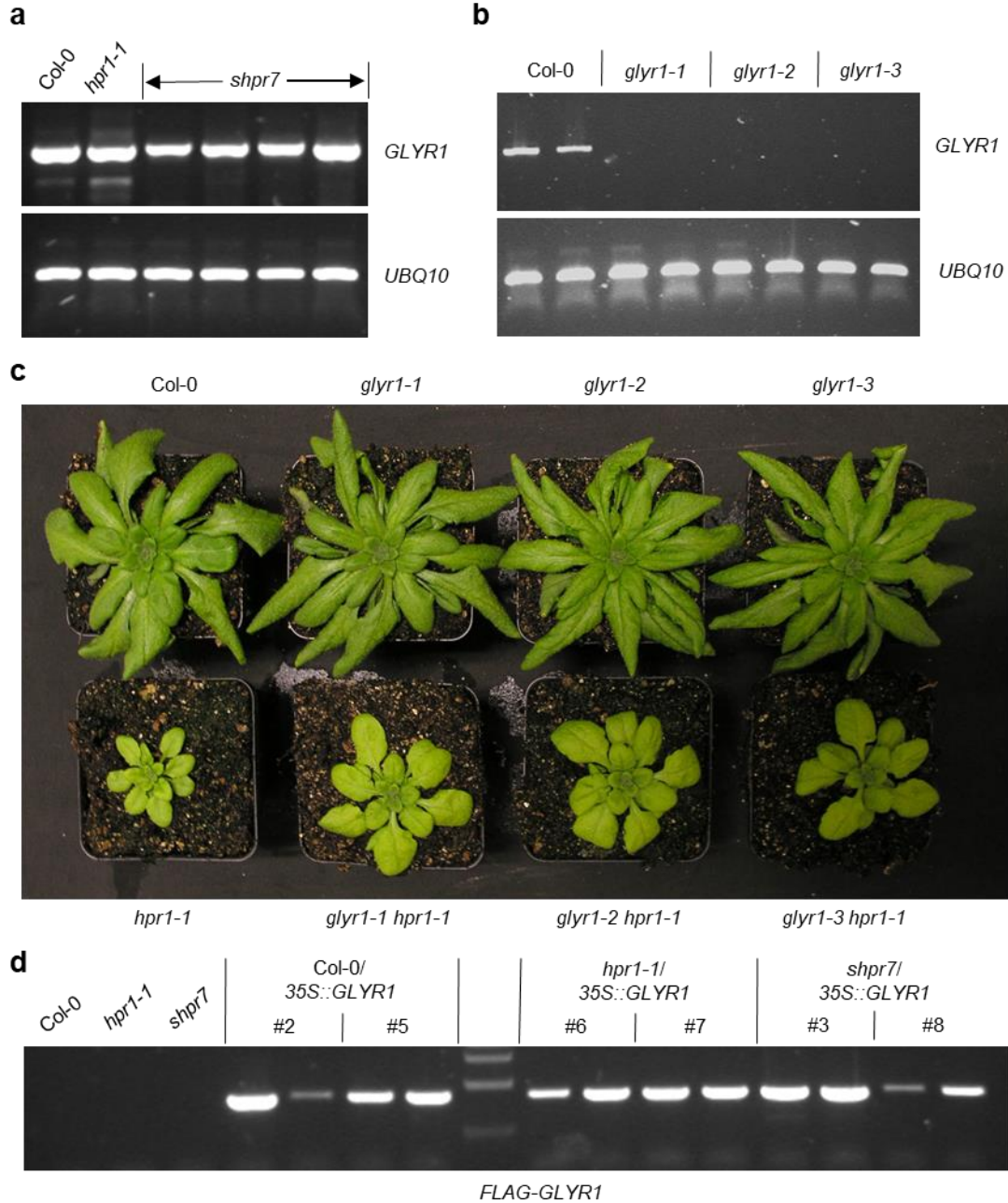


Figure A1. Characterizations of *shpr7*, T-DNA insertion lines of *GLYR1*, and *GLYR1*-overexpressing lines. (a) *GLYR1* expression in *shpr7* plants grown under 2 weeks of normal light followed by 4.5 weeks of high light. (b) *GLYR1* expression in the T-DNA insertion lines grown under 2 weeks of normal light followed by 3 weeks of high light. The expression of *UBQ10* was used as a control in (a) and (b). (c) The *glyr1* single mutants and *glyr1 hpr1* double mutants grown under 2 weeks of normal light followed by 2.5-week high light. (d) *FLAG-GLYR1* expression in transgenic lines grown under 2 weeks of normal light followed by 2.5 weeks of high light.

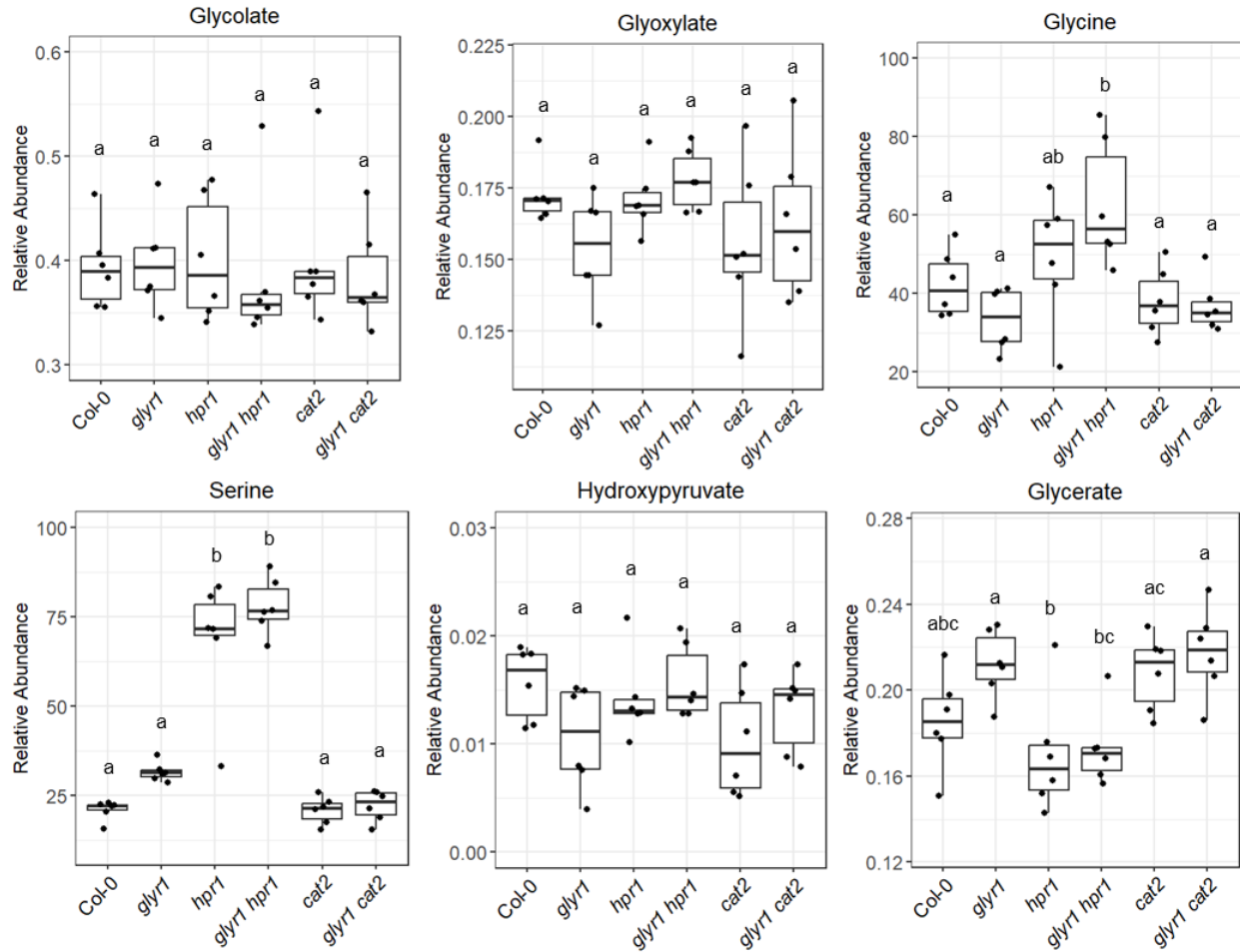


Figure A2. Metabolic profiling of plants grown under high CO₂. Plants were grown under high CO₂ for 3 weeks. Different letters indicate statistically significant differences ($p < 0.05$), which were determined by One-way ANOVA with Tukey's HSD test. Biological replicates: $n = 6$.

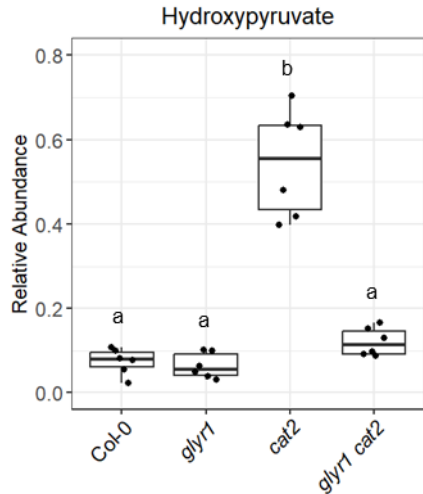


Figure A3. Profiling of transitional hydroxypyruvate in plants transferred to the photorespiratory environment. The same data of hydroxypyruvate was used as Fig. 2.5, but *hpr1* and *glyr1 hpr1* were removed to focus on *cat2* and *glyr1 cat2*. Plants were grown under 3 weeks of high CO₂ and normal light, and then transferred to ambient CO₂ and high light before lights were turned on. Leaf tissue was sampled after ~10 h. Different letters indicate statistically significant differences ($p < 0.05$), which were determined by One-way ANOVA with Tukey's HSD test. Biological replicates: $n = 6$.

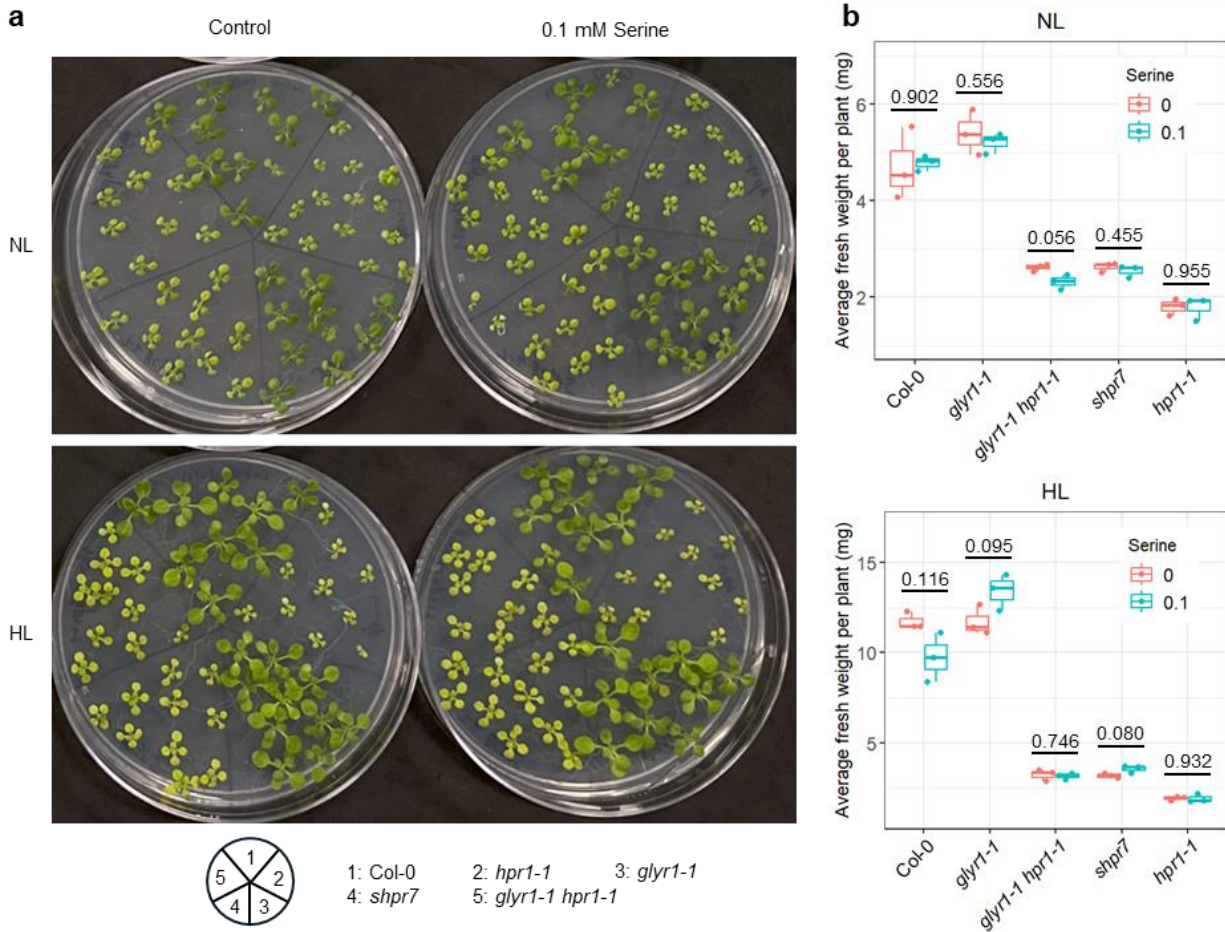


Figure A4. Plant growth after feeding with serine. Growth phenotype (a) and fresh weight (b) of 12-day-old seedlings on plates with or without serine under normal light (NL) or high light (HL) are recorded. The *p* values determined by Student's unpaired two-tailed *t*-test were labeled on the plot. Seedlings grown on the same plate were treated as a biological replicate. Biological replicates: *n*=3.



Figure A5. Characterizations of *hpr2-3*. (a) Schematic depiction of the *HPR2* gene and the position of the mutation in *hpr2-3*. (b) *HPR2* expression in *hpr2-3* in plants grown under 2 weeks of normal light followed by 2 weeks of high light. *UBQ10* was used as a control.

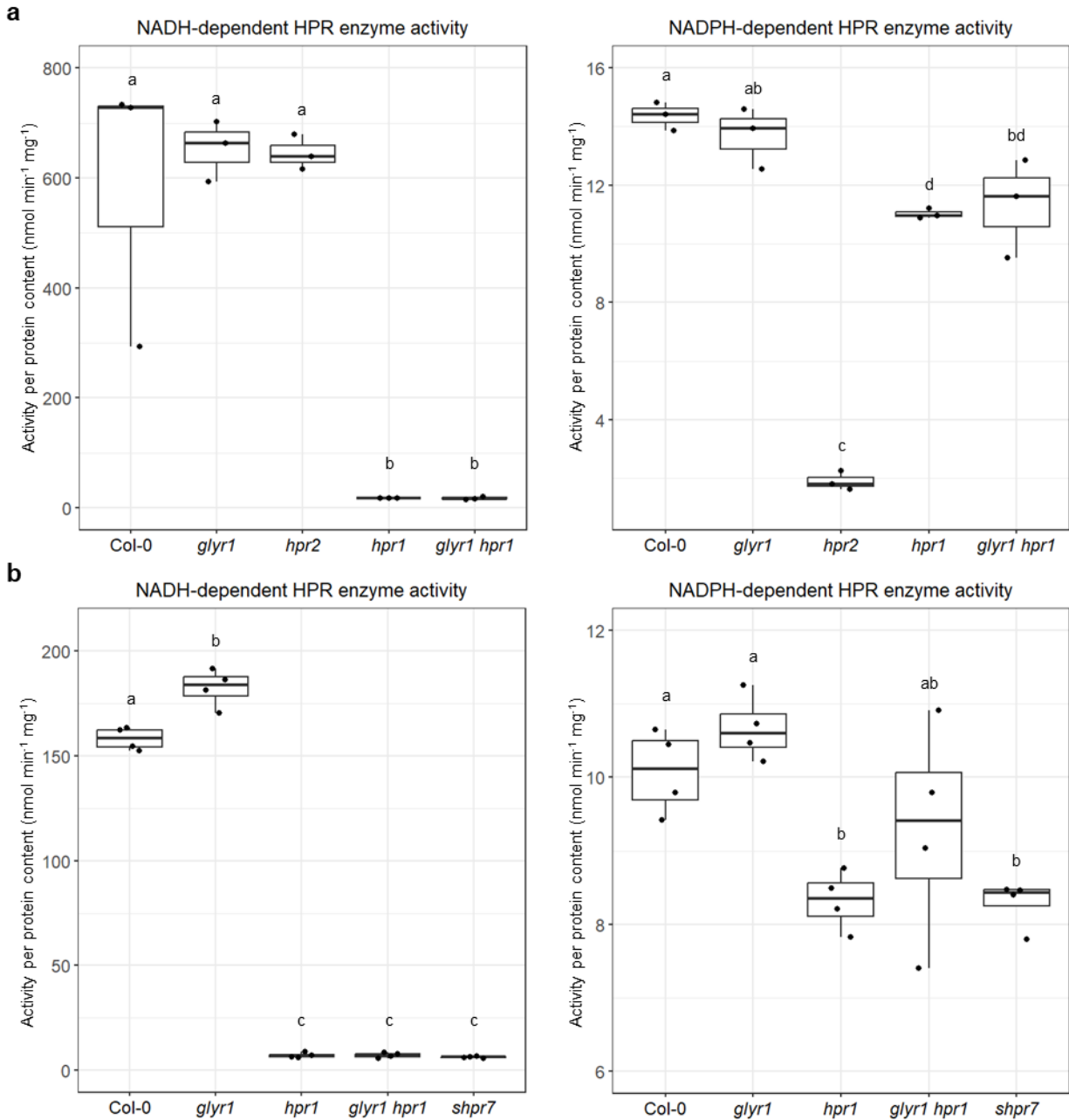


Figure A6. Hydroxypyruvate reductase (HPR) activities in plants. The NADH- and NADPH-dependent HPR enzyme activities in plants grown under 3-week high CO₂ and normal light followed by ~10 h ambient air and high light (**a**) and plants grown under 2 weeks of normal light followed by 2 weeks of high light (**b**) are shown. Different letters indicate statistically significant differences ($p < 0.05$), which were determined by One-way ANOVA with Tukey's HSD test. Biological replicates: $n=3$ for (a) and $n=4$ for (b).

Table A1. List of primers used in this study.

Primer name	Primer sequence (5'-3')	Purpose
SALK_LBb1.3	ATTTTGCCGATTTCGGAAC	Genotyping
SALK_067724_LP	GTTGAGTTTGGATATGGCCAC	Genotyping
SALK_067724_RP	ACCAAACATCGCGATTACAAC	Genotyping
SALK_076998_LP	ACATTTTGGAGCATTGACTGG	Genotyping
SALK_076998_RP	TCTGGTGCTCCTGTATGGAAC	Genotyping
SALK_053469_RP	GTTTTGCCATAGGCTCGGCTT	Genotyping
SALK_053469_LP	CGTCGTCGTCTCCATACCCAT	Genotyping
SALK_057410_LP	ACAATCAAACCCAAAATCCC	Genotyping
SALK_057410_RP	AAACGATCTCTTCCCAAGAC	Genotyping
SALK_202680_LP	CTCAGCCAATCCAAATGAGTG	Genotyping
SALK_202680_RP	CGGTGTTTTGGAGCAGATATG	Genotyping
SALK_203580_LP	GCTTGCAAAAGTTTGATCACC	Genotyping
SALK_203580_RP	GTTTGGGAATCATGGGAAAAG	Genotyping
SALK_105876_LP	CACTGGATTCCCTAAACATGC	Genotyping
SALK_105876_RP	CCCTTAGCTCCTAATGCATCC	Genotyping
GLYR1-att-F	ggggacaagttgtacaaaaaagcaggcttcATGGAAGTAGGGTTTCTGGGT	Cloning
GLYR1-att-R	ggggaccactttgtacaagaaagctgggtcCTATTCGCGGGAGAA TTTC	Cloning
GLYR1-CDS-F	ATGGAAGTAGGGTTTCTGGGT	RT-PCR
GLYR1-CDS-R	CTATTCGCGGGAGAATTCAC	RT-PCR
FLAG-GLYR1-F	GACTACAAAGACGATGACGACAAA	RT-PCR
UBQ10-F	TCAATTCTCTTACCGTGATCAAGATG	RT-PCR
UBQ10-R	GGTGTCAGAACTCTCCACCTCAAGAG	RT-PCR
HPR2-RT-F	ATGGAATCAATCGGAGTCCTTATGA	RT-PCR
HPR2-RT-R	CCAAATCCCAAATGTGTCACATGAC	RT-PCR